JST Presto Symposium on Mathematical Sciences towards Environmental Problems

June, 2008

Series #136. September, 2008

HOKKAIDO UNIVERSITY
TECHNICAL REPORT SERIES IN MATHEMATICS

#113 N. Ishimura, T. Ishiwata, T. Sakajo, T. Sakurai, M. Nagayama, T. Nara, K. Hayami, D. Furihata and T. Matsuo, 応用数理サマーセミナー「確率微分方程式」, 116 pages. 2006.

#114 T. Abe, 第 8 回 COE 研究員連続講演会『超平面配置と対数的ベクトル場の幾何』, 23 pages. 2006.

#115 H. Kubo and T. Ozawa, Sapporo Guest House Symposium on Mathematics 22 "Nonlinear Wave Equations", 67 pages. 2006.

#116 S. Okabe, 第 9 回 COE 研究員連続講演会『ある束縛条件下における平面弾性閉曲線のダイナミクス』, 31 pages. 2006.

#117 A. Suzuki, T. Ito, N. Sato, K. Shibuya, D. Hirose, Y. Maekawa and K. Matsumoto, 第 3 回数学総合若手研究集会 –他分野との学際的交流を目指して, 264 pages. 2007.

#118 T. Yamamoto, Y. Sato, N. Kataoka and H. Takagi, Proceedings of the conference on New Aspects of High-dimensional Nonlinear Dynamics, 73 pages. 2007.

#119 T. Yamamoto and T. Nakazi, 第 15 回関数空間セミナー報告集, 82 pages. 2007.

#120 K. Hirata, 第 10 回 COE 研究員連続講演会『正値調和関数に対する Martin 積分表現と非線形楕円型方程式の正値解の存在』, 25 pages. 2007.

#121 K. Izuchi, 第 12 回 COE 研究員連続講演会『 I）Segal-Bargmann 空間の巡回ベクトルについて II）2 重単位開円板上の逆シフト不変部分空間上のクロス交換子について』, 18 pages. 2007.

#122 T. Ozawa, Y. Giga, S. Jimbo, G. Nakamura, Y. Tonegawa, K. Tsutaya and T. Sakajo, The 32nd Sapporo Symposium on Partial Differential Equations, 73 pages. 2007.

#123 H. Kubo, T. Ozawa, H. Takamura and K. Tsutaya, Nonlinear Wave Equations, 53 pages. 2007.

#124 N. Ishimura, T. Sakajo, T. Sakurai, M. Nagayama, T. Nara, D. Furihata and T. Matsuo, 応用数理サマーセミナー 2007「計算ホモロジーとその応用」, 110 pages. 2007.

#125 S. Hattori, 第 15 回 COE 研究員連続講演会『分岐理論と有限平坦 Galois 表現』, 28 pages. 2008.

#126 T. Miyaguchi, M. Kon, R. Kamijo, S. Kawano, Y. Sato and D. Hirose, 第 4 回数学総合若手研究集会 –他分野との学際的交流を目指して, 298 pages. 2008.

#127 K. Saji, 第 13 回 COE 研究員連続講演会『波面とその特異点』, 15 pages. 2008.

#128 T. Nakazi and S. Miyajima, 第 16 回関数空間セミナー報告集, 105 pages. 2008.

#129 M. Kon, 学位論文 Doctoral thesis "Minimal submanifolds immersed in a complex projective space", 77 pages. 2008.

#130 S. Minabe, 第 14 回 COE 研究員連続講演会『開ミラー対称性における最近の進展』, 8 pages. 2008

#131 H. Kubo and T. Ozawa, Sapporo Guest House Symposium, Final "Nonlinear Partial Differential Equations", 73 pages. 2008.

#132 H. Kang, 第 16 回 COE 研究員連続講演会『CHAOS IN TRAVELING WAVES IN LATTICE SYSTEMS OF UNBOUNDED MEDIA』, 13 pages. 2008.

#133 G.-J. Chung, editor:Y. Kimura, Introduction to Various Models in Image Processing, 61 pages. 2008.

#134 H. Takagi and R. Uno, 研究会報告書『動的システムの情報論 (7)』, 110 pages. 2008.

#135 T. Ozawa, Y. Giga, S. Jimbo, G. Nakamura, Y. Tonegawa, K. Tsutaya and T. Sakajo, 第 33 回偏微分方程式論札幌シンポジウム, 72 pages. 2008.

JST Presto Symposium on Mathematical Sciences towards Environmental Problems

June, 2008

Organizers:
JST Mathematics Program, "Alliance for breakthrough between mathematics and sciences"
Hokkaido Unviersity Graduate School of Science (Department of Mathematics)

Co-organizers:
Research Center for Intergrative Mathematics (Hokkaido University)
Global Eco-Risk Management from Asian Viewpoints (Yokohama National University)

JST Symposium Organizing Committee:
Takashi Sakajo (Hokkaido University / Presto Researcher, Corresponding Organizer)
Yasumasa Nishiura (Hokkaido University / Research Supervisor)
Hiroshi Suito (Okayama University / Presto Researcher)
Katsuhiro Nishinari (University of Tokyo / Presto Researcher)
Masaharu Nagayama (Kanazawa University / Presto Researcher)
Takashi Amemiya (Yokohama National University)

Preface

Environmental problems are among the most important scientific challenges in the 21st century. They are the key themes that were discussed in the G8 Hokkaido Toyako Summit held at Hokkaido, Japan in July 2008. A number of researchers from various fields of sciences are now dealing with the problems intensively in recent years.

While mathematicians tend to pay less attention to such real-world problems, mathematical tools can be potentially applied towards environmental problems due to the intrinsic universality. The aim of this symposium was to overview how mathematics can contribute to these problems by inviting distinguished researchers from a wide range of disciplines related to environmental problems.

The topics were selected from various research fields such as global climate change, civil engineering, environmental hydraulics, environmental assessments, dermatology and ultraviolet, statistical treatment of infectious diseases and so on.

We had five invited speakers who provided the participants with wonderful research results and inspiring ideas. We also organized a poster session, where excellent 15 contributed posters were presented. The summary of these talks and the posters are collected in this proceedings.

This symposium was organized by "PRESTO" researchers which consist of young mathematicians seeking an innovative breakthrough from mathematics towards many other research fields. It is also supported as one of the events in "Sustainability Marathon" organized by Hokkaido University.

Takashi Sakajo
Department of Mathematics, Hokkaido University
Presto Researcher

"PRESTO" is a proposal-oriented research promotion of JST, a Japan's national agency.
http://www.jst.go.jp/kisoken/presto/index_e.html

Sustainability Marathon, Hokkaido University 2008.
http://sw2008.jp/english/index.html

Contents

JST Presto Symposium on Mathematical Sciences towards Environmental Problems

Dates: June 11 (Wednesday) - 13 (Friday), 2008

Venue: Room 8-309, Faculty of Science Building #8, Hokkaido University

Organizers: JST Presto Project,
Hokkaido University Graduate School of Science (Department of Mathematics)

Co-organizers: Research Center for Integrative Mathematics (Hokkaido University),
Global Eco-Risk Management from Asian Viewpoints
(Yokohama National University)

JST Symposium Organizing Committee:
Takashi Sakajo (Hokkaido University/Presto Researcher, Corresponding Organizer)
Yasumasa Nishiura (Hokkaido University/Research Supervisor)
Hiroshi Suito (Okayama University/Presto Researcher)
Katsuhiro Nishinari (University of Tokyo/Presto Researcher)
Masaharu Nagayama (Kanazawa University/Presto Researcher)
Takashi Amemiya (Yokohama National University)

URL: http://www.math.sci.hokudai.ac.jp/sympo/080611/index_en.html

June 11 (Wednesday)

14:00-15:00 Marco Picasso (IACS/Switzerland)
Numerical simulation of Rhone glacier between 1874 and 2100
*joint work with Guillaume Jouvet, Jacques Rappaz (EPF-Lausanne), Heinz Blatter, Martin Funk (ETH-Zurich)

15:30-16:30 Koji Kurihara (Okayama University)
Statistical approach for environmental problems based on spatial structure

June 12 (Thursday)

9:30-10:30 Mitsuhiro Denda (Shiseido Co., Ltd)
Aridification of modern cities and skin pathology

11:00-12:00 Axel Rossberg (IIASA/Austria)
The problem of biodiversity

14:00-15:00 Kiminori Itoh (Yokohama National University)
Will statistics give the sensitivity of the global climate system?

15:30-17:30 Poster Session

June 13 (Friday)

9:30-10:30 Tetsuro Tujimoto (Nagoya University)
River management for ecosystem conservation
- Policy-making support through mathematical modelling -

11:00-12:00 Discussion Time

Poster Session

Yousuke Amaya (Hokkaido University)
Charge simulation method for approximating the complex potential in a channel domain with multiple cyrindrical islands
*joint work with Takashi Sakajo

Kazunori Fujisawa (Okayama University)
Simultaneous analysis method of deformation and internal erosion for soil structures

Myungjin Na (Okayama University)
A study on appropriate selection of final waste disposal sites

Fumio Nakajima (Iwate University)
The paradox of enrichment

Shinji Nakaoka (University of Tokyo)
Mathematical study on microbial coexistence mediated by syntrophic association
*joint work with Chie Katsuyama, Yasuhiro Takeuchi, Kenji Katoh

Takashi Nakazawa (Okayama University)
Numerical and mathematical approaches to flow analyses in ponds induced by a water circulator

Takashi Nitta (Mie University)
Constructing the optimal solutions to the infinite horizon optimization problems as the limit of the optimal solutions to the finite horizon problems
*joint work with Dapeng Cai

Isamu Ohnishi (Hiroshima University)
A binary digit induced by multiple covalent modifications and its application to molecular rhythm
*joint work with Tatsuo Shibata and Kazumi Ebisu

Kazumichi Ohtsuka (University of Tokyo)
Real option valuation of social systems
*joint work with Katsuhiro Nishinari

Akiko Satake (Hokkaido University)
Modelling forest transition: Bistability of forested and abandoned landscapes

Kenichi Shibata (Yokohama National University)
Activities of algicidal bacteria and their influences on microbial communities

Hiroshi Suito (Okayama University)
Motion of aquatic plants interacting with water flows
*joint work with K. Tanino

Akiyasu Tomoeda (University of Tokyo)
Fuel loss and jams due to stopping at railroad crossings
*joint work with Katsuhiro Nishinari and Yoshiaki Harada

Daichi Yanagisawa (University of Tokyo)
Easing pedestrian jam for preventing global warming
*joint work with Katsuhiro Nishinari

Numerical simulation of Rhone's glacier from 1874 to 2100

Guillaume Jouvet, [a,1] Marco Picasso, [a] Jacques Rappaz, [a]
Heinz Blatter, [b] Matthias Huss, [c] Martin Funk [c]

[a] *Institut d'Analyse et Calcul Scientifique, EPFL, 1015 Lausanne, Switzerland*

[b] *Institute for Atmospheric and Climate Science, ETHZ, CH-8092 Zürich, Switzerland*

[c] *Laboratory of Hydraulics, Hydrology and Glaciology (VAW), ETHZ, CH-8092 Zürich, Switzerland*

Abstract

The numerical simulation of the motion of Rhone's glacier in the Swiss Alps is performed from 1874 to 2007, and then from 2007 to 2100. Given the shape of the glacier, the velocity of ice $\mathbf{u}$ is obtained by solving a 3D nonlinear Stokes problem. Then, the shape of the glacier is updated by computing the volume fraction of ice φ, which satisfies the transport equation

$$\frac{\partial \varphi}{\partial t} + \mathbf{u} \cdot \nabla \varphi = b\delta_{\Gamma_A}.$$

Here $b\delta_{\Gamma_A}$ is a source term acting only on the ice-air interface Γ_A which accounts for the accumulation or ablation of ice due to snow falls or melting.

A decoupling algorithm allows the two above problems to be solved using different numerical techniques. The nonlinear Stokes problem is solved on a fixed, unstructured finite element mesh made of tetrahedrons. The transport equation is solved using a fixed, structured grid made of smaller cells.

The numerical simulation is performed between 1874 and 2007. Then, a median climatic scenario is considered in order to predict the shape of the glacier from 2007 until 2100.

[1] Supported by the Swiss National Science Foundation

14 August 2008

1 Introduction

Since 1850, glaciologists have documented the retreat of the glaciers in the Swiss Alps. The motion of glaciers is relevant not only for the tourism industry but also for the future management of natural risks, hydroelectric plants and water supply for agriculture.

The dynamics of a glacier is the result of different phenomena. Due to snowfalls, ice is accumulating on the upper part of the glacier whereas it is melting on the lower part because of higher temperatures. Moreover, due to gravity, ice is flowing down to the valley. When studying ice flows during years or centuries, ice can be considered as an incompressible non-Newtonian fluid and the convected derivative can be disregarded. Therefore, given a glacier shape, the mass and momentum equations reduce to a nonlinear stationary Stokes problem. Mass conservation along the ice-air interface yields to a transport equation which can be used to determine the new glacier shape. A source term - the so-called mass balance - must be added to the right hand side of this transport equation in order to take into account ice accumulation or ablation due to snow falls or melting. This term contains the climatic input of the model and several scenario can be explored in order to predict the future retreat of Alpine glaciers.

Most of the numerical simulations presented so far in glaciology have been performed using Lagrangian or Arbitrary Lagrangian Eulerian methods. When considering ice flows during centuries, topological changes may appear so that Eulerian methods such as Level Set or Volume of Fluid (VOF) seem to be more appropriate. Level set methods in glaciology have been considered in [PF04] to compute the onset of crevasse formation in 2D. The VOF formulation has been used in [JPRB08] to recover stationary 3D glacier shapes.

In this paper, the dynamics of Rhone's glacier is computed in 3D for 227 years using the method presented in [JPRB08]. The determination of the mass balance is the result of 150 years of measurements performed by glaciologists; it corresponds to a parameter identification procedure that involves weather reports, climate prediction, measurements of ice flow, ice depth, snow falls and ice melting [HBF08]. Using this mass balance, the simulated glacier shape can then be compared to the measured one from 1874 to 2007. Then, a median climatic scenario is considered in order to predict the future shape of the glacier from 2007 to 2100.

The paper is organised as follows. The mathematical model is presented in the next Section and corresponds to the model already presented in [JPRB08]. The numerical procedure also corresponds to [JPRB08]. At each time step, the velocity computation is decoupled from the glacier shape computation, which allows different numerical techniques to be used for solving each of these two subproblems, as in [MPR03,BPL06]. The transport equation is solved on a fixed structured grid of small cells and SLIC post-processing is used to reduce numerical diffusion, see for instance [SZ99]. The nonlinear Stokes problem is solved using a fixed unstructured finite element mesh of tetrahedrons. The computation of the mass balance is presented in Section 4; it has been already published in [HBF08]. Numerical results are presented in Section 5. Computed shapes are compared to measured ones from 1874 to 2007. Finally, the predicted glacier shape in 2100 is reported when using a median climatic scenario taken from [HFBF08].

2 The mathematical model

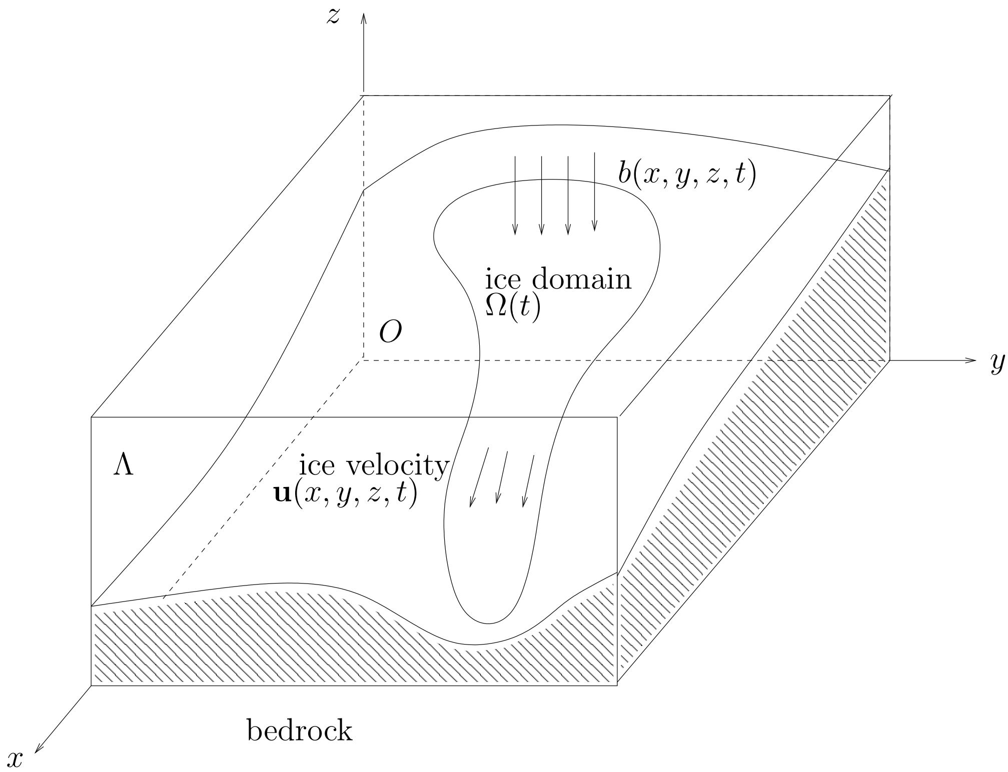

Fig. 1. Notations.

We are interested in computing the shape of a glacier between time $t = 0$ and $t = T$. Let Λ be a cavity of $\mathbb{R}^3$ in which the ice domain is contained. At time t the ice domain is denoted by $\Omega(t)$, the bedrock-ice interface is $\Gamma_B(t)$ and the ice-air interface is $\Gamma_A(t)$. Let Q_T be the ice region in the space-time domain :

$$Q_T = \{(x, y, z, t) \in \Lambda \times (0, T); (x, y, z) \in \Omega(t); 0 < t < T\},$$

and let $\mathbf{u} = (u, v, w) : Q_T \to \mathbb{R}^3$ and $p : Q_T \to \mathbb{R}$ be the ice velocity and pressure, respectively. When considering the motion of a glacier during years or centuries, ice can be considered as an incompressible non-Newtonian fluid. Moreover, a dimensionless scaling shows that inertial terms can be disregarded. Therefore, the mass and momentum equations reduce at time t to a stationary nonlinear Stokes problem in the ice domain $\Omega(t)$:

$$-2\text{div}(\mu\varepsilon(\mathbf{u})) + \nabla p = \rho\mathbf{g}, \tag{1}$$

$$\text{div }\mathbf{u} = 0. \tag{2}$$

Hereabove $\varepsilon(\mathbf{u}) = \frac{1}{2}\left(\nabla\mathbf{u} + \nabla\mathbf{u}^T\right)$ denotes the rate of strain tensor and Glen's flow law [Gle58,Hut83] holds for the viscosity $\mu = \mu(\mathbf{u})$. More precisely, for a given velocity field $\mathbf{u}$, the viscosity μ satisfies the following nonlinear equation:

$$\frac{1}{2\mu} = A\left(\sigma_0^{n-1} + \left(2\mu\sqrt{\frac{1}{2}\text{tr}\Big(\varepsilon(\mathbf{u})\varepsilon(\mathbf{u})\Big)}\right)^{n-1}\right), \tag{3}$$

where A is a positive number known as the rate factor, n is Glen's exponent and σ_0 is a regularisation parameter which prevents infinite viscosity for zero strain. It should be noted that A depends on ice temperature but, since temperature varies very little in most Alpine glaciers, A can be taken as a constant for Rhone's glacier.

The boundary conditions corresponding to (1) are the following. Since no force applies on the ice-air interface $\Gamma_A(t)$:

$$2\mu\varepsilon(\mathbf{u})\mathbf{n} - p\mathbf{n} = \mathbf{0}, \tag{4}$$

where $\mathbf{n}$ is the unit outer normal vector along the boundary of the ice domain $\Omega(t)$. Along the bedrock-ice interface $\Gamma_B(t)$, ice may slip or not, according to the roughness of the bedrock. However, for the sake of simplicity, only no-slip condition will be considered :

$$\mathbf{u} = \mathbf{0} \qquad \text{on } \Gamma_B(t). \tag{5}$$

We now turn to the model for the volume fraction of ice. As in [JPRB08], the presence of ice is defined by a caracteristic function $\varphi : \Lambda \times (0,T) \to \mathbb{R}$ defined by :

$$\varphi(x,y,z,t) = \begin{cases} 1, & \text{if } (x,y,z) \in \Omega(t), \\ 0, & \text{else.} \end{cases} \tag{6}$$

In absence of snowfalls or melting, the volume fraction of ice would satisfy

$$\frac{\partial\varphi}{\partial t} + \mathbf{u}\cdot\nabla\varphi = 0, \tag{7}$$

in a weak sense in the space-time ice domain Q_T. In other words, φ is constant along the trajectories of the fluid particles which are given by

$$\begin{pmatrix} x'(t) \\ y'(t) \\ z'(t) \end{pmatrix} = \begin{pmatrix} u(x(t), y(t), z(t)) \\ v(x(t), y(t), z(t)) \\ w(x(t), y(t), z(t)) \end{pmatrix}.$$

We refer for instance to [SZ99] for a review of numerical methods for solving the above equation.

In Alpine glaciers snow accumulates on the upper part of the glacier whereas ice melts on the lower part. The horizontal line at which $b = 0$ is called the equilibrium line of accumulation ELA and is around 3000 meters above sea level in the Alps. Therefore, a source term must be added to the right hand side of (7) to account for ice accumulation or ablation. Let $b(x, y, z, t)$ be the ice height added or removed along the ice-air interface $\Gamma_A(t)$ within one year, the so-called mass balance function. In our model, this quantity is a given quantity and corresponds to the climate input. It can be measured by glaciologists using stakes and simple empirical expressions are available. Recently [HBF08], a complex formula has been proposed for b which involves snow precipitations and ice melting. The coefficients involved in these formula are then the result of a parameter identification problem which takes into account measurements that have been reported on Rhone's glacier since 1874.

Given the mass-balance function b and following [JPRB08], equation (7) must be updated as follows :

$$\frac{\partial \varphi}{\partial t} + \mathbf{u} \cdot \nabla \varphi = b \delta_{\Gamma_A}, \tag{8}$$

where δ_{Γ_A} is the 3D Dirac (or delta) function on the ice-air interface Γ_A.

Let us sum up the model. Our goal is to find the volume fraction of ice φ in the whole cavity, the velocity $\mathbf{u}$ and pressure p in the ice domain satisfying equations (1), (2) and (8). Equation (1) must be supplemented with the boundary conditions (4) and (5). At initial time, the volume fraction of liquid $\varphi(x, y, z, 0)$, or equivalently the initial ice domain $\Omega(0)$, must be provided.

3 Numerical method

In order to decouple the computation of the volume fraction of ice φ to that of $\mathbf{u}$, p, a time discretization is proposed. Two different space discretizations are then used for solving the transport problem (8) and the nonlinear Stokes problem (1) (2). The transport problem is solved using a structured grid of small cells having size h, with goal to reduce numerical diffusion as much as possible. On the other side, since the numerical resolution of the nonlinear Stokes problem is CPU time consuming, an unstructured mesh of tetrahedrons with larger size H is used. The use of two different grids has shown to be very efficient for solving Newtonian [MPR03] and viscoelastic flows [BPL06] with complex free surfaces. A good compromize between accuracy and efficiency is to choose $H \simeq 5h$ with a time step such that the maximum CFL number (velocity times the time step divided by the cells spacing) is close to 5. This numerical method has already been presented in [JPRB08] in order to compute stationary glacier shapes.

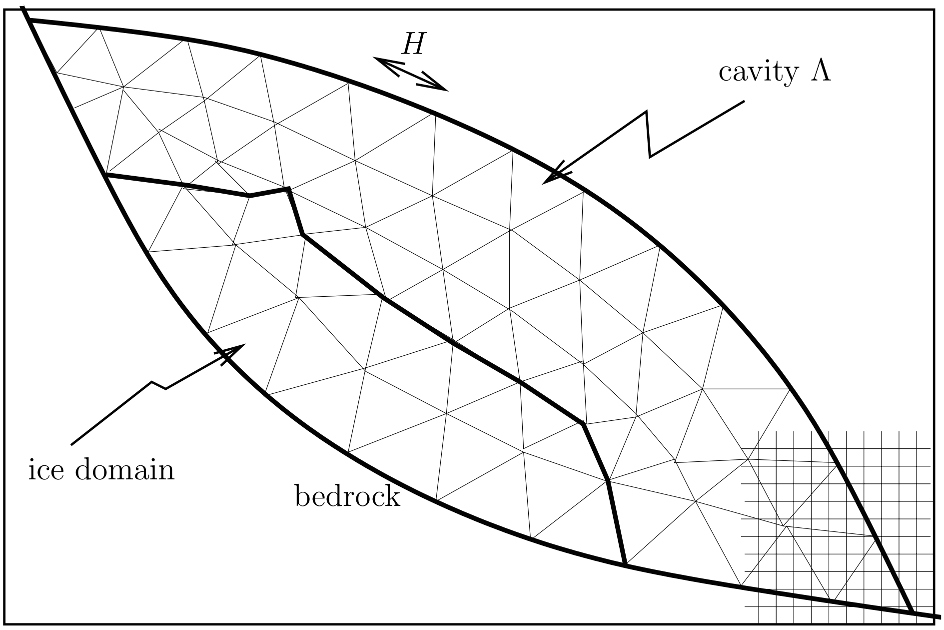

Fig. 2. The two grids (2D figure). The cavity Λ is meshed once for all with unstructured finite elements having size H. Then, at each time step, the ice region is the union of all the elements being filled with ice. The cavity is also covered with structured cells having smaller size $h \simeq H/5$.

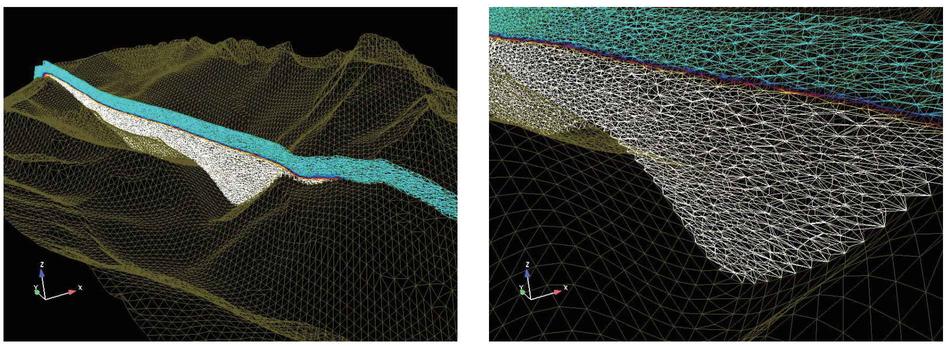

Fig. 3. Cut of the finite element mesh used for Rhone's glacier. Brown : bedrock, blue : cut of the cavity, white : cut of the ice domain at year 1874.

4 The mass balance function b

A model for the mass balance function b accounting for ice acculumation or ablation has been proposed in [HBF08]. The parameters involved in this model have been tuned in order to fit measured values from 1874 to 2007. Then a median climatic scenario [HFBF08] is considered in order to predict glacier shapes until 2100. It corresponds to an increase of 3.8^oC in temperature and a decrease of 6% in precipitations.

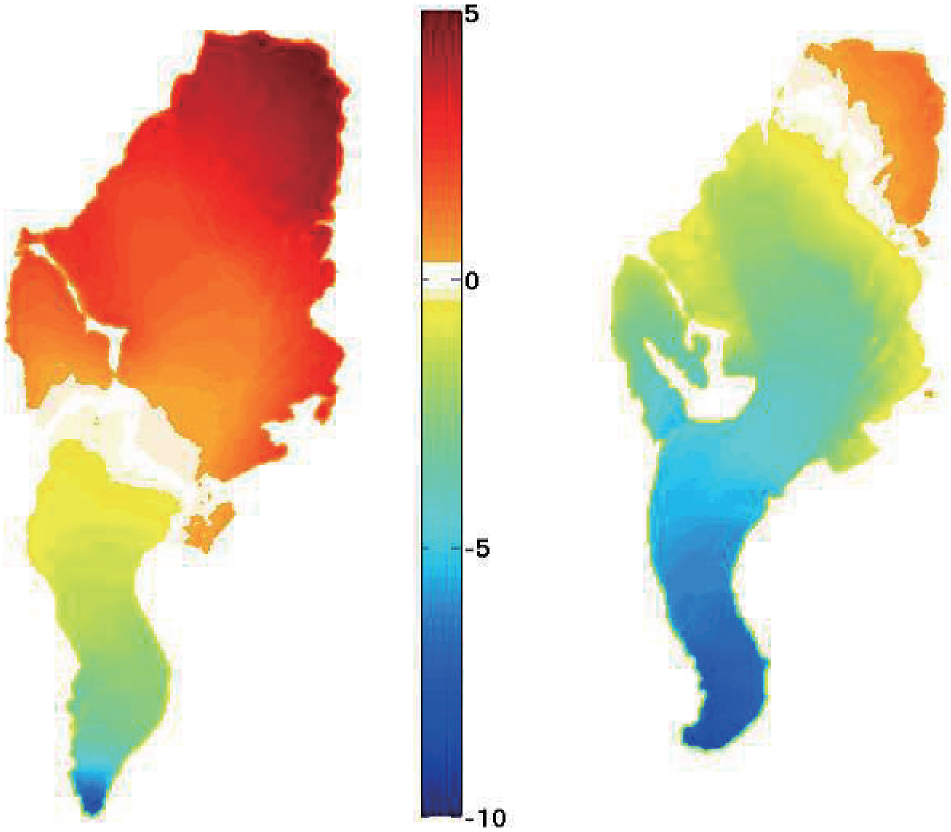

Fig. 4. The mass balance function b at year 1913 (left, cold year) and 2003 (right, hot year).

5 Numerical results

The cavity Λ is contained in the block $(0, 4000) \times (0, 10000) \times (1700 \times 3600)$. At each vertex (x_i, y_j) of a structured grid in the Oxy plane, the bedrock elevation $B(x_i, y_j)$ and the initial ice thickness $T(x_i, y_j)$ are provided, $i = 1, 80$, $j = 1, 200$. The mesh stepping in the x, y directions is 50 m. A triangular finite element mesh of the bedrock is then generated. A triangular finite element mesh of the top surface of the cavity Λ is also generated by adding 150 m to the initial ice thickness. Then, a Delaunay unstructured mesh of tetrahedrons is generated between the bedrock and the top surfaces using TetMesh-GHS3D [FG08], thus filling the cavity Λ with tetrahedrons of typical size 50 m. The MeshAdapt remesher [Dis03] is used in order to refine the mesh in the Oz direction only (mesh size 10 m). The final mesh of the cavity has 240147 vertices. The number of vertices of the cavity contained in Ω^0 is 84161. The block $(0, 4000) \times (0, 10000) \times (1700 \times 3600)$ containing the cavity Λ is cut into $400 \times 1000 \times 200$ structured cells. As in [MPR03] a hierarchic data structure is used in order to activate the cells and decrease the required memory. The time step is half a year. All the computations have been performed on an AMD Opteron 242 CPU with less than 8Mb memory. The simulation is performed with $A = 0.08$ from 1874 to 2007 and requires one week of CPU time. The initial and final glacier shapes are reported in Fig. 5.

Starting from the measured shape of the glacier in 2007, the numerical simulation of the motion of Rhone's glacier is then performed until 2100 using the median climatic scenario discussed in Section 4. The results are displayed in Fig. 6. Clearly, when using such a scenario, the glacier would almost disappear in 2100.

Vol.= 2.8 km^3

Vol.= 2.1 km^3

Fig. 5. Simulation over the period 1874-2007.

References

[BPL06] A. Bonito, M. Picasso, and M. Laso. Numerical simulation of 3D viscoelastic flows with free surfaces. *J. Comput. Phys.*, 215(2):691–716, 2006.

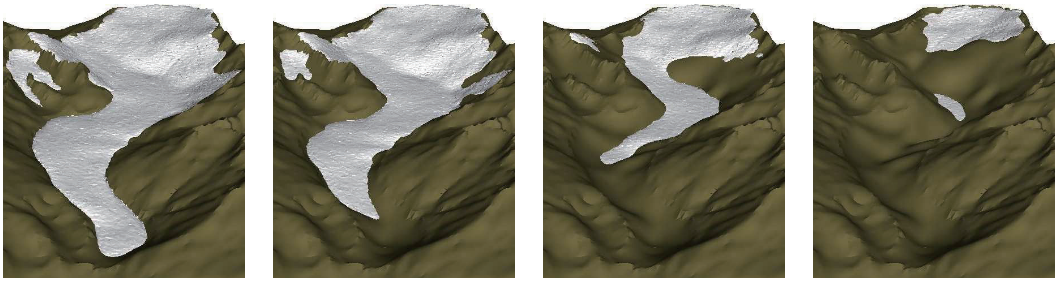

Fig. 6. Simulation over the period 2007-2100.

[Dis03] Distene S.A.S., Pôle Teratec - BARD-1, Domaine du Grand Rué, 91680 Bruyères-le-Chatel, France. *MeshAdapt : A mesh adaptation tool, User's manual Version 3.0*, 2003.

[FG08] P. Frey and P.-L. George. *Mesh generation.* ISTE, London, second edition, 2008. Application to finite elements.

[Gle58] J.W. Glen. The flow law of ice. *IUGG/IAHS Symposium of Chamonix IAHS Publication*, 47:171183, 1958.

[HBF08] M. Huss, A. Bauder, and M. Funk. Determination of the seasonal mass balance of four alpine glaciers since 1865. *Journal of Geophysical research*, 2008.

[HFBF08] M. Huss, D. Farinotti, A. Bauder, and M. Funk. Modelling runoff from highly glacierized alpine drainage basins in a changing climate. *Hydrological Processes*, 2008.

[Hut83] K. Hutter. *Theoretical Glaciology.* Reidel, 1983.

[JPRB08] G. Jouvet, M. Picasso, J. Rappaz, and H. Blatter. A new algorithm to simulate the dynamics of a glacier: theory and applications. *Journal of Glaciology*, 2008.

[MPR03] V. Maronnier, M. Picasso, and J. Rappaz. Numerical simulation of three-dimensional free surface flows. *Internat. J. Numer. Methods Fluids*, 42(7):697–716, 2003.

[PF04] A. Pralong and M. Funk. A level-set method for modeling the evolution of glacier geometry. *J. Glaciology*, 50(171):485–491, 2004.

[SZ99] R. Scardovelli and S. Zaleski. Direct numerical simulation of free-surface and interfacial flow. *Ann. Rev. Fluid Mech.*, 31(7):567–603, 1999.

Statistical Approach for Environmental Problems based on Spatial Structure

Koji Kurihara† and Fumio Ishioka‡

†*The Graduate School of Environmental Science, Okayama University, 3-1-1 Tsushima-naka Okayama 700-8530, Japan, kurihara@ems.okayama-u.ac.jp*

‡*The School of Law, Okayama University, 3-1-1 Tsushima-naka Okayama 700-8530, Japan, fishioka@law.okayama-u.ac.jp*

1. Introduction

The increased level of interest is the concern in society for environmental issues and their relation to the health of individuals. It is important to investigate the areas of significant risk (hotspot) about the effect on the human health status to make early warning for infectious diseases and so on. Most environmental phenomena investigated by sampling geographic space have spatial components. The important roll of statistical analysis for spatial data is to build a model and to make clear the structure of data based on spatial information. There are some typical problems of spatial analysis for geostatistical data, lattice data and point patterns. We focus on lattice data over a fixed subset D of d-dimensional Euclidean space. We deal with the 0/1 event data over the entirety of a partitioned spatial region. Data can be collected directly within each region. These data are known as a kind of spatial epidemiological data, cellular data, irregular lattice data and so on. Several methods have been proposed to detect the hotspots areas. From the perspective of the spatial autocorrelation, Anselin (1995) proposed a local Moran's *I* statistics which was able to locate spatial associations. Recently, the hotspot detection by scan statistics based on the likelihood ratio is a popular method. Kulldorff (1997) detected the hotspots, significant cluster (zone) for the lattice data, based on spatial scan statistic with Binomial and Poisson models. The circular window zone for scanning is defined around one lattice (county) seat. The zone consists of counties whose county seat exists within the circle. Thus we can only detect the circular cluster based on this circular scan. Echelon analysis (Myers et al. 1997) is useful to investigate the cellular surface analysis by systematically and objectively determining topological structure and change. The echelon dendrogram represents the surface topology of lattice data and hierarchical structure of these data. Regional features such as hotspots and trends are shown in an echelon dendrogram. The candidates of hotspots are given as the top echelon in the dendrogram, and some extended approaches are proposed for health and environmental data (Ishioka et al. (2007), Kurihara (2004), Kurihara et al. (2000, 2006), Myers et al. (2006), Tomita et al. (2008)). Therefore we can detect the hotspots of any size and shape for spatially aggregated lattice data based on proposed technique with spatial scan statistic and echelon analysis. The purpose of this paper is to classify any types of lattice data based on their spatial hierarchical structure and to detect the hotspots with regional features. In section 2, we explain the spatial scan statistics. In section 3, we introduce echelon analysis for some types of lattice data. In section 4, we demonstrate the proposed technique with some illustrations on environmental and epidemiological data.

2. Spatial Scan Statistics

The spatial scan statistics is a test statistics to detect the areas with significantly high or low rates. There is one area Z, which is a subset of whole area G. Individuals within area Z have population probability p_1 of the attribute, whereas the population probability for individuals outside of the area Z is p_2. The probabilities for all individuals are mutually independent. The null hypothesis is H_0: $p_1=p_2=p$, and the alternative hypothesis is H_1: $p_1>p_2$, then we have a high attribute rate in an area Z. Let $n(G)$ be the total population in whole area G, and $n(Z)$ be the population within area Z. The $c(G)$ is the total number of attributes in all of area G and $c(Z)$ is the number of the attributes within area Z. Then we consider the model based on the Poisson distribution. The probability of in the study area is given by

$$f(Z) = \exp[-p_1 n(Z) - p_2(n(G) - n(Z))] \frac{[p_1 n(Z) + p_2(n(G) - n(Z))]^{c(G)}}{c(G)\ !} . \tag{2.1}$$

The density function $f(x)$ of a specific point being observed at location x is

$$\begin{cases} \dfrac{p_1 n(x)}{p_1 n(Z) + p_2(n(G) - n(Z))} & if \;\; x \in Z \\ \\ \dfrac{p_2 n(x)}{p_1 n(Z) + p_2(n(G) - n(Z))} & if \;\; x \notin Z \end{cases} . \tag{2.2}$$

We can therefore write the likelihood function as

$$L(Z, p_1, p_2) = \exp[-p_1 n(Z) - p_2(n(G) - n(Z))] \frac{[p_1 n(Z) + p_2(n(G) - n(Z))]^{c(G)}}{c(G)\ !}$$

$$\times \prod_{x_i \in Z} \frac{p_1 n(x)}{p_1 n(Z) + p_2(n(G) - n(Z))} \prod_{x_i \notin Z} \frac{p_2 n(x)}{p_1 n(Z) + p_2(n(G) - n(Z))} . \tag{2.3}$$

$$= \frac{\exp[-p_1 n(Z) - p_2(n(G) - n(Z))]}{c(G)\ !} p_1^{\ c(Z)} p_2^{\ c(G)-c(Z)} \prod_{x_i} n(x_i)$$

To maximize the likelihood function (2.3), we calculate the maximum likelihood function conditioned to area Z. The maximum likelihood estimator $\hat{p}_1 = \dfrac{c(Z)}{n(Z)}$ and $\hat{p}_2 = \dfrac{(c(G) - c(Z))}{(n(G) - n(Z))}$ are substituted.

$$L(Z)=\frac{\exp[-c(G)]}{c(G)\,!}\left(\frac{c(Z)}{n(Z)}\right)^{c(Z)}\left(\frac{c(G)-c(Z)}{n(G)-n(Z)}\right)^{c(G)-c(Z)}\prod_{x_i} n(x_i)\,. \tag{2.4}$$

The likelihood ratio $\lambda(Z)$ is maximized over all subset areas of whole areas to detect the hotspots.

$$\lambda(Z)=\underset{Z}{Max}\,L(Z)\big/L_0=\frac{\left(\frac{c(Z)}{n(Z)}\right)^{c(Z)}\left(\frac{c(G)-c(Z)}{n(G)-n(Z)}\right)^{c(G)-c(Z)}}{\left(\frac{c(G)}{n(G)}\right)^{c(G)}}\,. \tag{2.5}$$

Here, L_0 is the following likelihood function under the null hypothesis.

$$L_0=\sup_p\frac{\exp[-pn(G)]}{c(G)\,!}\,p^{c(G)}\prod_{x_i} n(x_i)=\frac{\exp[-c(G)]}{c(G)\,!}\left(\frac{c(G)}{n(G)}\right)^{c(G)}\prod_{x_i} n(x_i)\,. \tag{2.6}$$

The test statistics $\lambda(Z)$ is also written as

$$\lambda(Z)=\left(\frac{c(Z)}{e(Z)}\right)^{c(Z)}\left(\frac{c(G)-c(Z)}{e(G)-e(Z)}\right)^{c(G)-c(Z)}, \tag{2.7}$$

where $e(Z)$ is the expected value of the attribute within area Z, and $e(G)=c(G)$. An area Z, where the value of λ becomes the maximum, is suitable as the hotspot.

3. Echelon Analysis

3.1 Basic idea

The echelon approach aggregates the areas in which the values have identical topological structure and produce a hierarchically related structure of these areas based on connective (neighbor) information among cells. One-dimensional spatial lattice data has the position (i) and the value h_i on the horizontal and vertical lines, respectively. For D_1 divided lattice (interval) data, data are taken at the interval $l_1(i)=(i-1,i],\, i=1,2,\ldots,D_1$. Table 1 shows the 25 intervals named from A to Y in order and their values (e.g., A=1 and Q=7).

Table 1: One-dimensional spatial lattice data.

i	1	2	3	4	5	6	7	8	9	10	11	12	13	14	15	16	17	18	19	20	21	22	23	24	25
ID	A	B	C	D	E	F	G	H	I	J	K	L	M	N	O	P	Q	R	S	T	U	V	W	X	Y
h(i)	1	2	3	4	3	4	5	4	3	2	3	4	5	6	5	6	7	6	5	4	3	2	1	2	1

At first, we define the neighbor information of spatial lattice data $l_1(i)$, say $NB(i)$. The $NB(i)$ indicates the spatial positions between each cell, and it is given by

$$NB(i) = \begin{cases} \{i+1\}, & i=1 \\ \{i-1, i+1\}, & 1 < i < D_1 \\ \{i-1\}, & i = D_1 \end{cases} \cdot \tag{3.1}$$

We can make the cross sectional view of topographical map like Figure 1, based on $NB(i)$ and value of each cell. There are nine numbered parts with same topological structure in these hills. These parts are called echelons. These echelons consist of peaks, foundation of peaks and foundation of foundation. The numbers 1,2,3,4 and 5 are the peaks of hills. The numbers 6 and 7 are the foundations of two peaks. The number 8 is the foundation of two foundations. The number 9 is the foundation of foundation and peak and also called as the root. The graphical representation is given by the following dendrogram shown in Figure 2.

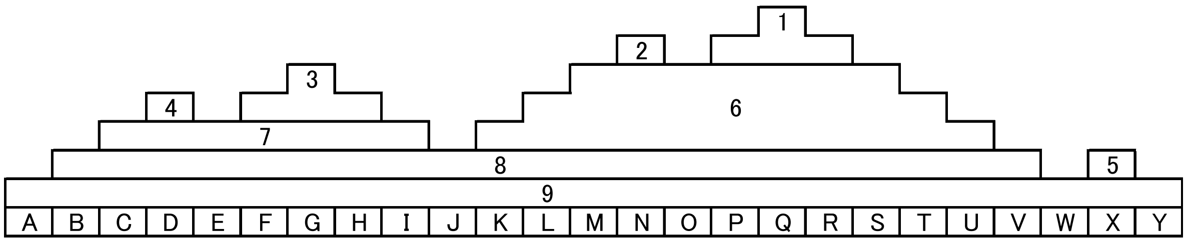

Figure 1: The hypothetical set of hillforms in one-dimensional spatial lattice data.

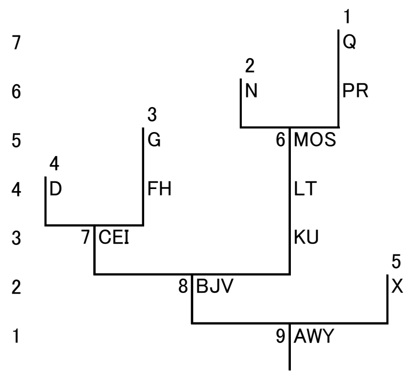

Figure 2: The echelon dendrogram for one-dimensional spatial lattice data.

3.2 Echelon analysis for two and three dimensional spatial lattice data

Two dimensional spatial lattice data, such as remote sensing data or mesh data, are given as the cells of digital value $h_{i,j}$ over the $D_1 \times D_2$ array data:

$$l_2(i, j) = \{(x, y) \mid x_{i-1} \le x \le x_i, y_{j-1} \le y \le y_j,\} \; i = 1,2,\ldots, D_1,\; j = 1,2,\ldots, D_2 \tag{3.2}$$

The neighbor information of cell $l_2(i, j)$ is given as

$$NB(l_2(i,j)) = \{(a,b) \mid i-1 \le a \le i+1, j-1 \le b \le j+1\} \cap \{(a,b) \mid 1 \le a \le D_1, 1 \le b \le D_2\} - \{(i,j)\} \quad (3.3)$$

where $A - B = A \cap \{B^c\}$ for the sets of A and B. Here, B^c denotes the complement of B. For such 2D data with a digital value over a 5×5 array shown in the left side of Figure 3, the echelon dendrogram shown in the right side of Figure 3 is produced by the following steps.

	A	B	C	D	E
1	2	24	8	15	3
2	10	1	14	22	5
3	4	13	19	23	25
4	20	21	12	11	17
5	16	6	9	18	7

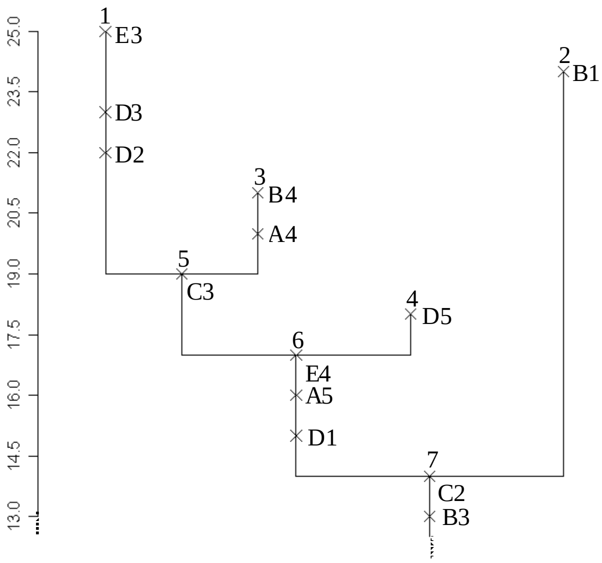

Figure 3: Digital data over 5×5 array and their echelon dendrogram.

Algorithm-E: To find the peaks and foundation of echelon

Step E-1) Find the peaks

The digital values in the peak are greater than the values of neighboring cell of same peak. There are four peaks in this 5-by-5 array. The maximum value in this array is 25. The value of 25 belongs to the fist peak. The maximum value among connected data to 25 is 23. The value of 23 is greater than the values of neighboring cell of 25 and 23. Thus the value of 23 belongs to the fist peak. The maximum value among connected data to 25 and 23 is 22. The value of 22 is greater than the values of neighboring cell of 25, 23 and 22. Thus the value of 22 belongs to the fist peak. The maximum value among connected data to 25, 23 and 22 is 19. But the value of 19 is not greater than 21 which is connected to 19. Thus the value of 19 does not belong to the first peak. As a result, the first peak consists of the values of 25, 23 and 22, and its echelon number is 1. These values are greater than the values of neighboring cell of first peak. In the same manner, second peak consists of 24, and third peak consists of 21 and 20, and the fourth peak consists of 18. These echelon numbers are 2, 3 and 4, respectively.

Step E-2) Find the foundations of the peaks and foundations

The maximum value except the values of four peaks is 19. The value of 19 is the foundation of the peaks whose echelon numbers are 1 and 3. The echelon number of this foundation is 5.

The echelon number 5 is a parent of echelon numbers of 1 and 3. This relationship is expressed as 5(1 3) using echelon numbers. Similarly, we can find the foundation 6 for echelon numbers 4 and 5, and foundation is 7 for echelon numbers of 2 and 6. These relationship is expressed as 7(2 6(5(1 3) 4)) using echelon numbers.

Three dimensional spatial lattice data consist of overlapped two-dimensional (2D) spatial data. These data are also considered as cubic data that consist of $D_1 \times D_2 \times D_3$. Therefore, neighbor information of cell $l_3(i, j, k)$ is given as

$$\begin{aligned} NB(l_3(i,\ j,k)) = &\{(a,b,c)\,|\, i-1 \le a \le i+1,\ j-1 \le b \le j+1,\ k-1 \le c \le k+1\} \\ &\cap \{(a,b,c)\,|\, 1 \le a \le D_1,\ \ 1 \le b \le D_2,\ 1 \le c \le D_3\} - \{(i,j,k)\} \end{aligned} \tag{3.4}$$

where i=1,2,…,D_1, j=1,2,…,D_2, and k=1,2,…,D_3.

For 3D data with a digital value over a $4 \times 4 \times 3$ array shown in the left side of Figure 4, the echelon dendrogram shown in the right side of Figure 4 is also produced by the similar steps of Algorithm-E.

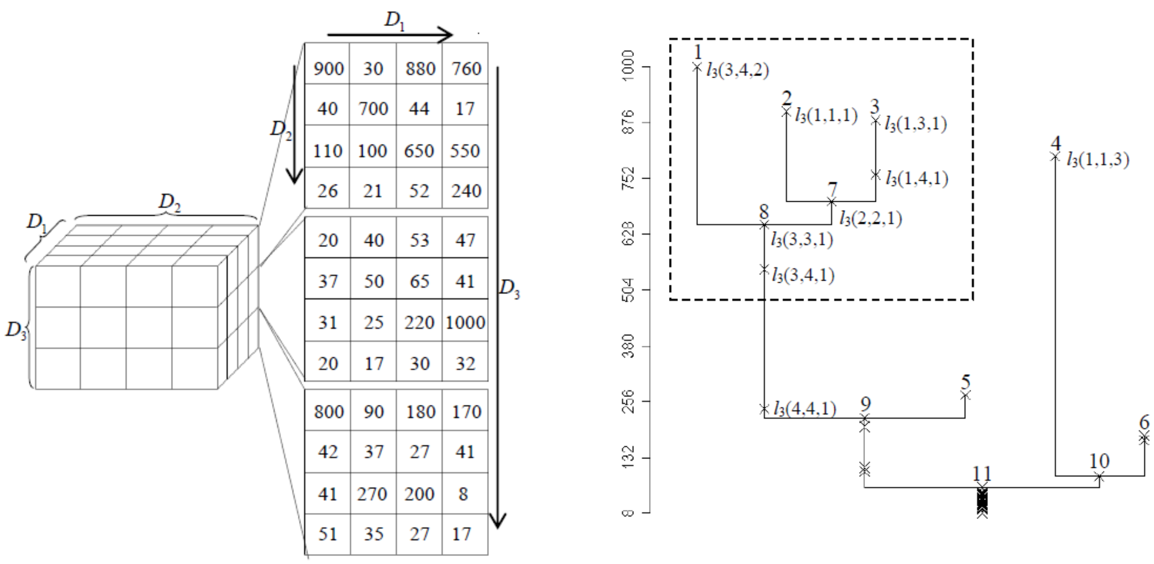

Figure 4: Digital data over $4 \times 4 \times 3$ array and their echelon dendrogram.

We use the echelon technique to seek areas Z where the test statistics is maximized. Through scanning based on echelon, we can detect the candidates of hotspots using the following procedures.

Algorithm-H: To detect the candidate of hotspots

Step H-1) Draw the echelon dendrogram for specified spatial data

Step H-2) Scan the areas from the upper echelon to the bottom, based on the hierarchical structure determined in Step H-1.

Step H-3) Detect the candidate of hotspots, which takes the maximum natural logarithm of test statistics $\lambda(Z)$.

3.3 Echelon analysis for multivariate spatial data using PCA

Echelon analysis has been applied only to univariate spatial data. As a result, it is impossible to detect the hotspots on the multivariate spatial data. We propose a technique of echelon analysis for multivariate spatial data with principal component analysis (PCA) which is the one of the multivariate dimension reduction techniques. We can detect the candidate of hotspots for multivariate spatial data using the following procedures.

Algorithm-M: To detect the candidate of hotspots for multivariate spatial data

Step M-1) Dimension reduction of the multivariate spatial data using the principal component analysis

Step M-2) Characterize the factors for each principal component

Step M-3) Draw the echelon dendrogram using principal component scores to detect the hotspots

Step M-4) Scan the regions from the upper echelon to the bottom, on the basis of the hierarchical structure of Step M-3

StepM-5) Detect the hotspots, which take the maximum log λ based on the likelihood ratio calculated to the factors detected on the StepM-2

4. Applications

4.1 Hotspot detection for 3D lattice data in the event of leachate-leaking accident

At final-disposal sites, the possibility exists of a leachate accident of waste material to groundwater because of liner sheet rupture. As an application of our study, we detect the hotspot with statistically significant pollution area for the simulated process of leachate advection-diffusion in the event of a leachate leaking accident. Figure 5 shows expected processes of leachate advection-diffusion in the event of a leachate-leaking accident at the three time points.

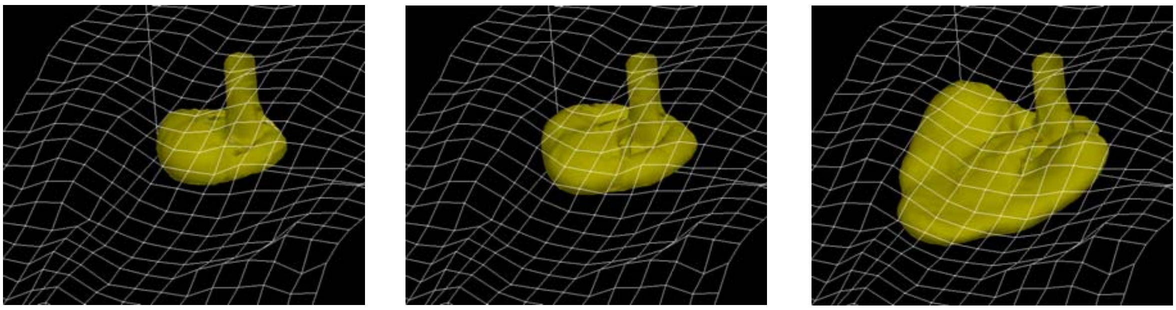

Figure 5: Simulation results of leachate advection-diffusion in the event of a leachate-leaking accident at the three time points. (t=1,2,3)

This consists of the physical space (x, y, z). Therefore, it can be said that these are 3D lattice data. These data consist of

$$\{D_1 \times D_2 \times D_3 \mid D_1 \in \{1,2,\dots,61\},\ D_2 \in \{1,2,\dots,101\},\ D_3 \in \{1,2,\dots,41\}\}; \tag{4.1}$$

Each cell has leachate concentration C computed by solving the advection-diffusion equation. Because the volume of the leachate concentration data is huge, i.e. $61 \times 101 \times 41 = 252601$, we grouped the cells as

$$\{D_1 \times D_2 \times D_3 \mid D_1 \in \{1,2,\dots,16\},\ D_2 \in \{1,2,\dots,26\},\ D_3 \in \{1,2,...,11\}\} \tag{4.2}$$

and detected statistically significant pollution area (hotspot) based on echelon structure using spatial scan statistics. Table 2 shows the calculated result of the spatial scan statistics and the number of hotspot cells in each time.

Table 2: Result of hotspot detection for each time.

	$\log \lambda(Z)$	Number of hotspot cells	Ratio of hotspots
t=1	137.27	40	0.0087
t=2	183.86	47	0.0103
t=3	310.54	104	0.0227

4.2 Hotspots detection for 5 leading causes of death of Korea

We detect the candidate of hotspots for the 5 leading causes of death among the 16 counties of Korea in 2001. It is collected to promote national prosperity and to formulate the policy for health by Korea National Statistical Office in 2001. The mortality statistics were compiled in accordance with the World Health Organization (WHO) regulations, which specify that member nations classify causes of death. The 5 leading causes of death of Korea in 2001 are shown in Table 3.

(1) Malignant diseases (i.e. Cancer)
(2) Cerebrobascular diseases
(3) Diseases of heart
(4) Diabetes mellitus
(5) Chronic lower respiratory diseases

Thus we shall limit ourselves to these 5 leading causes in this study. We calculate the standardized mortality ratio (SMR) as a common intensity measurement and then apply the principal component analysis (PCA). We detect hotspots on the first principal component (PCA). Eigen values and vectors of PCA are shown in Table 4.

As the coefficients of the first component are all positive, it can be interpreted as an overall measure of the five variables. The echelon dendrogram using the score of the first component is shown in the left side of Figure 6. We calculate the spatial scan statistics according to Poisson model by aggregating regions for the echelon from the upper county in each peaks. The area Z with the maximum log $\lambda(Z)$ becomes the candidates of hotspots. The result of hotspots for the PC1 are six counties (Busan, Ulsan, Gyeongnam, Gyeongbuk, Daegu and Jeonnam) in the first peak, where the spatial statistics $\lambda(Z)$

=1255.26. Using the spatial scan statistics, we can detect the candidates of hotspots which take maximum likelihood. We can also detect various shapes of hotspots. The second component represents a contrast between habitual disease (Heart diseases and Diabetes mellitus: positive sign) and the remaining variables (Cancer, Cerebrovascular diseases and Chronic lower respiratory diseases ; negative sign). Thus the habitual disease in PC2 can be interpreted as the main cause of death. In similar manner, the hotspots for PC2 turned out Seoul and Gyeonggi in the second peak, where the spatial statistics $\lambda(Z)$ =319.51 in the right side of Figure 6.

Table 3: The 5 leading causes of death of Korea in 2001.

counties	Total population	Cancer	Cerebrovascular diseases	Diseases of hearts	Diabetes mellitus	Chronic lower respiratory
Seoul	10263336	10077	5573	2823	1911	1139
Busan	3770536	4789	2853	1916	1000	688
Daegu	2525109	2903	1634	718	586	416
Incheon	2564598	2629	1813	724	518	373
Gwangju	1383765	1389	661	325	292	174
Daejeon	1403164	1370	868	352	250	217
Ulsan	1055618	915	557	281	209	167
Gyeonggi	9544494	9408	5953	2747	1870	1424
Gangwon	1552407	2274	1573	633	468	389
Chungbuk	1496520	2241	1511	466	373	365
Chungnam	1918137	3230	1981	740	553	514
Jeonbuk	2006454	3179	1979	692	570	552
Jeonnam	2099308	3953	1943	997	828	778
Gyeongbuk	2784704	4973	3329	1296	1005	992
Gyeongnam	3106502	4902	2735	1369	848	822
Jeju	546889	624	331	172	98	91

Table 4: Eigen values and vectors of PCA.

	I	II	III	IV	V
Cancer	0.4396	-0.5579	-0.2744	-0.4609	0.4559
Cerebrovascular diseases	0.4212	-0.1571	0.8764	0.1515	0.0824
Diseases of hearts	0.4156	0.6428	0.0400	-0.6086	-0.2053
Diabetes mellitus	0.4599	0.4085	-0.2898	0.5714	0.4596
Chronic lower respiratory	0.4951	-0.2900	-0.2664	0.2604	-0.7294
Eigen values	3.2463	0.7269	0.5166	0.3556	0.1547
Cumulative contribution ratio	0.6493	0.7946	0.8980	0.9691	1.0000

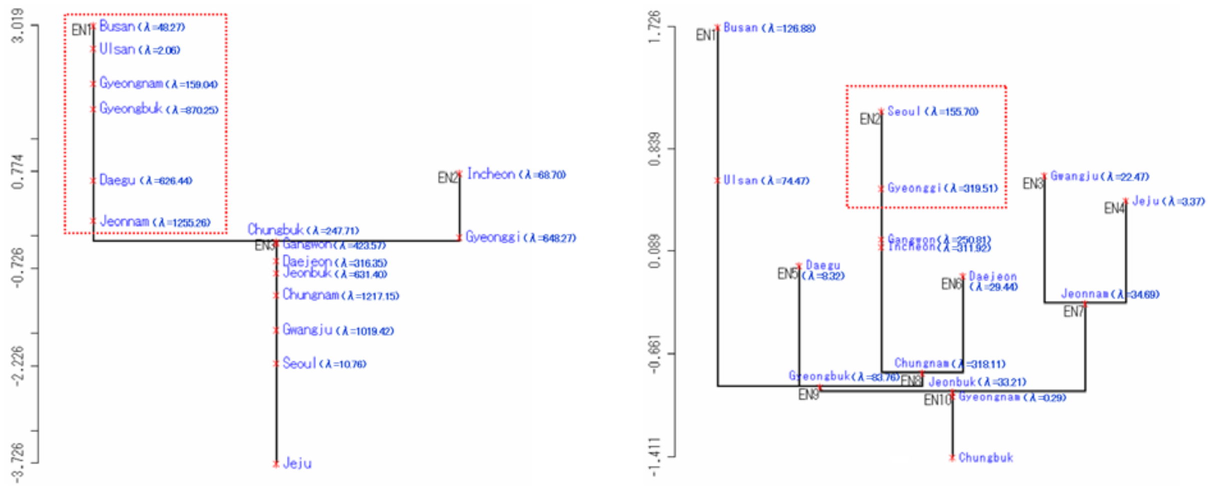

Figure 6: Echelon dendrogram of PC1(left) and PC2(right).

5. Conclusion

It is important to investigate the areas of significant risk (hotspots) about the effect on the human health status to make early warning for infectious diseases and so on. We can easily find the candidates of hotspots for any types of spatial data based on spatial scan statistics and echelon spatial hierarchical structure.

References

Anselin, L. (1995). Local indicators of spatial association-LISA., *Geographic Analysis*, 27, 93-115.

Ishioka, F., Kurihara, K., Suito, H., Horikawa, Y. and Ono Y. (2007). Detection of hotspots for three-dimensional spatial data and its application to environmental pollution. *Journal of Environmental Science for Sustainable Society*, 1, 15-24.

Kulldorff, M. (1997). A spatial scan statistics. *Communications in Statistics*, *Theory and Methods*, 26, 1481-1496.

Kurihara, K. (2004). Classification of geospatial lattice data and their graphical Representation. *Classification, Clustering, and Data Mining Applications* (Edited by D. Banks et al.), Springer, 251-258.

Kurihara, K., Myers, W.L. and Patil, G.P. (2000). Echelon analysis of the relationship between population and land cover patterns based on remote sensing data. *Community Ecology*, 1, 103-122.

Kurihara, K., Ishioka, F. and Moon, S. (2006). Detection of Hotspots on Spatial Data by Using Principal Component Analysis. *Journal of the Korean Data Analysis Society*, 8(2), 447-458.

Myers, W. L., Patil, G. P. and Joly, K. (1997). Echelon approach to areas of concern in synoptic regional monitoring. *Environmental and Ecological Statistics*, 4, 131-152.

Myers, W. L., Kurihara, K., Patil, G. P. and Vraney, R. (2006). Finding upper level sets in cellular surface data using echelons and SaTScan. *Environmental and Ecological Statistics*, 13(4), 379-390.

Tomita, M., Hatsumichi, M. and Kurihara, K. (2008). Identify LD blocks based on hierarchical spatial data. *Computational Statistics & Data Analysis*, 52(4), 1806-1820.

The Problem of Biodiversity

Axel G. Rossberg
Queen's University Belfast

September 1, 2008

Abstract

After pointing out the severity of current biodiversity loss, I argue that the lack of an appropriate theory of biodiversity is one of the main obstacles standing in the way of an appropriate response. Reasons for this lack are investigated, followed by the discussion of a promising route towards building a theory of biodiversity.

1 The Great Collapse

Have you ever wondered what it would have been like to live during one of the great mass extinctions on earth? Well, just look around you. It is happening again. Right now [1].

According to the synthesis report on biodiversity by the Millennium Ecosystem Assessment [2], current extinction rates are 100 to 1000 times higher than they were throughout paleontological times, where extinctions and the creation of new species were in balance. Projections see this figure increase to about 10.000 to 100.000 over the next fifty years [2]. When looking at particular, well-studied groups of species and applying the IUCN-World Conservation Union criteria for threats of extinction, it is found that [2, 3] "some 12% of birds, 25% of mammals, and at least 32% of amphibians are threatened with extinction over the next century." By another account [4], there are about 50-150 species lost every day. About one every fifteen minutes. Seriously.

The reasons for this catastrophic collapse of biodiversity (I shall here focus on diversity in terms of the number of species) are well known. Among the main environmental pressures are the loss of natural habitats to human use; the inability of native species to compete with invasive alien species introduced by humans or the complete re-organization of ecosystems by invasive species, anthropogenic climate change, and over-harvesting. It has been estimated that [3] "90% of the total weight of large predators of the ocean such as tuna, swordfish, and sharks has disappeared in modern times.[...] In some sea areas, the total weight of fish available to be captured is less than a hundredth of that caught before the onset of industrial fishing." Further pressures on the world's ecosystems result from the fact 40% to 50% of the fresh water running off the land is used by humans, who instead doubled the production of biologically usable nitrogen compared to natural levels, further upsetting the balance of nature [2].

2 So what?

While the Millennium Ecosystems Assessment does an excellent job in summarizing the difficult scientific work that has led to our current understanding of biodiversity loss and making it accessible to the public (and one would wish more people read it), it also reveals our poor understanding of the consequences of all this. Why should we worry?

The Assessment's main line of the argument refers to the value of services provided by ecosystems to humans. These are services such as the provisions of clean air and water; regulation and stabilization of the environmental; production of food, fiber, and fuel; and recreational, aesthetic and ethic values. But do we really need all of the estimated 5 million to 30 million species on earth to profit from these services? Ethical considerations aside, wouldn't we be just as well off with only half of the estimated eight million species of insects, centipedes and millipedes? Or only a thousands of them? It is well known that most species on earth are rare, having population densities of only a hundredth or a thousands of those few, dominant species that we are all familiar with (a phenomenon which is by itself not well understood [5]). It is not obvious what all the rare species are good for. In fact, while it is stressed that even on plain economic grounds more must be done to protect nature, the Assessment concedes that [2] "the total amount of biodiversity that would be conserved based strictly on utilitarian considerations is likely to be less than the amount present today (medium certainty)."

Yet, there are several ways in which each and every species could have its role in the working of nature and its value to us; and each of these has, to some extent, been demonstrated empirically. (1) Ecosystems seem to "function" the better the more species they contain [6]. The "function" most often considered in experiments, however, is simply production of biomass, and the effect seems to scale with the logarithm of the number of species, thus rapidly becoming weaker as the number of species increases. Furthermore, most systems investigated had a rather simple structure, consisting, for example, only of plants. (2) Rare species may serve as an "insurance" [7]. In the case that environmental conditions change such that one of the dominating species cannot maintain its population and its role in the system, one of the rare species could take over in a diverse system. (3) Rare species might be filling small ecological "niches" left open by the dominant species, and thus closing the ecosystems up against the invasion of alien species. [8] (4) Each species, rare or abundant, might carry in its genome or by its phenotype, some information useful for technical or medical applications.

The reason why we are currently unable to make a better case out of these considerations, in particular of (1) to (3), is the complexity of real ecosystems. The body of empirical results is not without contradictions. What is found for one system is not found for another one. Setting experiments up slightly differently or asking slightly different questions, one often gets different answers [6, 8].

3 A theory of biodiversity?

A theory that would organize the accumulated empirical data regarding the role of biodiversity, that would explain under which conditions what kind of outcome of impoverished biodiversity must be expected, is missing. We are therefore unable to extrapolate the empirical findings to the relevant scales of space, time and species number, and to the actual functional and trophic complexity of ecosystems, as would be necessary to assess their implications for us, humans. This lack of understanding of the role of biodiversity in nature is a direct consequence of our poor understanding of the *structure* of biodiversity. While there is plenty of data revealing consistent patterns in the relationships between the numbers of species and their abundances, their sizes, their phylogenetic groupings, their trophic levels, the size of areas studies and its geographic latitude, as well as dependencies on the size, age, and degree of isolation of the ecosystems they live in, a coherent theory that would make sense of much of this data is missing. Lack of such a theory of biodiversity, and the ensuing inability to put experiments on the role of biodiversity into context, are, I believe, at the core of the current problem of biodiversity.

Without a strong underlying theory, the debate on merits and necessity of biodiversity conservation will fall prey to selective readings and interpretations of disparate data by stakeholders, much as we have experienced it in the debate on global warming until recently. The question is, however, if such a theory can be found, and if it was found, if we would hear about it. Even 13 years after John Lawton's inspiring essay on the question of ecological theory [9] the WIWACS (World Is Infinitely Wonderful And Complex School), which holds that ecology is theory resistant, has still many followers. Even worse, it is by now standard to sell the observation of a correlation between two quantities as a "prediction" or "explanation", as if this was all we could hope for. Rightfully appalled by a tradition of theoretical ecology (allegedly going back to G. E. Hutchinson [10]) by which models may be unrealistically simple or even wrong, if only they are thought provoking, and by the habit of theorists to argue for their models by "plausibility" rather than their ability to reproduce observations, any ecological theory today is met with scepticism. Theoretical ecologist are regularly forced to hide the essence of their work, their models and derivations, in appendices, of which some aren't even printed. As a result, it is unclear what exactly is said; concepts and predictions remain fuzzy, only adding to the confusion. If somebody came forward with a general theory of biodiversity today, which would necessarily be of some mathematical complexity, chances are slim that any ecological journal would publish it. Even with his comparatively simple neutral theory, S. P. Hubbell's initially met stiff resistance, which he eventually evaded by publishing it as a book [11]. But how far are we really from understanding biodiversity at its basis?

4 Yes, we can (understand biodiversity)!

Selfishly, I may here advertise the Population Dynamical Matching Model—described in an online appendix [12]—as an example for the degree of realism that has now been reach in modeling biodiversity in complex, multitrophic communities. After some struggle with reviewers and editors, we were at least able to smuggle a detailed characterization of the model steady state into an article otherwise concerned with one particular model application [13].

The model describes the population dynamics and evolution of species interacting in a food web. Basically, each species is characterized by its total biomass, which is determined by population dynamics, and the mean body mass of individuals, which varies over 15 orders of magnitude, plus ten other abstract evolving traits, which together determine the trophic interaction structure. The set of species in a community evolves by invasions, speciations, and extinctions. Thus, we have a characterization of communities in terms of body sizes, biomasses (or abundances), and a trophic interaction structure. Jonsson et. al [14] suggested to break down the discussion of community structure by first considering each of these three aspects separately, then combinations in pairs, and finally considering the structure as a whole. To make a long story short: on each of these levels of description the model reaches semi-quantitative agreement with empirical data for pelagic aquatic communities [13].

Body sizes of species are distributed fairly evenly over 14 orders of magnitude, with somewhat more small than large species and the distribution dropping off sharply at about $10\,\mathrm{kg}$. The distribution has a slight dip about $0.1\,\mathrm{g}$, corresponding to the frequently observed gap in size distributions between fish and zooplankton. Only primary producers are unrealistically squeezed into a single size class. *Biomasses* of species—or abundances within a give size class—are distributed approximately log-normally, spreading over about three orders of magnitude, consistent with typical empirical data. *Food web topology* reproduces that of empirical data sets by 13 different measures. The *distribution of species over trophic levels*, with higher trophic levels becoming less sharp and less diverse, agrees with empirical data as well. The *exponent relating body size to abundance* is approximately -1 in agreement with observations. And, finally, the *ordering of species by trophic level* follows largely that by size and abundance (top predators are large and rare), but some deviations are found, as is the case in nature.

Thus, apart from aspects related to spacial distribution, the mapping of the structure of biodiversity onto a mechanistic model has here largely been successful. We are now working on an analysis of the mechanisms generating this structure by an inspection of the Population Dynamical Matching Model and simplified model variants. Since the model displays all structural features listed above at the same time, we can expect that the explanations found for each of these features will be consistent with each other, a point which is not generally clear for simpler models [5].

With a good understanding and further verification of model structure and dynamics, we will then be able to address, in a reliable form, specific questions regarding the role of biodiversity for ecosystem functioning and utility.

References

[1] Eldredge N (2001). The sixth extinction. Accessed Sep 2008.

[2] Millennium Ecosystem Assessment (2005) Ecosystems and Human Well-being: Biodiversity Synthesis. Washington, DC: Island Press.

[3] Millennium Ecosystem Assessment (2005) Ecosystems and Human Well-being: Synthesis. Washington, DC: Island Press.

[4] Sepkoski J (1997) Biodiversity: past, present, and future. J Paleontol 71:533.

[5] McGill BJ, Etienne RS, Gray JS, Alonso D, Marti J Anderson HKB, et al. (2007) Species abundance distributions: moving beyond single prediction theories to integration within an ecological framework. Ecology Letters 10:995–1015.

[6] Hooper DU, III FSC, Ewel JJ, Hector A, Inchausti P, et al. (2005) Effects of biodiversity on ecosystem functioning: a consensus of current knowledge. Ecol Monog 75:3–35.

[7] Yachi S, Loreau M (1999) Biodiversity and ecosystem productivity in a fluctuating environment: The insurance hypothesis. Ecology 96:1463–1468.

[8] Stachowicz JJ, Fried H, Osman RW, Whitlatch RB (2002) Biodiversity, invasion resistance, and marine ecosystem function: Reconciling pattern and process. Ecology 83:2575–2590.

[9] Lawton J (1995) Webbing and WIWACS. OIKOS 72:305–306.

[10] Justus J (2008). Emergence of the stability-diversity-complexity debate of community ecology. At annual meeting of the Ecological Society of America, Milwaukee.

[11] Hubbell SP (2001) The Unified Neutral Theory of Biodiversity and Biogeography. Princeton, NJ: Princeton University Press.

[12] Rossberg AG, Ishii R, Amemiya T, Itoh K (2008). The top-down mechanism for body-mass–abundance scaling – Appendix A: Model details. `http://www.esapubs.org/archive/ecol/E089/031/appendix-A.pdf`.

[13] Rossberg AG, Ishii R, Amemiya T, Itoh K (2008) The top-down mechanism for body-mass–abundance scaling. Ecology 89:567–580.

[14] Jonsson T, Cohen JE, Carpenter SR (2005) Food webs, body size, and species abundance in ecological community description. Adv Ecol Res 36:1–84.

Will Statistics Give the Sensitivity of the Global Climate System?

Kiminori Itoh
Graduate School of Engineering, Yokohama National University
79-7 Tokiwadai, Hodogaya-ku, Yokohama 240-8501, Japan.

Abstract. I discuss here mathematical analyses associated with the estimation of climate sensitivity (λ), a fundamental property of our climate system. Despite its importance, however, a large gap exists between model-based and observation-based values of λ. Statistics seems to be effective to characterize λ although a further progress is necessary.

1. What is the climate?

"The climate" can be regarded as a system consisting of the atmosphere, oceans, land, and cryosphere while the conventional definition of climate is "long-term weather statistics" [1]. The state of each subsystem of the climate system is represented by characteristic state variables. For instance, the state of the atmosphere can be described by the variables such as temperature, humidity, clouds, winds, precipitation, trace gases and aerosol distribution. In a similar manner, the state of the ocean can be represented by temperature, salinity, currents, and marine biota.

"Externals" of the climate system will affect the states of the climate; primarily important externals are the sun, volcanic emissions, anthropogenic emission of greenhouse gases, and changes in the land-use.

Although the strongest greenhouse gas is water vapor, the most famous greenhouse gas is carbon dioxide because its extensive release from human activity is thought to increase the global temperature and to cause climate changes.

2. Radiative forcing and climate sensitivity

The greenhouse gases trap heat (infrared radiation) emitted from the earth surfaces, and finally increase the temperature. This function is approximated as TOA (Top of the Atmosphere) radiative forcing, RF. For instance, the RF corresponding to the increase in carbon dioxide concentration during the past 250 years (from 280 ppm to 370 ppm) is around 1.5 W/m^2. That is, a heat source of this magnitude is placed at the TOA (tropopause, in reality) to express the radiative effect of the CO_2 increase. For some aerosols, RF is large negative; that is, they have a cooling effect although the value of RF's are not accurately estimated.

It is usually assumed that RF's from different sources can be added to give total RF. The coefficient connecting the total RF (ΔRF) and the change in temperature (ΔT) is the climate sensitivity (λ) as Eq. 1 shows.

$$\Delta T = \lambda \Delta RF \qquad (1)$$

Sometimes, depending on authors, λ^{-1} is used instead of λ as the definition of the climate sensitivity.

3. Feedback in the climate system.

When RF is given to the climate system, the system will respond. The most basic response of the climate system is to attain the thermal equilibrium between solar radiation (mostly visible light) absorbed by the earth surface and infrared radiation from the atmosphere to the space. Besides this, changes in the climate system associated with the addition of different kinds of RF's are important. For instance, the doubling of carbon dioxide concentration gives a temperature increase of 1-1.5 ℃ after the system reached a new thermal equilibrium state. This increase in temperature would increase the amount of water vapor (due to evaporation) in the atmosphere to give another temperature increase. Thus, in this case, positive feedback has taken place. On the other hand, when the water vapor is converted into cloud, reflection of sun light will increase to give a decrease in temperature; this is negative feedback. These mechanisms are called water vapor-cloud feedback, which largely affect the magnitude of λ in Eq. 1.

4. Estimation of the climate sensitivity

Until recently, the values of λ had been estimated mainly by model-based computer simulations because observation-based estimation was difficult. Typical values are 0.54 ～ 1.22 K/W m^{-2}, which give 2.0 ～ 4.5 ℃ (central value, 3.0 ℃) for the doubling of carbon dioxide.

However, thanks to the development of global observations (e.g., satellite-based temperature measurements), it is now becoming to be able to estimate λ "experimentally" (that is, estimation based on observations). Table 1 shows those values in the form of ΔT at doubled CO_2, together with some information including methods employed.

Table 1. Recent observation-based $\Delta T2\times CO_2$

1. Forster & Gregory, J. Climate, 2006
   *Energy budget from satellite data
   1.0 ～ 4.1℃ Central value **1.6℃**
2. Schwartz, J. Geophys. Res., Nov. 2007
   *Based on oceanic heat capacity, and time constant of temperature changes
   0.6 ～ 1.6℃ Central value **1.1℃**
3. Chylek et al., J. Geophys. Res., Dec. 2007
   *Insolation change due to aerosol, and heat transfer to ocean
   0.9～1.8℃ Central value **1.3℃**

4.1. Forster & Gregory's work

Their work [2] is epochal in a sense that it showed effectiveness of observation-based measurements of λ. They followed the definition of λ to estimate its value. They utilize the energy budget (shortwave input minus longwave output) and global temperature variations observed with satellites. Figure 1 shows their typical result; the vertical axis (Q-N) denotes the energy budget, and the horizontal axis (DT) the global temperature change. From the slope, they obtained λ. Their result that the central value for λ is 1.6 K/Wm^{-2} is surprising because it is only about half that based on the models. They suggested other important points as well; only one model out of ten IPCC (International Pannell on Climate Change) AR4 models fitted their results on the radiation from clouds. Moreover, they claim that the standard approach using volcano eruptions for testing climate models is not adequate.

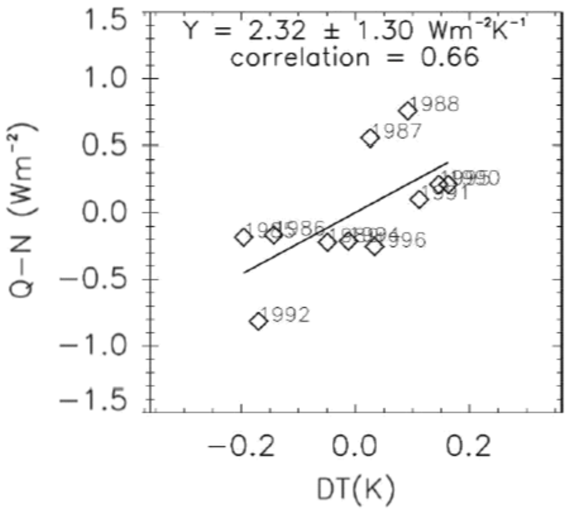

Fig. 1. Relation between energy budget and temperature changes observed by satellites (from Forster & Gregory, 2006).

4.2. Schwartz's work.

Schwartz [3] employed statistical approach, so that I describe his results a little in detail here. His idea is based on Eq. 2, where the solar radiation Q and the earth radiation E are considered.

$$dH/dt = C\, dT_S/dt = Q - E. \qquad (2)$$

Here, H is the heat content in the climate system, C the effective heat capacity of the climate system, and T_S the global and annual mean surface temperature. Q is expressed as γJ where γ is planetary coalbedo (= 1 – albedo: where albedo stands for whiteness or reflectance) and J is a quarter the solar constant. By considering Stefan-Boltzmann relation, $E = \varepsilon\sigma T_S^4$, Eq. 3 is obtained.

$$C\, dT_S/dt = \gamma J - \varepsilon\sigma T_S^4 \qquad (3)$$

For small perturbations (step-function radiation forcing, in particular), Eqs.4 and 5 are assumed.

$$F = Q - E \qquad (4)$$

$$T_S = T_{S,0} + \Delta T_S \tag{5}$$

Thus, Eqs. 6 and 7 hold.

$$\Delta T_S(t) = \Delta T_S(\infty)\,(1 - e^{-t/\tau}) \tag{6}$$
$$\Delta T_S(\infty) = F/(4\,\varepsilon\sigma T_S^3) = \lambda F \tag{7}$$

For τ and λ, Eqs. 8 and 9 are obtained.

$$\tau = \quad C/(4\,\varepsilon\sigma T_S^3) = C\,T_{S,0}\,/(\gamma J) \tag{8}$$
$$\lambda = T_{S,0}\,/(\gamma J) \tag{9}$$

From Eqs. 8 and 9, λ is obtained as Eq. 10.

$$\lambda = \tau\,/\,C \tag{10}$$

Thus, the climate sensitivity can be obtained from the heat capacity of the climate system and the response time constant of the climate system against the change in RF.

Schwartz estimated the heat capacity C from the measurements of ocean heat content and the global surface temperature observed during recent 40 years as shown in Fig. 2. His result was $C = 16.7 \pm 7.0$ W yr m^{-2} K^{-1}, which corresponds to ca. 100 m of the ocean layer. The heat content down to the depth of 3000 m was not very different from other depths; this shows inhomogeneous heating of the oceans. Moreover, the heat content largely fluctuates due to unknown processes.

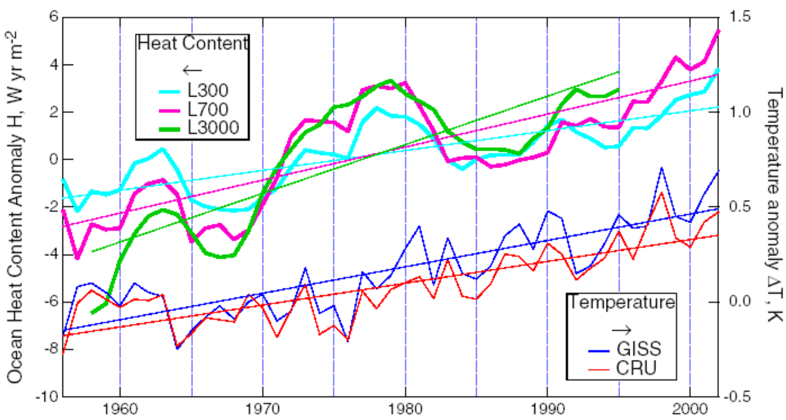

Fig. 2. Estimation of effective heat capacity from the ocean heat content and global mean temperature. From Schwartz 2007.

The response time was estimated from autocorrelation of the global mean temperature anomaly data as shown in Fig. 3. The top figure is the original temperature anomaly data, the middle (normalized residual) is obtained by removing trend, and the bottom is the autocorrelation (r) of the residual data with lag Δt.

Schwartz assumes a first-order Markov process, and approximates that r decays exponentially. From this assumption, the time constant is estimated by calculating the slope of ln r versus t. Thus, he obtained 5 ± 1 yr as the asymptotic value of τ.

From the values of C and τ, using eq. 10, the value of λ is obtained as follows.

$$\lambda = \tau/C = 0.30 \pm 0.14\ \mathrm{K/(W\ m^{-2})} \quad (11)$$

Corresponding ΔT for doubled CO_2 concentration is,

$$\Delta T_{2xCO_2} = 1.1 \pm 0.5\ \mathrm{K} \quad (12)$$

There arise several questions on this estimation. The first question is whether the small λ is theoretically reasonable or not. The second question is whether the analysis is reasonable or not.

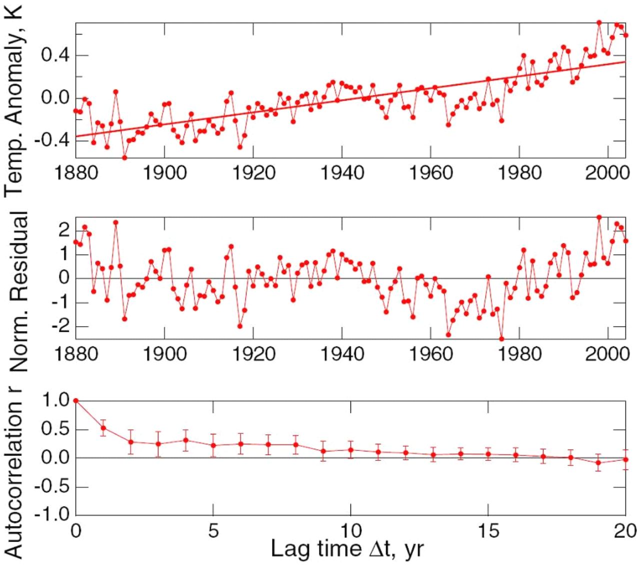

Fig. 3. Top, original temperature data: middle, trend-removed time series: bottom, autocorrelation r with lag Δt. From Schwartz 2007.

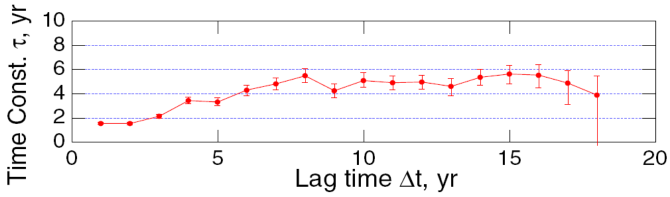

Fig. 4. Time constant obtained from the slope of ln r vs. t. From Schwartz 2007.

On the first point, it is known that most climate models give considerably longer time constants, 20～30 yr, which result in large values of λ. Thus, it is essential whether or not the time constant can be such short from the theoretical point of view. As a conclusion, it is basically possible when the treatment of Dickinson and Schaudt (hereafter, DS 98) [4] is considered. They employed zero-dimensional model to analyze the behavior of time response of the atmosphere-ocean system, and have shown that overall time constant of the system could be much shorter than the time constant of each subsystem. Thus, DS 98 theoretically supports the estimation of Schwartz. Conversely, the estimation Schwartz can be regarded to support the theoretical conclusion of DS98.

On the second point, that is, the analysis of Schwartz might be questionable because it assumes a simple exponential form for the decay of τ, neglecting long memory in the climate system. The strongest reason for this question is, for instance, that the climate system should be multi-exponential at least, and it should have long memory. In fact, DS98 shows the time dependence of their zero-dimensional system is not simple exponential. Moreover, the value of r tends to be negative for long t. It should be noted, however, that the analysis of Schwartz also takes into account that the autocorrelation curve is non-exponential by considering the asymptotic behavior of τ as shown in Fig. 4. Thus, for the first approximation, the assumption of Schwartz seems valid.

5. Statistical analysis of Kärner.

Kärner [5, 6] has employed the analysis of increments in the temperature time series data, instead of the temperature itself. This is because the temperature is often non-stational; that is, its time-mean is not constant. In fact, Schwartz has removed the time trend from the temperature data in his analysis. Kärner has shown that the increments of the temperature time series have rather stable distribution, and hence, show persistency [5].

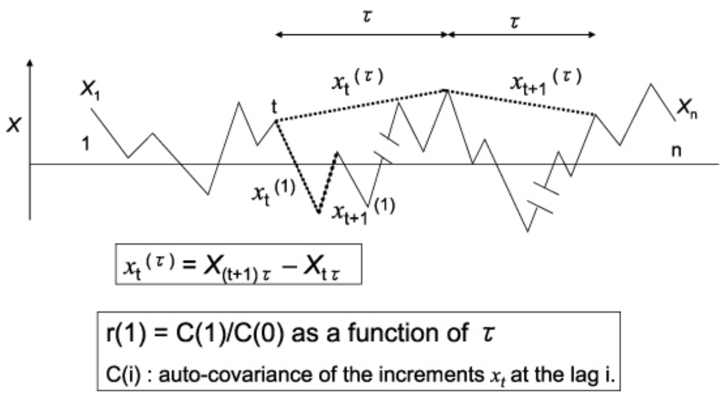

Fig. 5. Estimating autocorrelation of increments with different ranges. From Kärner 2005.

According to his idea, the autocorrelation of the increments will reflect the property of feedback mechanisms in the system [6]. When the autocorrelation is positive, there is a tendency that increments continue to have the same sign, and hence, positive feedback prevails. Conversely, for the negative autocorrelation, the feedback in the system should be negative.

Figure 5 explains the procedure for estimating autocorrelation between increments with different ranges. The discrete time series X_t has n members. Increments $x_t^{(\tau)}$ are calculated for different range of steps τ, and then, auto-covariance is obtained with changing lag. The quantity r(1) (C(1) normalized by C(0)) in Fig. 5 shows, according to its definition, relation between the increments. In particular, based on Kärner's idea, it represents the feedback in the system.

The temperature data measured by the satellites were employed in his analysis because they cover the whole earth except a small area of the polar regions.

Figure 6 shows typical data for the monthly temperature anomaly observed by satellites (measured with microwave sounding units); Kärner used daily data also, although not shown in the Fig. 6 for the sake of simplicity.

In addition, the positive peaks at 1983 and at 1992 for the stratosphere temperature are the result of large volcanic eruptions, which induced temperature decreases in the troposphere. The positive peak at 1998 for the troposphere is due to a large El Niño.

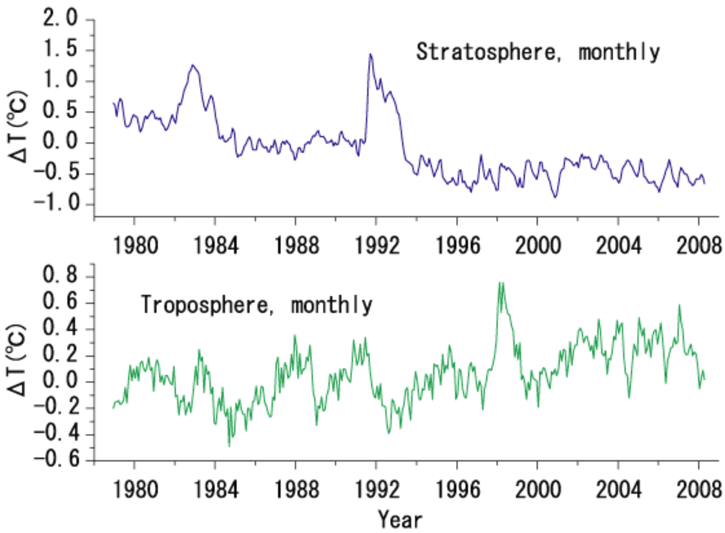

Fig. 6. Monthly temperature anomaly data for stratosphere (top) and troposphere (bottom). From http://www.nsstc.uah.edu/data/msu/

Figure 7 shows the correlation r(1) of increments of each temperature data (stratosphere, troposphere and solar radiation) as a function of increment range.

For the troposphere and the solar radiation, r(1) is mostly negative except for short increment range (several days). On the other hand, r(1) for the stratosphere takes positive values for the increment range up to around 50 days. According to Kärner's discussion, this shows that feedback in the troposphere is largely negative.

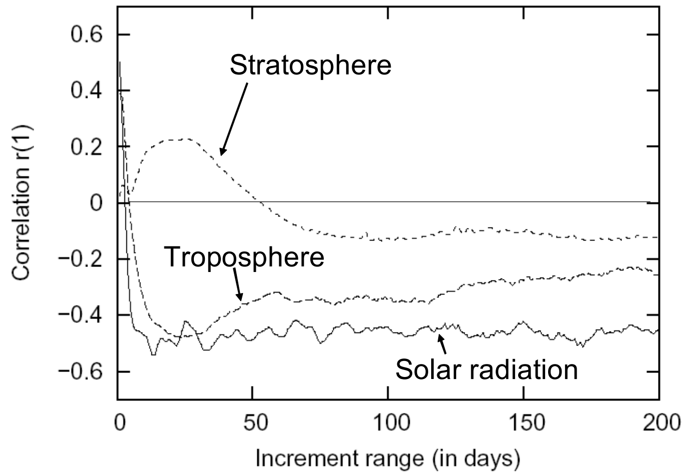

Fig. 7. Correlation of increments of temperature data (Kärner 2005) for stratosphere, troposphere and solar radiation.

6. Origin of negative feedback.

A question, then, arises; what is the origin of the negative feedback climate in the troposphere? Kärner considers different possibilities; e.g., the negative feedback of the solar radiation directly determines the sign of feedback in the troposphere. He even suggests that day-and-night cycle itself might induce the negative feedback.

It is, however, necessary to consider the origin of the negative feedback from more physical point of view if possible.

Spencer et al. discussed how tropical clouds respond to changes in surface temperature [7].

They identified 15 temperature oscillations during the period of 2000 – 2005 as shown in fig. 8 A, where averaged temperature change is plotted as a function of time (day) with the temperature peak placed at time zero. They showed that clouds consisting of ice largely decreased during the course of the temperature change (Fig. 8 B). This means that longwave radiation from the earth to the space increases during this period, which suggests a mechanism called "infrared iris," a controversial idea related to negative feedback of the climate system.

Although detailed mechanisms of the feedback as well as exact values of λ are still to be clarified, the negative feedback suggested by Kärner and other researchers thus seems plausible.

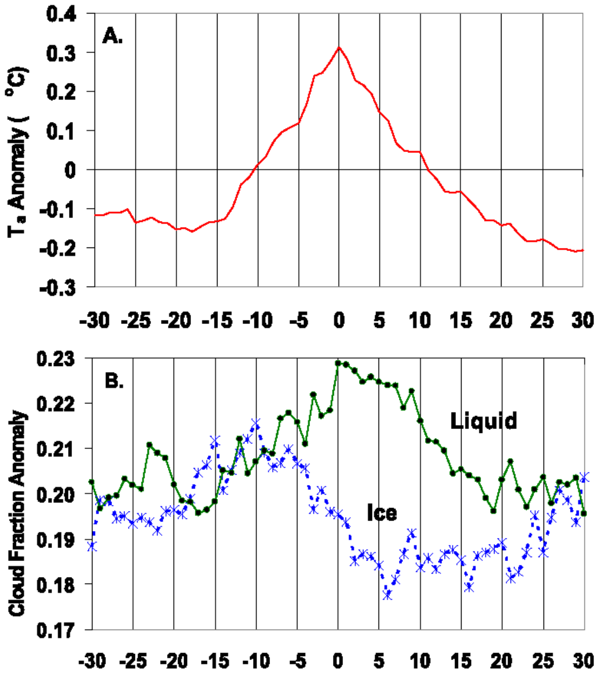

Fig. 8. Temperature changes (A) and cloud changes (B) associated with tropical intraseasonal oscillations. (Spencer et al., 2007)

References.

1) Radiative Forcing of Climate Change, National Research Council (NRC) of the National Academies (2005).

2) P. M. De F. Forster and J. M. Gregory, The Climate Sensitivity and Its Components Diagnosed from Earth Radiation Budget Data, J. Climate, 19 (2006) 39-52

3) S. E. Schwartz, Heat Capacity, Time Constant, and Sensitivity of Earth's Climate System, J. Geophys. Res., VOL. 112, D24S05, doi:10.1029/2007JD008746, 2007

4) Dickinson and Schaudt, Analysis of Timescales of Response of a Simple Climate Models, J. Climate, 11 (1998) 97-106.

5) O. Kärner, On nonstationarity and antipersistency in global temperature series, J. Geophys. Res., Vol. 107, NO. D20, 4415, doi:10.1029/2001JD002024, 2002

6) O. Kärner, Some examples of negative feedback in the Earth climate system, Central European Journal of Physics, 3 (2005) 190–208.

7) R. W. Spencer, W. D. Braswell, J. R. Christy, and J. Hnilo, Cloud and radiation budget changes associated with tropical intraseasonal oscillations, Geophys. Res. Lett., 34, L15707, doi: 0.1029/ 2007GL029698, 2007

River Management for Ecosystem Conservation
- Policy-Making Support through Mathematical Modelling -

Tetsuro TSUJIMOTO

Professor, NHRI, Department of Civil Engineering, Nagoya University
Furo-cho, Chikusa-ku, Nagoya, 464-8603, Japan, e-mail: ttsujimoto@genv.nagoya-u.ac.jp

ABSTRACT

Human activity is developed on a river basin, which is a unit of hydrological cycle of the surface of a globe, In a river basin, rainfall is converted to flow regime in a river. Not only water but also various materials are transported along a river, and they support various organisms. Our activity is closely related to these processes and river basin management is a key for sustainability of human activity. In particular, management of rivers must be efficient where the above processes are dynamic.

Since the revision of River law in 1997, ecosystem conservation has become one of the objectives of river management, and we have tackled with the research topics how to recognize the mechanism of river ecosystem where it would be described quantitatively and mathematical modelling is one of powerful means.

We regard ecosystem as an interrelating system among (1) physical basement, (2) material cycles focusing on the bioelements and (3) biological aspects, and mathematical models to describe respective subsystems are developed in addition the interactions among subsystems. This paper introduces the framework of mathematical modelling and some examples, where it is able to how we are able to recognize not only degradation of ecosystem by human impacts but also rehabilitation effects by new policies and measures of river management.

Keywords: *River basin management, Ecosystem, Habitat, Biophilic elements cycle, Mathematical modeling*

INTRODUCTION

The discipline of "civil engineering" has a mission to support national land grand design, construction and management which create various functions to sustain human activities, The functions are summarized as disaster prevention, resources development and environment management (against pollution and for ecosystem conservation), and these functions are accomplished by facilities (infrastructure), institutional framework and citizen behaviour. Civil engineering includes such wide aspects. In civil engineering, river engineering is responsible to river-basin management based on hydro-science and engineering (hydrology and hydraulics). National land is divided into many river basins, and water policy is to keep the following functions: flood control, water resources management and river-basin ecosystem conservation.

Figure 1 shows a comparison of river basins between Chubu district in Japan and Boston district in USA by satellite photos, and we can recognize intensive contrasts in Chubu river basin. The climatic and geographic characteristics of Japan bring such contrasts in landscape, and particularly in Japan, we have to take care about the river basin in grand design of our homeland. It implies that recognition of national land is a complex of river basins not a complex of merely administrative divisions.

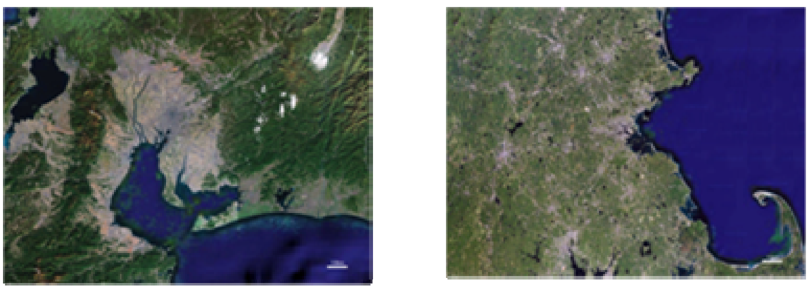

(a) River-basin complex around Ise bay (b) River-basin complex around Boston bay

Fig.1 River basin characteristics

River basin is defined as a catchment in hydrology and/or geography, and it is a pan to receive precipitation where runoff process appears. Runoff implies the conversion from precipitation ($r(t)$=hyetograph) to flow discharge in river system ($Q(t)$=hydrograph), and it is a part of "hydrological cycle" which is constituted by precipitation, runoff and evapo-transpiration. Precipitation and evapo-transpiration sustains the hydrological cycle (water cycle), but between these two processes water travels globally (climatic circulation), but on the global surface a river basin limits the area of the behaviour of water. In this sense, a river basin is a unit of hydrological cycle on the surface of the globe. In a river basin, a conversion from $r(t)$ to $Q(t)$ is the first one when we discuss on mathematical modelling, and it is called "runoff model". In these hundred years, many runoff models have been developed based on modelling physical process and stochastic recognition (impulse response model), and some of them have been useful in policy making process depending on the purpose.

Hydrological cycle in river basin takes a role not only of conveying water but also sediment and various materials including biophilic elements. In transport process of biophilic elements, they change the form: inorganic (nutrients) to organic matters, and they sometimes form biomass. In this sense the hydrological cycle drives even bio-aspects related to various organisms. The word "ecosystem" includes physical basement and material cycles as well as bio-aspects, and it is driven by the hydrological cycle. Thus, a river basin is an assembly of fluxes where a flux implies not only a route but also include transport rate.

From the viewpoint of water policy, water is related to flood control and water resources, sediment is related to debris, erosion-deposition issues and fluvial morphology, and bioelement-transport is concerned with water quality and ecosystem. Thus, river basin management or water cycle management (integrated water resources management) is very important for human activity toward sustainability. However, we have not to forget the above-mentioned functions are most effective in a river as an axis of a river basin, and we can say that river management is efficient and in addition various policy can be applied in river areas most of which is owned by public while most of the other river basin by private. It should be added that river management brings fair polices for various functions: levee and flood-control dam constructions instead of special protection of limited areas, public water resources from river flow instead of limited sources (springs) and groundwater which causes severe ground subsidence. Few people occupying the area protected against flood agree that the owned area is utilized for ecosystem conservation. However, river management is insistently a part of river-basin management.

As for river management, the central government enacted "river law" in 1896 to strengthen the flood control countermeasures, then revised it in 1964 to establish river management for water resources development incorporated to flood control, and then in 1997 revised it again to add river environment in objectives of river management as well as flood control and water resources development.

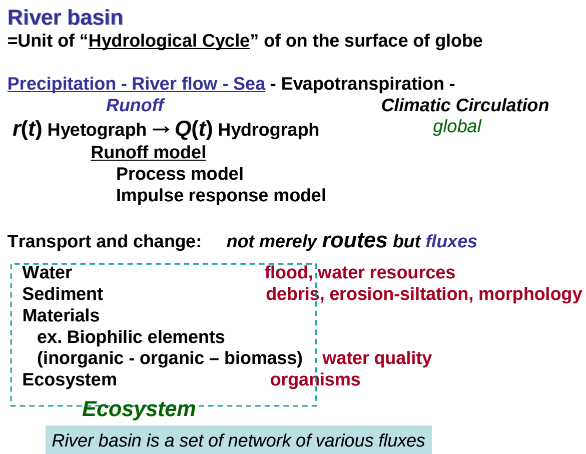

Fig.2 River basin as a unit of water policy

When we discuss a water policy, the following framework, the flow as vision-scenario-design-operation (see Fig.3), is focussed on. This framework should accompany the "accountability" and/or "assessment" which require fairness and transparency. In the visions, we have to clarify the functions necessary for sustainability of human activities. Functions are to be produced by processes in prepared infrastructures with natural system of river basin, and these processes should be reasonably described so that fair explanation how they create the required functions. We may say mathematical modelling is expected to be one of powerful means to keep fairness and transparency.

When we mention the functions, the required levels should be discussed from the social reality. For example, when we say the safety against flood, we set the level such as once 200 years and so on. That is an introduction of the concept of "return period", which needs an assistance of statistical modelling.

Because we often don't have enough datum, we would get a reasonably estimated value. In fact, various techniques have been developed in our fields, academically and practically. The return period concept has been employed when we discuss a designed drought in water resources policy, too. However, we have not proposed any standard for ecosystem yet, because we have not yet well understand ecosystem as a target for national land grand design. Hence, we, river engineers and researchers, started a cooperative study with other disciplines to hydrology and hydraulics such as biology, ecology and limnology. In addition to interdisciplinary cooperative study, river engineer had to make a framework how to recognize the ecosystem, otherwise innumerable information about ecosystem could not be taken into account in policy making.

RIVER ECOSYSTEM

We regard ecosystem as an interrelating system among (A) physical basement, (B) biological aspects, and (C) material cycles focusing on the bioelements such as N, P, C, O, *etc*. (see Fig.4). Subsystem (A) is also an interrelating subsystem among morphology, flow and sediment transport in a river, which is specified as "fluvial hydraulics", and it must not be forgotten that vegetation growth and decay affect the fluvial processes intimately. Subsystem (B) has three different aspects: Growth of individual, population change by breeding and interaction among species represented by "food web" and "species diversity". Subsystem (B) is supported by (A) as habitat, and related to (C) through production-assimilation and metabolism-decomposition. In subsystem (C), materials exist in some forms: inorganic (nutrients) or organic, furthermore in biomass, and they are transported and changed in forms through physical, chemical and biological processes. Transport and changing processes require peculiar morphology and flow dynamics, and in this sense (C) is supported by (A) as similarly as (B) by (A). Summarizing the above, we have three subsystems, which form interrelating systems respectively, and they are interacted one another.

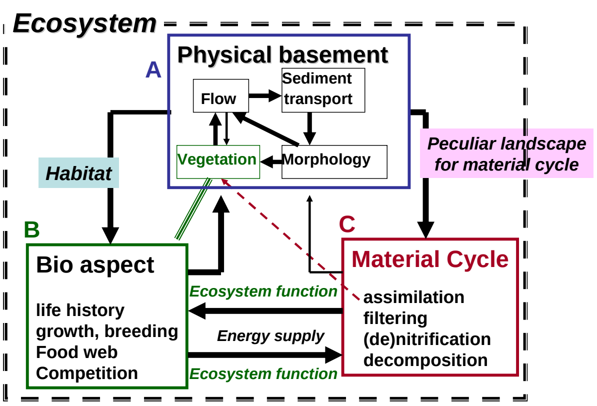

Fig.3 River ecosystem

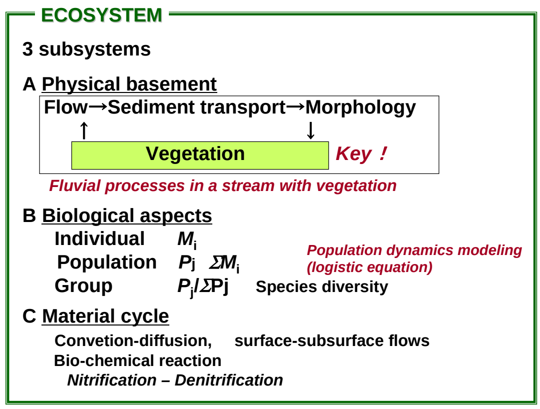

Fig.4 Three subsystems constituting river ecosystem

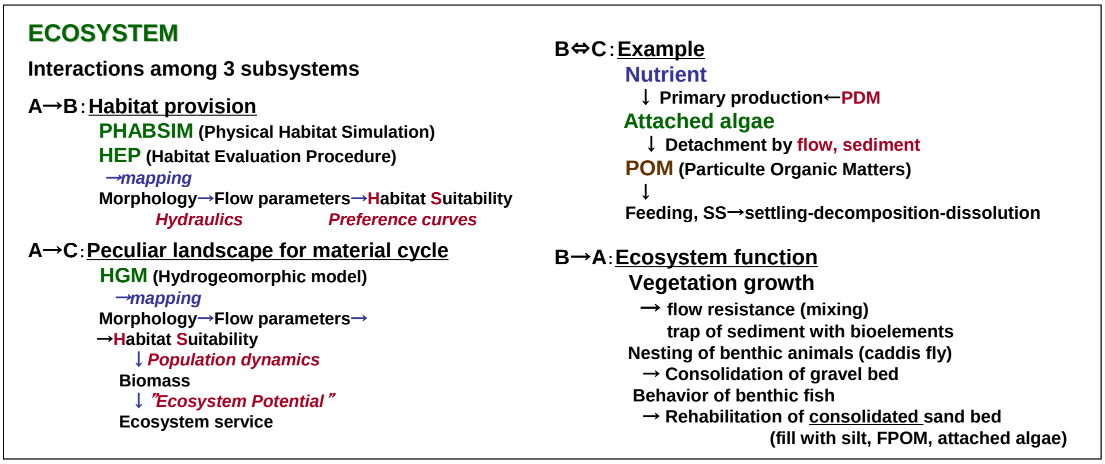

Fig.5 Interactions among 3 subsystems constituting ecosystem

As above-mentioned, we recognize the ecosystem as a complex of three subsystems (see Figs.3 and 4) and the interaction among them (see Fig.5). We should develop mathematical models to describe the respective subsystems: fluvial process, bio-material cycles, and behaviours of organisms; and in addition, we have to develop mathematical models to describe interactions among subsystems: Habitat provision ((A) to (B)), providing specialized landscape elements for peculiar processes in material cycles, changing of bioelements between biomass and non-biomass forms ((B)~(C), and biological actions to change physical process ((B) to (A)). In Fig.4, some interactions are shown. As for habitat suitability, the mathematical modelling was developed as PHABSIM (Physical Habitat Simulation) or HEP (Habitat Evaluation Method). In order to specify the morphology for respective processes in material cycle, HGM (hydro-Geo-Morphological modelling) is available.

Some examples from mathematical modelling for respective aspects will be introduced in the following part of this paper, where model for fluvial processes in streams with vegetation, habitat suitability evaluation and biomass dynamics are introduced based on the recent results from our laboratory. In particular, the author would show how we are able to recognize not only degradation of ecosystem by human impacts but also rehabilitation effects by new policies and measures of river management through applying such mathematical modelling. With suitable habitat and specially prepared site of material cycle, biomass must grow and its aspect can be analyzed by "Population Dynamics Modelling". Bio-aspects sometimes affect the physical basement: Vegetation growth and decay affect the flow resistance, some species of benthic animal brings consolidation of a bed, and behaviour of some species of benthic fish rehabilitates a sand bed degraded by silt deposition or by attached algae.

FLUVIAL PROCESSES IN STREAMS WITH VEGETATION

Physical basement of river ecosystem is subjected to fluvial processes, and proper description of fluvial process affected by riparian vegetation is a key. When a river is discussed, it is important to focus on the hierarchy of landscape in scales: river basin, river from headwater to sea, segment, reach, unit, and sub-unit scales. In particular, river management should be taken into account from upstream to down stream, but segment is an important scale, where physical processes are similar. Classification into mountain river, gravel-bed river (in fluvial fan), sandy river (in alluvial plain) and estuary is particularly significant. The physical processes are under similarity in a segment and it is mainly subjected to the substratum diameter and the stream slope. The detailed characteristics of segment are represented by those of reach which is repeated in a segment. For example, a photo in Fig.6 is a sandy river segment and sand bars appear aternately, and we say that it has such a "structure". When we close up into a unit of reach, a sand bar, we find more detailed morphology, which is sub-unit scale and is often called "texture" (see Fig.7). The "structure" is determined by fluvial process caused by major flood while the "textures" are by usual floods.

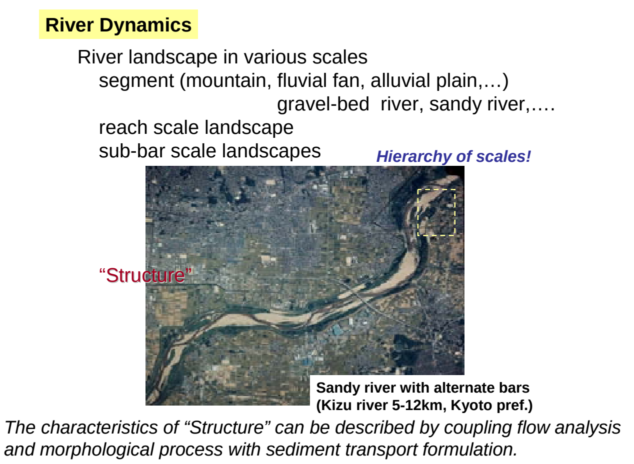

Fig.6 "Structure" in sandy-bed segment

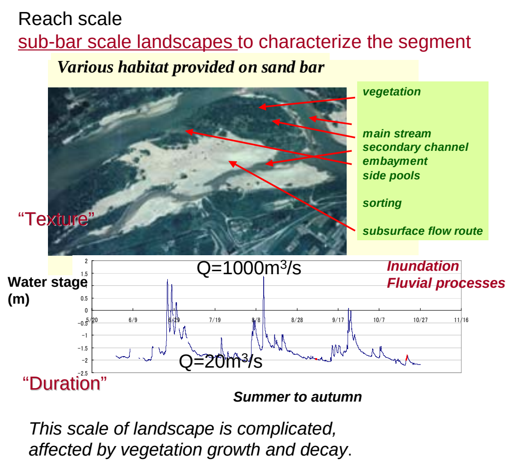

Fig.7 Reach scale characterized by "textures"

The structure can be analyzed by using depth-averaged 2D flow with transport equation of sediment, and in particular numerical simulation techniques have been developed. Fig.8 is an example of numerical simulation of alternate bars evolution, and such rather regular sand bars can be reproduced numerically.

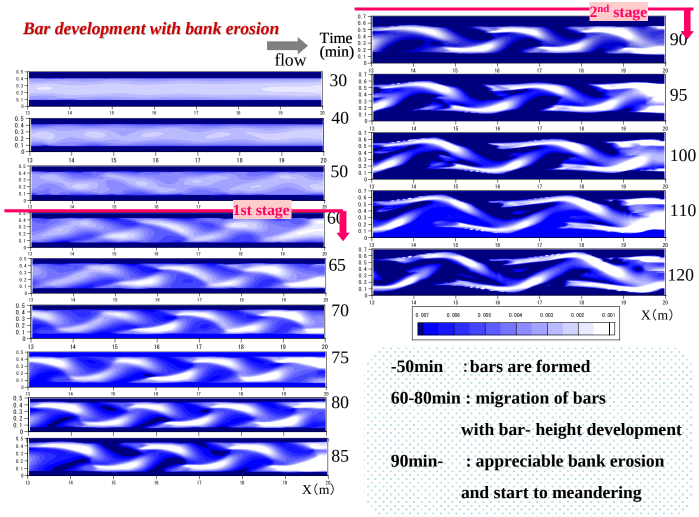

Fig.8 Numerical simulation of evolution process of alternate bars

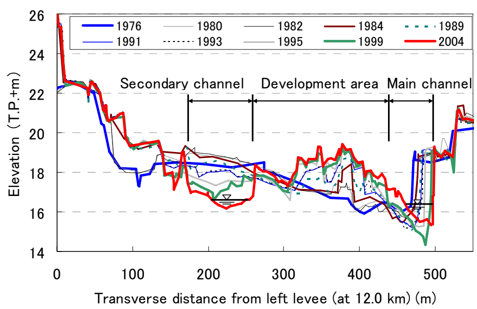

Fig.9 Transition of sand bar geometry affected by vegetation growth

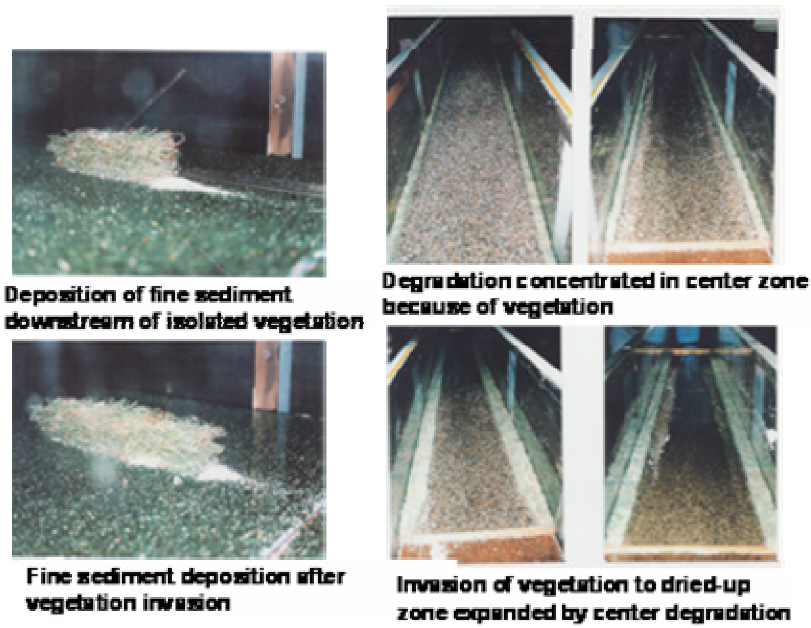

Fig.10 Laboratory experiment for fluvial processes affected by vegetation

Figure 9 shows the transition of bar geometry represented by cross-section survey of actual sand bar, and simple geometry in early 70's have changed to complicated one. The characteristics are formation and development (diversification) of longitudinal ridges with vegetation, which are examples of fluvial processes affected by vegetation growth, and the elementary processes have been checked by laboratory experiments shown in Fig.10. In fundamental laboratory experiments, artificial porous medium was employed instead of real vegetation, and polystyrene particles instead of sand. Such experiments where elementary processes are abstracted have been utilized for process modelling in mathematical calculation (for example, how to describe "vegetated region" and how to assume the location and its enlargement).

An approach to fluvial processes in streams with vegetation was well developed (Tsujimoto, 1999), and various processes governing river-landscape transition have been described mathematically. However, we often require an additional model concerning with vegetation strategy which is related to the subsystem (B) (growth-decay model). For example, Fig.11 shows the enlargement of vegetation-covered area after dam construction, which caused the decrease of magnitude of annual maximum flood discharge. In order to simulate such process, we derived the scenario to represent the strategy of vegetation growth, shown in Fig.12: Vegetation-covered area increases with G% annually, and individual trees grow gradually. While, major floods destructs vegetation without dam control, but minor floods after dam construction cannot destructs vegetation with grown trees.

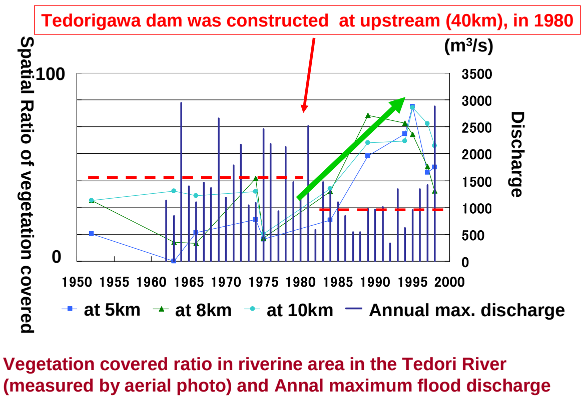

Fig.11 Enlargement of vegetation-covered area after dam construction (Tedori river)

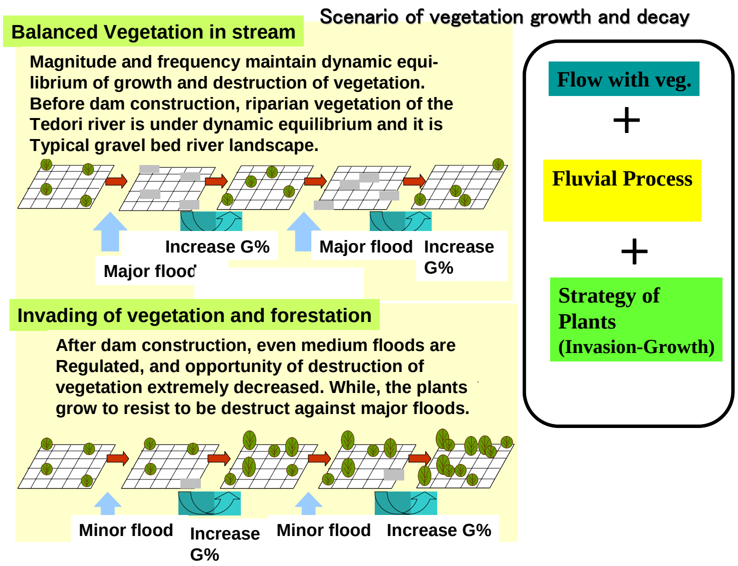

Fig.12 Scenario prepared for description of vegetation growth and decay

BIO-ASPECTS OF ECOSYSTEM

Bio-aspects are also represented by a mathematical model, particularly by the so-called population dynamics model (PDM). Its simple expression is written as follows for biomass of an individual or for population of one species. It often accompanies more terms, and multiple equations are prepared for different species. For example, if a single species is focussed on, its temporal change on biomass per unit area, $M(t)$, can be expressed as follows, for example.

$$M(t) = \mu M_0 \left(1 - \frac{M_{eq}}{M}\right) + D(t)$$

where M_0=initial biomass per unit area, μ=growth rate, M_{eq}=maximum biomass per unit area (environmental capacity); and $D(t)$=loss of biomass (death) due to disturbance, for example; and t=time.

Figure 13 shows an example for growth of attached algae in a gravel river. While, attached algae is detached eventually by bedload transport during flood, and the biomass shows temporal fluctuation (Tsujimoto & Tashiro, 2004).

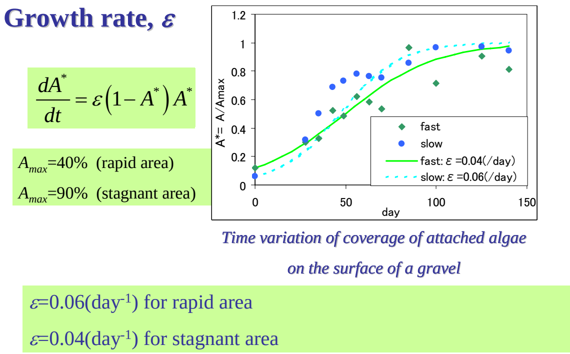

Fig.13 Application of PDM for attached algae

Sometimes the growth of organisms is not so simple. For example, we have developed the growth model of *Flagmites Japonica*, a plant growing on a sand bar, where the condition of supplying water with nutrients is not good. Active uptake during better condition and its storage in their roots are a strategy of those plants, and such a process is described by coupling a usual growth model with SPAC (Soil-Plant-Atmosphere Continuum) model.

HABITAT SUITABILITY ANALYSIS

In order to make a habitat map for a peculiar species of organisms, the preference curves are prepared, which relate the habitat suitability with the physical parameters. In other words, the preference curves are mapping functions to convert the maps of the physical indices to a habitat-suitability map which shows spatial distribution of habitat potential. The preference curve $f_s(\xi_s)$ implies habitat suitability ranging in [0,1] against a physical parameter, ξ_s (s designates one of the physical parameters). Considering multiple parameters, the "composite habitat suitability" Ξ_z is obtained as

$$\Xi_z = \prod_{s=1}^{N}\left[f_s(\xi_s)\right]^{p_s}, \quad \sum_{s=1}^{N} p_s = 1$$

where N=number of physical parameters included in consideration (s=1, 2, …, N); and z designates the landscape elements. The above techniques follow the so-called PHABSIM (Physical Habitat Simulation) or HEP (Habitat Evaluation Procedure).

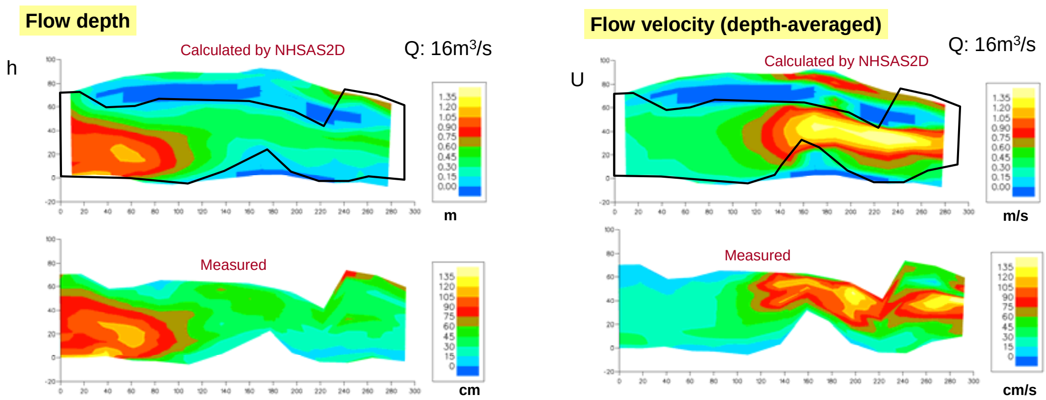

Fig.14 Physical parameters mapping in a reach of a gravel river segment (Yahagi river)

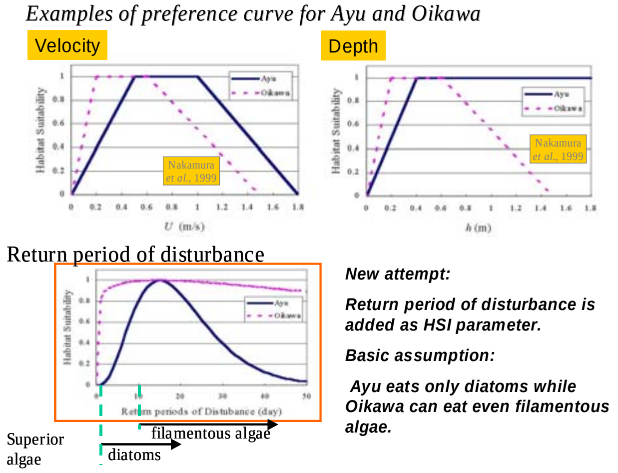

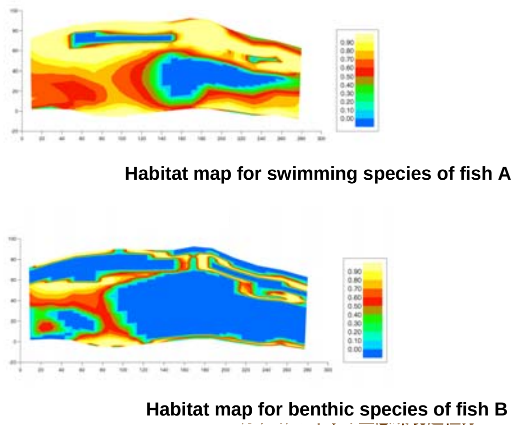

Fig.15 Examples of preference curves for some species of fish

Fig.16 Examples of habitat maps for fish

On discussion of habitat, we have to take care about the “life cycle” of the target organism. For example, an organism requires not only daily habitat but also spawning site, hatchery, nursery, feeding (hunting) site and emergency refuge for floods and/or draught. For example, “temporary waters” such as embayment and side pools provide emergency refuge during flood. Side pools are connected one another by subsurface flow usually, but during flood, they becomes submerged and connected from downstream opening back water area (embayment), and there are tranquil zones even when the upstream entrance breaches at the peak of flood (see Fig.17). Moreover, such temporary waters supply spawning site, hatchery, nursery for some species of fish. Particularly in this segment of the Kizu river, it is utilized by an endangered species, *Acheilognathus longipinnis Regan* (see Fig.18). For the above-mentioned argument, numerical simulation for detailed flow affected by complicated morphology and vegetation should be carried out to confirm the habitat suitability.

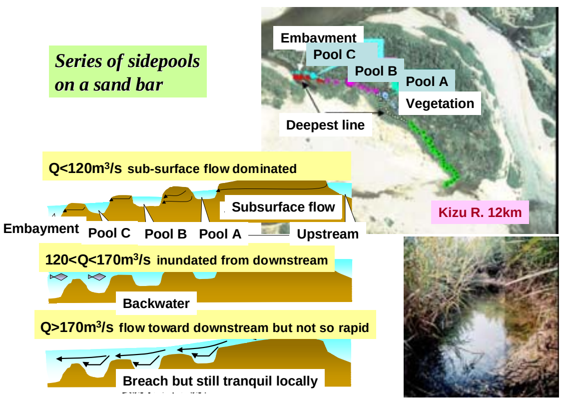

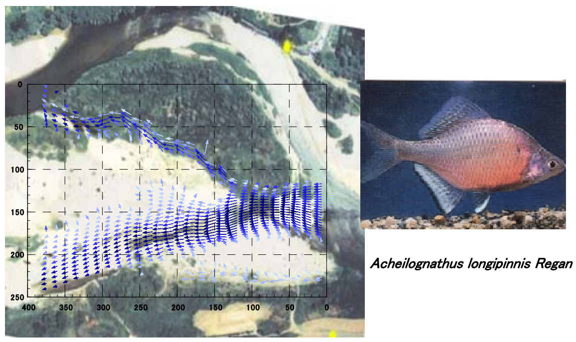

Fig.17 Temporary waters to provide habitat

Fig.18 Information on detailed flow and fish

MATERIAL CYCLE RELATED TO BIOASPECTS IN RIVER ECOSYSTEM

Figure 19 shows the time series of water quality monitored at longitudinally different three points of the Kizu river. Nitrate-ion and Chloride-ion concentrations are shown (In Fig.19, J-00 means January 2000, for example). As for the former (NO_3^-), a typical seasonal pattern can be recognized as it decreases in summer season, and there are small differences among the data monitored at different points though there are several tributaries in to the river with heavier ion load. On the other hand, the latter (Cl^-) hardly show a typical seasonal pattern. The former is affected by bio-chemical action and its activity is higher in summer, while the latter cannot be affected by bio-chemical action. Thus, the data shown in Fig.19 has become a motivation for a research on reaction of ecosystem to the river. River has a function to support ecosystem, while ecosystem brings a function, and that can be often regarded as “ecosystem service”. Fig.19 suggests one of the examples of ecosystem service. The scenario is as follows: The segment in 2-30km of the Kizu river contains many sand bars, and water is conveyed not only by surface flow but also by subsurface flow which is stimulated by the existence of sand bars. Fig.20 shows the relation between the sand bar pattern (characterized by vegetation and secondary channel) and the subsurface flow behaviour, and we can recognize it by mathematical calculation of subsurface flow as well as excellent monitoring in the fields.

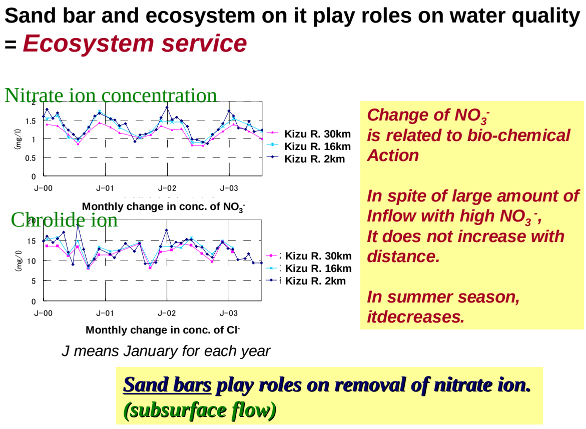

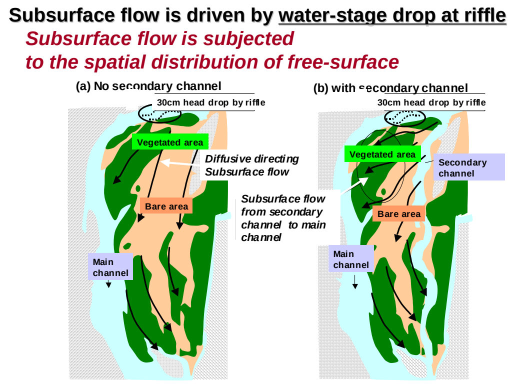

Fig.19 Temporal and spatial changes in water qualities along the Kizu river

Fig.20 Sand bar characteristics and subsurface flow

When we expect that the recognition of river ecosystem supports an ecosystem conservation policy, a concept "ecosystem service" is strategically employed: Physical basement of rivers supports bio-aspects or various organisms, and it reversely acts as an advantage for rivers or human activity, and one of examples are water purification through ecosystem service introduced in the above. If so, we can start an argument such what parts (elementary landscape units) of a bar are functionally efficient for water purification to be preserved, or how many bars must be preserved among many sand bars in a segment.

In order to clarify the function of elementary landscapes of a sand bar, various techniques to quantify the function are employed in the field study. Fig.21 shows one of them, where "stable isotope method" is applied. We measured not only nitrate-ion concentration (NO_3^-) but also the ratio of Nitrate isotope (heavier nitrogen), $\delta^{15}N$. Decreases of both the concentration and NO_3^- and $\delta^{15}N$ indicates denitrification (emission of nitrogen gas to the atmosphere), and it is pure purification (out release of N from the river system). Based on such field studies, we can specify the function of elementary landscapes of a sand bar. In a sand bar, vegetated area shows an intensive function of denitrification because the organic matters produced from vegetation requires Oxygen or the subsurface flow layer is intercepted from the atmosphere with impervious fine soil trapped by vegetation brings anaerobic condition (low dissolved oxygen condition), where is a good habitat for anaerobic bacteria to contribute denitrification.

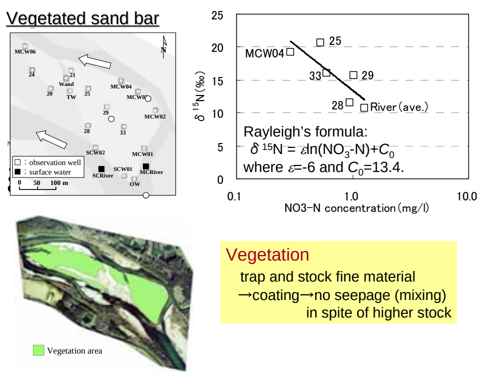

Fig.21 Stable isotope method to specify material-cycle process

For the time being, we cannot evaluate all the ecosystem service, but important ecosystem service can be added up as potential how it replaces fossil fuels and it may become an index of "value " to explain why the river ecosystem should be conserved.

As for a summary of this chapter, Fig.22 (Nohara 2007, from the report of the special coordination fund for promoting science and technology for sustainable national land management 2006-10, "Research and development in assessment and restoration for eco-compatible management of river basin complex around Ise bay” supported by Ministry of Education, Culture, Sports, Science and Technology, Japan) .is an intuitive sketch which suggests where and how the respective elementary landscape units play roles for providing habitat, and how the biomass functions in various process of material-cycle regarded as “ecosystem service” in a river landscape.

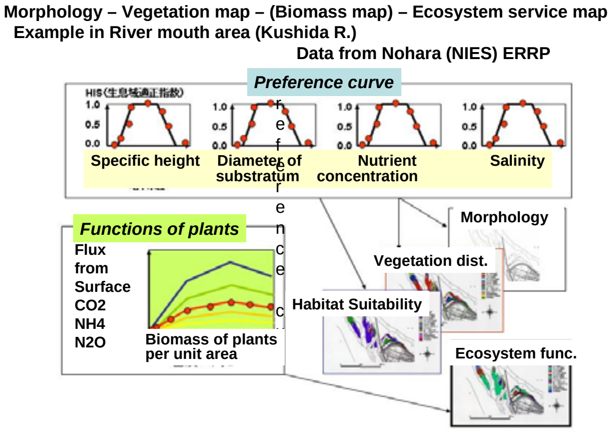

Fig.22 Elementary landscape units and their functions

CONCLUSION

The author sincerely appreciates Dr. T. Sakajo who provided him an opportunity to give an invited lecture on PRESTO Seminar in Hokkaido University, on the 13th June 2008, and this paper has been reproduced from the contents of this lecture. In this paper, it is explained how the river ecosystem is recognized as the process-complex or an interacting system. The research corporation among hydrology, hydraulics, biology, ecology and limnology has been efficient to bring various modelings, which is able to be employed in policy making for river and river-basin management, particularly in its accountability or assessment process. All processes included in the system have been clarified through not necessarily perfect observations or monitoring in the fields. Understanding of the field data is an important part, and various mathematical tools are expected such as data processing, statistical analysis, stochastic forecasting, and GIS techniques. On modeling the system, dynamism is an important aspect not only in physical processes but also in bio-processes, and various mathematical techniques are expected to be engaged. And, the process of policy making, based on the system, various conversions (morphology to flow characteristics, to habitat suitability, to biomass, to ecosystem service and so on) are necessary, and it requires mapping techniques in mathematics. Numerical tools have now become familiar to us, but meanwhile a kind of intuition for the processes or a system comes from rather based on mathematical relations for example relations among equations and solutions. In this sense, we expect interdisciplinary networks not only with several natural sciences in understanding of a system but also with mathematics in data processing, analyzing the processes, algorithm for accountability and intuition to the processes.

REFERENCES

Teramoto, A, S. Nakamura and T. Tsujimoto (2003) Bank erosion with bar migration, *Int. Sym. Disaster Mitigation & Basinwide Water Management*, Niigata, Japan, B06, CD-ROM.

Tsujimoto, T. (1999) Fluvial processes in a stream with vegetation, *Jour. Hydraul. Res*., IAHR, Vol.37, No.6, pp.789-803.

Tsujimoto, T. (1999) Sediment transport processes and channel incision: Mixed size sediment transport, degradation and armouring, *Incized River Channels*, edited by S.E. Darby and A. Simons, John Wiley & Sons Ltd., Chapt.3, pp.37-66,

Tsujimoto, T and T. Tashiro (2004) Application of population dynamics modeling to habitat evaluation –Growth of some species of attached algae and its detachment by transported sediment, *Hydroecol. Appl*., Tome 14, Vol.1, pp.161-174.

Tsujimoto, T., Y. Toda and M. Obana (2008) Assessment framework of eco-compatible management of river basin complex around Ise bay, Advances in Hydro-Science & Eng., ICHE (CD-ROM).

Charge simulation method for approximating the complex potential in a channel domain with multiple circular islands

Yousuke AMAYA * and Takashi SAKAJO †

Figure 1: The Nile, an example of the river region with many sand islands.

1. Introduction

In dealing with environmental problems in rivers, it is important to describe how chemical and biological particles are advected by the river flows. However, the description of river flow itself is generally difficult, since the flow domain has a complex topography as we see in Figure 1. Moreover, the dispersion of such particles are in general non-uniform; Some pollutants spread over the whole river, while the others stay around stagnation points of the flow. Thus as the first step of the mathematical treatment toward the river environments, we need to develop a numerical method to generate flows in complex domains with which the particles float.

In the present article, we propose a numerical method to construct a uniform flow in a specific domain called "river region", which is a channel region with many obstacles like sandbanks inside. The mathematical devices are the theory of perfect fluids in two-dimensional planar space and the elliptic functions.

2. Charge simulation method

Charge Simulation Method (CSM) is a well-known fast and accurate computational method to solve the Poisson equations[1]. For a given domain $\Omega \subset \mathbb{C}$, let us consider the Poisson equations for the function $g(z)$,

$$\Delta g(z) = 0 \quad \text{in } \Omega, \tag{1}$$

$$g(z) = b(z) \quad \text{on } \partial\Omega, \tag{2}$$

where $b(z)$ is a given function on the boundary $\partial\Omega$. CSM approximates the function $g(z)$ with a linear combination of fundamental solutions at N charge points $z = \zeta_1, \zeta_2, \ldots, \zeta_N$ as follows.

$$G(z) = Q_0 + \sum_{i=1}^{N} Q_i \log|z - \zeta_i|, \tag{3}$$

in which $Q_1, \ldots, Q_N$ are unknowns with the constraint $\sum_{i=1}^{N} Q_i = 0$. We determine Q_i numerically so that the equation (3) satisfies the boundary condition (2) at given collocation points $z_1, \ldots, z_N$ along the boundary, i.e. $G(z_i) = b(z_i)$ for $i = 1, \ldots, N$. This is equivalent to the following $(N+1)$-dimensional linear equation

*Department of Mathematics, Hokkaido University, E-mail: s063002@math.sci.hokudai.ac.jp
†Department of Mathematics, Hokkaido University, E-mail: sakajo@math.sci.hokudai.sc.jp

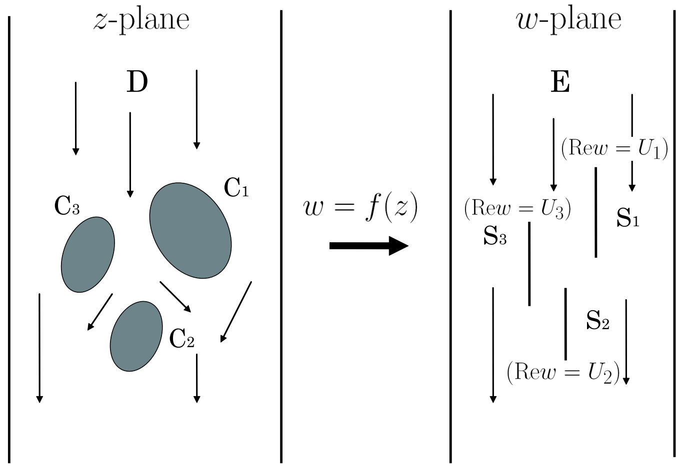

Figure 2: Conformal mapping from the complex z-plane to the complex w-plane

$$\begin{cases} Q_0 + \displaystyle\sum_{i=1}^{N} Q_i \log|z - z_i| = b(z_i), \qquad (i = 1, \cdots, N), \\ Q_1 + \cdots + Q_N = 0, \end{cases} \tag{4}$$

which is solved numerically by the LU-decomposition method. CMS has a nice disposition in terms of the error estimate between the exact solution and the approximate solution. Since the error estimate attains its maximum at the boundary of the domain due to the maximum principle, we can define the maximum error by $E = \max_{1\le j\le N} |G(z_j) - g(z_j)|$ in which $g(z)$ and $G(z)$ represent the exact mapping and the approximate mapping respectively. When the charge points are properly set and the domain has sufficiently smooth boundaries, the maximum error decreases with $O(\tau^N)$ for some $0 < \tau < 1$, which depends on the shape of the domain. (See, e.g., Katsurada and Okamoto[3].)

3. Conformal mapping to the parallel slit domain

We propose how to construct the uniform flow in the river region by constructing a conformal mapping from the complex z-plane to the complex w-plane via CSM. see Figure 2. We consider the region D in the z-plane as a standard river region. Namely, the uniform flow is confined in a channel-like region with two long straight boundaries, in which there are cylindrical sandbanks $C_1, \ldots, C_d$. Next, we consider the region T in the w-plane as a channel region with parallel slits $S_1, \ldots, S_d$. The complex potential of the flow in D is mapped to a uniform flow in T by a conformal mapping $w = f(z) = z + H(z)$. (e.g., See Nehari[6].) CMS approximates the function $H(z)$.

For the sake of simplicity, we assume that the left and right doundaries of the region D correspond to the imaginary axis and Re$z = \alpha$ in the z-plane respectively, and that the flow is periodic in the imaginary direction with period 2π. Then, because of the principle of reflection, the flow in D must be symmetric with respect to both imaginary axis and the other right boundary as we see in Figure 3. Therefore, let D' denote the reflecting image of D. The union $D \cup D'$ is the basic computational region that covers the whole z-plane double periodically. As the fundamental solution to describe this flow in CSM, we adopt the elliptic functions. First, Weierstrass ζ-function is defined by

$$\zeta(z) = \frac{1}{z} + \sum_{\omega\in\Omega'} \left(\frac{1}{\omega} + \frac{1}{z-\omega} + \frac{z}{\omega^2} \right), \tag{5}$$

in which $\omega_1 = \alpha,\ \omega_2 = 2\pi i$ and $\Omega' = \{n\omega_1 + m\omega_2 \mid n, m \in \mathbb{Z}\} \setminus \{0\}$, Second, the elliptic theta function of type 1 is given by

$$\vartheta_1(z) = 2\sum_{n=1}^{\infty} (-1)^n h^{\frac{(2n-1)^2}{4}} \sin(2n-1)\pi z, \tag{6}$$

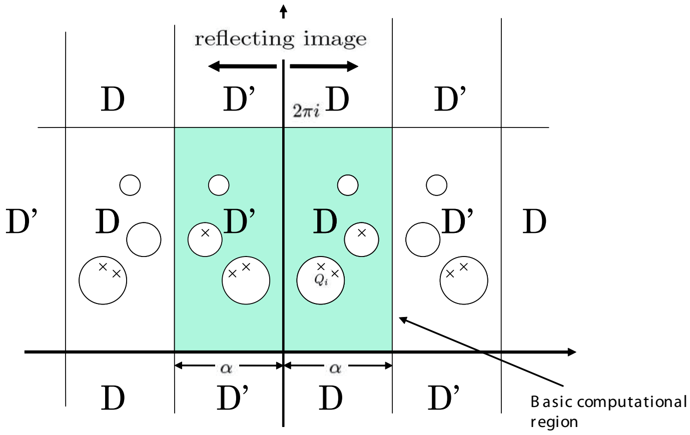

Figure 3: Doubly periodic computational region.

in which $h = e^{\frac{\omega_2}{\omega_1} i\pi}$. These two elliptic functions are connected through the following relation,

$$\zeta(u) = \frac{2\eta}{\omega_1} u + \frac{d}{du} \log \vartheta_1 \left(\frac{u}{\omega_1} \right), \qquad \eta = \zeta \left(\frac{\omega_1}{2} \right). \tag{7}$$

Now, the complex potential for the flow is approximated by the linear combination of the elliptic theta functions:

$$\begin{aligned} H(z) &= Q_0 + \sum_{l=1}^{n} \sum_{i=1}^{N_l} Q_{li} \sum_{\omega} (\log |z - \zeta_{li} - \omega| - \log |z + \overline{\zeta_{li}} - \omega|) \\ &= Q_0 + \sum_{l=1}^{n} \sum_{i=1}^{N_l} Q_{li} \left\{ -\frac{z}{\omega_1} + \log \left(\frac{\vartheta_1 \{(z - \zeta_{li})/\omega_1\}}{\vartheta_1 \{(z + \overline{\zeta_{li}})/\omega_1\}} \right) \right\}, \end{aligned} \tag{8}$$

in which n is the number of the islands, N_l is that of the charge points in C_l and the collocation points on C_l and ζ_{li} is the position of the i-th charge point inside C_l. When the channel domain has the infinite length in the imaginary direction, namely $\omega_2 = \infty$, the approximating function (8) is equivalent to

$$H(z) = Q_0 + \sum_{l=1}^{n} \sum_{i=1}^{N_l} Q_{li} \log \left(\frac{\sin \{(z - \zeta_{li})\pi/\omega_1\}}{\sin \{(z + \overline{\zeta_{li}})\pi/\omega_1\}} \right). \tag{9}$$

(e.g., see Hurwitz and Courant [5].) Note that the actual computation of the ϑ_1 function can be carried out by truncating the inifinite product representation of ϑ_1.

4. Numerical method of infinite channel

Here we consider the river region with $\omega_2 = \infty$, the infinite channel. The equation (9) is not suitable for actual numerical computations because of the logarithmic singularity in the fundamental solution. To avoid the appearance of the branch singularities, we substract

$$0 = \sum_{l=1}^{n} \sum_{i=1}^{N_l} Q_{li} \log \left(\frac{\sin \{(z - \zeta_{l0})\pi/\omega_1\}}{\sin \{(z + \overline{\zeta_{l0}})\pi/\omega_1\}} \right) \tag{10}$$

from the function (9), in which ζ_{l0} and $-\overline{\zeta_{l0}}$ are the positions of additional charge points, which leads us to

$$H(z) = Q_0 + \sum_{l=1}^{n} \sum_{i=1}^{N_l} Q_{li} \left\{ \log \left(\frac{\sin \{(z - \zeta_{li})\pi/\omega_1\}}{\sin \{(z - \zeta_{l0})\pi/\omega_1\}} \right) - \log \left(\frac{\sin \{(z + \overline{\zeta_{li}})\pi/\omega_1\}}{\sin \{(z + \overline{\zeta_{l0}})\pi/\omega_1\}} \right) \right\}. \tag{11}$$

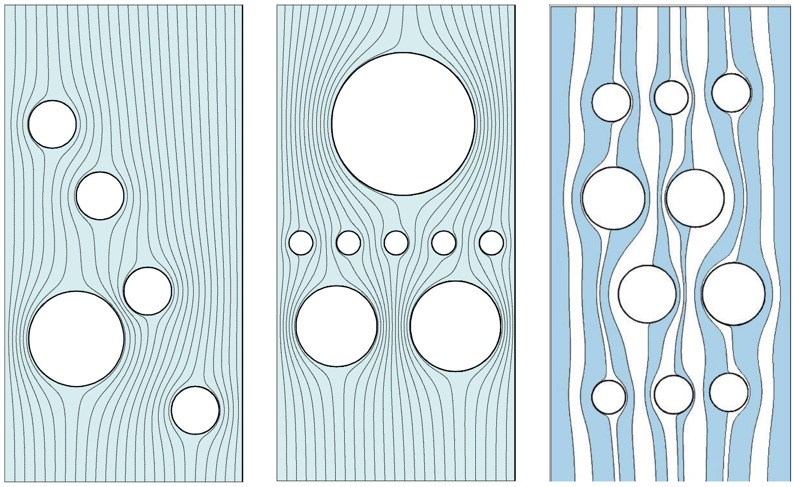

Figure 4: Computational results.

At the infinity, the flow is uniform because the flow is not affected by islands. Thus, we have $Q_0 = 0$. As a result we can compute the approximating conformal mapping by solving the following linear equation for Q_{li} and U_{mj}:

$$\sum_{l=1}^{n}\sum_{i=1}^{N_l} Q_{li}\left\{\log\left|\frac{\sin\{(z_{mj}-\zeta_{li})\pi/\omega_1\}}{\sin\{(z_{mj}-\zeta_{l0})\pi/\omega_1\}}\right| - \log\left|\frac{\sin\{(z_{mj}+\overline{\zeta_{li}})\pi/\omega_1\}}{\sin\{(z_{mj}+\overline{\zeta_{l0}})\pi/\omega_1\}}\right|\right\} - U_{mj} = -\mathrm{Re}(z_{mj})$$

$$\text{for} \quad m = 1,\ldots,n, \quad \text{and} \quad j = 1,\ldots,N_l. \tag{12}$$

$$\sum_{i=1}^{N_l} Q_{li} = 0, \qquad \text{for} \quad l = 1,\ldots,n.$$

in which z_{mj} is the position of the j-th collocation point on the boundary of the island C_m. We give three comptational results in Figure 4. The number of the collocation points and the charge points is $N_l = 64$. Let r_m and $\delta_m \in \mathbb{C}$ denote the radius and the center of C_m. Then, the positions of the collocation points inside C_m and the charge points on C_m are given by $z_{mj} = \delta_m + r_m \exp(2\pi ij/N_l)$ and $\zeta_{mj} = \delta_m + 0.7r_m \exp(2\pi ij/N_l)$ for $j = 1,\ldots,N_l$. The additional charge points for each island C_m are put at $\zeta_{m0} = \delta_m$.

References

[1] K. Amano, D. Okano, H. Ogata, H. Shimohira and M. Sugihara, "A systematic scheme of numerical conformal mappings of unbounded multiply-connected domains by the charge simulation method", Information Processing Society of Japan Journal, **42** (3) (2001), 385-395.

[2] H. Ogata, "Numerical conformal mapping of periodic structure domains", Japan J. Indust. Appl. Math., **19** (2002), 257-275.

[3] H. Okamoto and H. Katsurada, "A mathematical study of the charge simulation method 1", J. Fac. Sci. Univ. Tokyo, Sect.IA, Math., **35** (3) (1998), 507-518.

[4] E.R. Johnson and N.R. McDonald, "The motion of a vortex near two circular sylinders", Proc. Royal Soc. A, **460** (2004), 939-954.

[5] A. Hurwitz, and R. Courant, "Vorlesungen über allgemeine Funktionentheorie und elliptische Funktionen", Springer-Verlag (1964).

[6] Z. Nehari, "Conformal Mapping", Dover, New York (1975), General Pub., Tronrto (1952).

SIMULTANEOUS ANALYSIS METHOD OF DEFORMATION AND INTERNAL EROSION FOR SOIL STRUCTURES

Kazunori Fujisawa
Graduate School of Environmental Science
Okayama University
Okayama, Japan

INTRODUCTION

Recently, failures of embankments such as irrigation ponds and levees have been reported because of frequent occurrences of storm rainfall, together with significant economic and environmental damages. Piping, as the result of internal erosion of embankments, is a primary cause of embankment breaks. The inner states of embankments are needed to be estimated to take appropriate measures for the prevention of embankment failures. In this study, the equation of the conservation of soil particles inside of embankments is introduced to the conventional soil-water coupled equations, which enables internal erosion, i.e. transport of soil particles, and deformation of embankments to be calculated simultaneously. This approach offers a straightforward method to solve the complex phenomena of soil structures, such as piping.

GOVERNING EQUATIONS

Governing equations to analyze the deformation and the internal erosion of soils are given as follows:

$$\frac{\partial}{\partial x_j}\left(\dot{T}_{ij} + T_{ij}L_{kk} - T_{ik}L_{jk}\right) + \rho\dot{g}_i = 0 \quad , \tag{1}$$

$$\frac{\partial q_i}{\partial x_i} + \dot{\theta} + \theta L_{ii} = 0 \quad , \tag{2}$$

$$\dot{n} - (1-n)L_{ii} = E\,R_s \quad , \tag{3}$$

where t , x_i , T_{ij} , L_{ij} , ρ , g_i , θ , q_i , n and E denote time, Cartesian coordinates, Cauchy stress tensor, velocity gradient tensor, density of soil mass, gravity acceleration, volumetric water content, flux of pore water, porosity and erosion rates of soils, respectively. Erosion rates of soils are defined as the volume of eroded soil particles included in unit area within unit time. R_s in Eq. (1) denotes the internal surface area per unit volume of soils, where soil particles are eroded. A dot above the variables in Eqs. (1) to (3) means Lagrangian time differentiation. Eqs. (1) and (2) have been conventionally used to analyze the deformation of soils as the soil-water coupled problem. In this study, Eq. (3) is introduced to express the internal erosion of soils.

In order to solve the three equations above simultaneously, the change of the material parameters of soils governing the deformation has to be considered because internal erosion of soils decrease the density and change the particle size distribution. However, the studies on the alteration of the material characteristics of soils due to internal erosion have not been carried out up to now. Therefore, in this paper, the deformation of soils is neglected and the internal erosion is analyzed. In this case, Eq. (1) is not necessary, so that the governing equations are reduced as follows:

$$\frac{\partial n}{\partial t} = E\,R_s \quad , \tag{4}$$

$$\frac{\partial \theta}{\partial t} + \frac{\partial q_i}{\partial x_i} = 0 \ , \ q_i = k\,\frac{\partial h}{\partial x_i} \quad , \tag{5}$$

where h and k denote hydraulic head and permeability of saturated or unsaturated soils, respectively, and Darcy's law is applied to describe the flow in porous media. It has been empirically known that erosion rates of soils can be given as the following form as a function of applied shear stress on the pore wall τ (Reddi & Bonala, 1997):

$$E = \alpha(\tau - \tau_c) \quad , \tag{6}$$

where α is the erodibility coefficient expressing the rate of change of erosion rate; and τ_c is the critical shear stress which determines the onset of erosion. In order to obtain the applied shear stress τ, the following equation is available (Reddi, Lee & Bonala, 2000):

$$\tau = \rho_w g I\sqrt{2K/n} \quad , \tag{7}$$

$$K = \frac{k\mu}{\rho_w g} \quad , \tag{8}$$

where ρ_w , I , K and μ denote the water density, hydraulic gradient, intrinsic permeability and the viscosity of water (1.005x10^{-3} kg/m/s). The porosity and the intrinsic

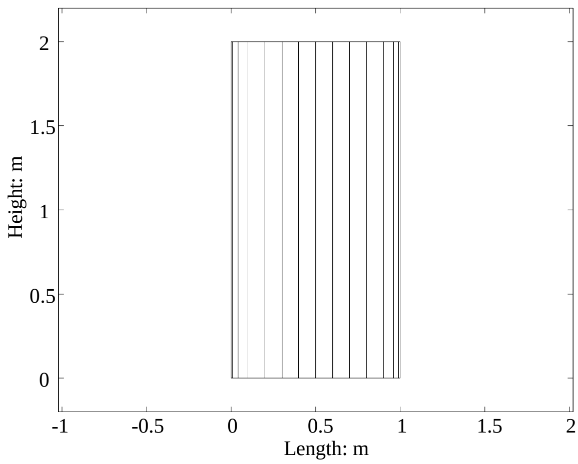

Figure 1: Finite element mesh of 1.0x2.0 m soil block for simple numerical test of internal erosion.

permeability are sufficient for computation of shear stress exerted onto pore walls. The internal surface area per unit volume R_s can be calculated from the particle size distribution curve of the soil.

EXAMPLES OF NUNERICAL ANALYSIS

To solve Eqs. (4) and (5), finite element method (FEM) was applied and the simple numerical test was conducted first. Fig. 1 shows the used finite element mesh. The number of the element was 14. The initial porosity was given as 0.31. The value of the critical shear stress was given as 0.8×10^{-5} kPa and the erodibility coefficient 0.51×10^{-6} m/kPa/s. The water pressure of 9.8 kPa was applied on the left side and 0 kPa on the right side. The undrained condition was imposed on the top and the bottom. When the gradient of the water pressure is applied as the boundary conditions, the pore water flowed rightward in Fig.1 and the internal erosion was induced. However, the state of internal erosion became steady, where the internal erosion did not happen, after the fine particles of the soil were fully eroded and erodible soil particles vanished. Fig. 2 shows three particle distribution curves, one of which presents the initial particle distribution. Other two curves show the steady particle distributions of the soils with the initial permeability of 0.5×10^{-6} and 1.0×10^{-6}. It is found that the soil with the initial permeability of 0.5×10^{-6} keeps more of fine particles than the other with the initial permeability of 1.0×10^{-6}. This result was obtained since the soil with smaller permeability is denser and the soil particles were restrained from moving.

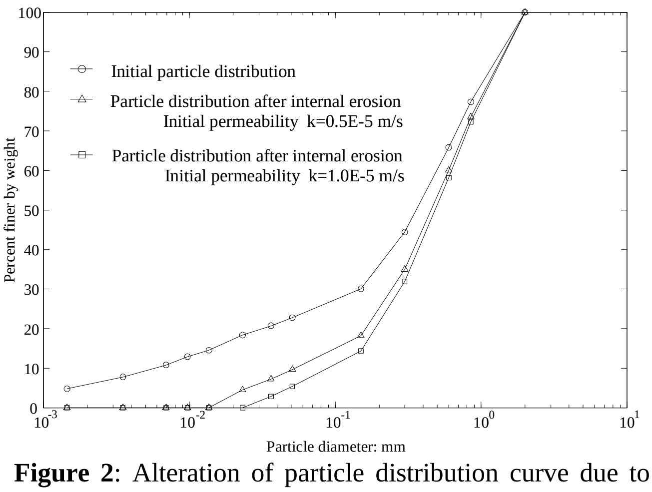

Figure 2: Alteration of particle distribution curve due to internal erosion from the initial state (○) to the steady state (△ and □), where internal erosion stops.

Next, the effect of initial imperfection was investigated, giving a scar at the center of the right side of a 1.0x2.0m soil block. Figs. 3 and 4 shows the finite element mesh and the numerical result of the pore water flux and the porosity distribution in a soil block which has been subjected to internal erosion for 166 hours. The values of the material parameters used in this analysis are the initial porosity of 0.31, the initial permeability of 1.0×10^{-6}, the critical shear stress of 0.8×10^{-5} kPa and the erodibility coefficient of 0.51×10^{-6} m/kPa/s. These values are similar to the previous analysis presented above, but the value critical shear stress is different. The water pressure of 9.8 kPa was applied on the left side and 0 kPa on the right side. The undrained condition was imposed on the top and the bottom. The pore water flowed rightward. As shown in Fig. 3, the internal erosion concentrated to the scar, the porosity just upstream of it increased rapidly, and the internal erosion of the soil block developed backward. These results were obtained when the shear stress exerted by the pore water flow onto the pore wall is slightly greater than the imposed critical shear stress.

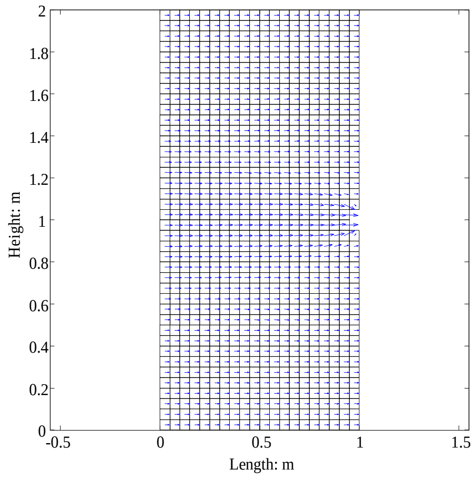

Figure 3: Finite element mesh and pore water flux in a 1.0x2.0m soil block which has a scar at the center of its right side (166 hours after internal erosion started).

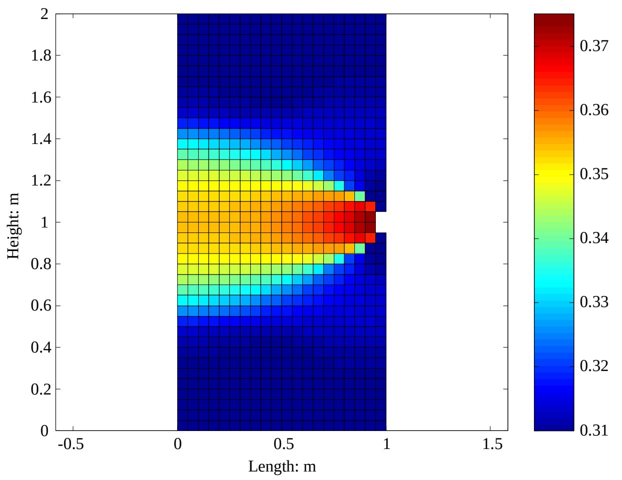

Figure 4: Finite element mesh and porosity distribution in a 1.0x2.0m soil block which has a scar at the center of its right side (166 hours after internal erosion started).

REFERENCES

Reddi L.N. and Bonala M.V.S. (1997), Critical shear stress and its relationship with cohesion for sand-kaolinite mixtures, *Canadian Geotechnical Journal*, **34**, 26-33.
Reddi L.N., Lee I-M. and Bonala M.V.S. (2000), Comparison of internal and surface erosion using flow pomp test on a sand-kaolinite mixture, *Geotechnical Testing Journal*, **23**(1), 116-122.

A Study on Appropriate Selection of Final Waste Disposal Sites

Myungjin NA* and Koji KURIHARA**

* Graduate School of Environmental science, Okayama University 1-1, Tsushima-Naka, 3-chome, Okayama 700-8530, Japan, E-mail: mjna@ems.okayama-u.ac.jp

** Graduate School of Environmental science, Okayama University, 1-1, Tsushima-Naka, 3-chome, Okayama 700-8530, Japan, E-mail: kurihara@ems.okayama-u.ac.jp

1. Introduction

Some wastes are recycled for creating a recycling society these days, but most remain buried in the ground or burned. In other words, construction of final waste disposal sites can not be avoided. This study presents a method for determining a final waste disposal site from the three perspectives of physical, social, and environmental factors. The area of study was Okayama Prefecture. We used 1km mesh data to estimate spatial distribution. The analysis was performed easily using the network ability of GIS (geographic information system).

2. Exclusionary Rule

An exclusionary approach begins by identifying areas that are inappropriate for use because they have particular land features such as endangered species or wetlands. Areas which judged to be inappropriate by exclusionary criteria in table1 were excluded from candidate sites for the facility.

Table 1 Exclusionary criteria

Item	Exclusionary criteria
Hydrology	river, flood-prone area
Landform	fault area, steep slope area, collapse area, landslide area
Ecology	nature conservation area, wildlife refuge
Location	major road, airport
Land use	natural park, use district
Sociality	cultural resource

3. Factors Considered in Siting

(1) Economic factor

The 'waste disposal flow chart' announced by the Ministry of the Environment in 2003 is shown in Fig.1. Optimal location is considered from this waste disposal network. If a new final disposal site is constructed, the area that minimizes target function will be selected as that optimal site. The target function is

$$f_{\mathrm{EF}} = \sum_{a\in At_2} d \cdot r \cdot x_a \cdot TC_a + \sum_{a\in At_3} (1-d) x_a \cdot TC_a + \sum_i TP_i \cdot \delta_i \qquad (1)$$

where the right side indicates transport cost of remaining waste, direct transport cost of final disposal, and the cost for locating the final disposal site facility in turn. Other costs were not considered because they do not change greatly according to location.

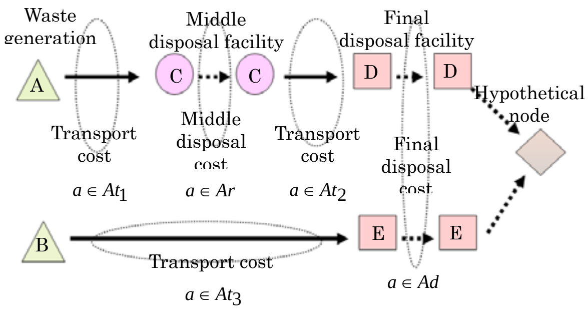

Fig.1 Waste disposal flow chart

(2) Social factor

The results of survey which was conducted in Saitama Prefecture were used to analyze social factors. We have analyzed using covariance structure analysis of statistical method to understand awareness of residents toward the final waste disposal facility. Fig.2 shows the covariance structure model.

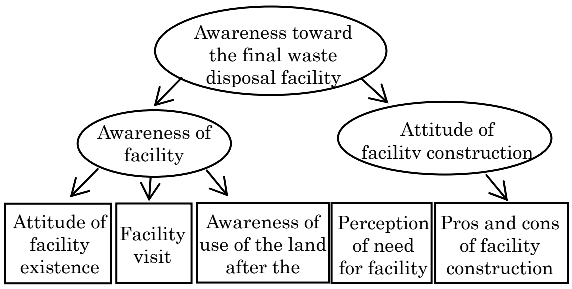

Fig.2 Covariance structure model

Covariance structure model by each age group was constructed from recoding data. We assume that awareness structure of whole nation is equal, and calculated awareness of residents in Okayama Prefecture using following function,

$$f_{\mathrm{SF}} = 1 - \sum_k I_{k,i} \frac{P_{k,i}}{T_i} \quad (2)$$

where k is age group's number, i is mesh number, I is awareness of residents, T is total population, and P is the population of age group. The area that minimizes value of this function will be selected as that optimal site. It means degree of public opposition.

(3) Environmental factor

Safety aspects must be also considered with economic and social factors. The regions that have final waste disposal facilities might be exposed to dangers through alteration and degradation of impermeable liners, leaching of contaminated water into groundwater following precipitation, and degradation of the disposal site by an earthquake. The considered environmental factors are average attitude, annual rainfall, gradient, and ground hardness.

4. Calculating weights of each factor by AHP

In order to consider simultaneously three factors, we need relative weights for each factor. In this study, the relative weights were obtained from AHP (Analytic Hierarchy Process). The AHP is a structured technique for helping people deal with complex decisions. We made a pairwise comparison matrix for each factor, and calculated eigen values and vectors. The elements of the eigen vector corresponding maximum eigen value are relative weights for each factor.

Table 2 Relative weights for each factor

Factor	Weight
Environmental factor	0.540
Economic factor	0.297
Social factor	0.163

Factor	Weight
Ground hardness	0.467
Gradient	0.277
Average attitude	0.160
Annual rainfall	0.095

5. Selecting final candidate site

The site selection model based on relative weights of each factor is

$$f(y) = \sum_{i=1}^{n} w_i f_i \quad (3)$$

where n is the number of factors, w_i is weight of i factor, and f_i is the standardized value of i factor. The area that minimizes value of this function will be selected as that optimal site. Fig.3 shows the proposed final candidate sites.

Fig.3 Proposed final candidate site

6. Conclusion

Determining the location of a final waste disposal facility is an important component of the waste management process. Three factors considered in this study must be considered simultaneously when determining the location. This study constructed site selection model to find appropriate location for the facility, and proposed several candidate sites.

References

1) Ministry of the Environment: About the state of general waste discharge and disposal (in Japanese), WWW Page, http://www.env.go.jp/recycle/waste/ippan.html, 2005.

2) Myungjin NA, Koji KURIHARA and Naokazu GION: Optimal Allocation of Final Waste Disposal Sites Based on Physical and Social Factors, *Journal of Environmental Science for Sustainable Society*, Vol.1, pp.25-32, 2007.

3) Satty, T. L.: The Analytical Hierarchy Process : Planning , Priority Setting , Resource Allocation, *New York : McGraw Hill*, 1980.

The paradox of enrichment

Fumio Nakajima
Department of Mathematics, Faculty of Education, Iwate University
Morioka 020-8550, Japan
e-mail: fnaka@iwate-u.ac.jp

August 10, 2008

1 Introduction.

It is natural to expect that an increasing the supply of food for human beings may support an increasing its populations. However, to the contray in 1963, Huffaker, Shea and Herman reported in their experiments the destabilization of a stable exploitation ecosystem which resulted in the extinction of both the exploiter (an acarophagous mite) and its victim (an herbivorous mite). This fact was confirmed by Luckenbill in 1973 who conducted more sophisticated experiment using the protozoan of a paramecium aurelia and its predator didinium nasutum and showed that the enrichment of the system by supplying excess bacteria resulted in the extinction of the paramecium aurelia. In 1971, Rosenzweig appealed that the increasing the supply of limiting nutrients or energy tends to destroy the steady state, and thus that human beings must be very careful in attempting to enrich an ecosystem in order to increase its food yield ; this concept is now known as the paradox of enrichment. On the other hand, as the theoretical studies of this paradox Rosenzweig and Harrison stated several mathematical models, which are the type of Lotka-Volterra equations, and showed numerically the situation of the extinction. The purpose of this paper is to state a new type of model for predator-prey system, by which we shall prove the paradox of enrichment rigorously but not numerically.

2 Main result

Our model is the following. Let $x(t)$ and $y(t)$ be the populations of prey and predator for time t, respectively :

$$\frac{\dot{x}(t)}{x(t)} = a - g(x(t)) - b\frac{y(t)}{x(t)}, \quad \frac{\dot{y}(t)}{y(t)} = -c + d\frac{x(t)}{y(t)} \quad \left(\cdot = \frac{d}{dt}\right) \tag{1}$$

where $x(t) > 0$, $y(t) > 0$, a, b, c and d are positive constants and $g(x)$ is a continuous, non-negative valued function. In (1), a represents the birth rate per capita of prey, c the death rate per capita of predator and $g(x)$ the effect of circumstances caused by x. We assume simply that $g(x) = x$ for $0 < x < e$ and for some number $e > a + c$, and $g(x) = e$ for $x \geq e$. Moreover assume that $ac > bd$, and hence we may see that the point $E := (x^*, y^*)$, where $x^* = a - \frac{bd}{c}$ and $y^* = \frac{d}{c}x^*$, is an equilibrium point. Our result is the following :

Theorem 1
Assume that $ac > 2bd - c^2$. Then E is asymptotically stable, and there exists a special solution $(x_0(t), y_0(t))$ such that $x_0(0) > x^*$ and $y_0(0) = y^*$ and that $x_0(t) \to 0$ and $y_0(t) \to 0$ as $t \to \infty$. Moreover for any solution $(x(t), y(t))$ with $x(0) > x_0(0)$ and $y(0) = y^*$ there exists a positive number T such that $y(T) > 0$ and $x(t)$ approaches zero as t approaches T.

Remark 1 The proof of Theorem 1 is a kind of phase plane method, and we may see that $y_0(t) > y^*$ for some $t > 0$. Moreover the existence of T may be observed in the data of [1] and [2]. The author thinks that the conclusion of Theorem 1 may describe the paradox of enrichiment.

We shall comment on the existence of non-constant periodic solution of (1). The following fact is known as [Example 1,5].

Theorem 2
Assume that $a = \frac{2bd}{c} - c$ and $bd > c^2$. Then there exists two continuously differentiable function $a(\varepsilon)$ and $w(\varepsilon), a(0) = a$, and $w(0) = \frac{\pi}{\sqrt{bd - c^2}}$, such that (1), where $a = a(\varepsilon)$, has a non-constant $w(\varepsilon)$-periodic solution $(x(t, \varepsilon), y(t, \varepsilon))$, which is close to E as ε is sufficiently small.

Theorem 2 was proved by the method of Hopf bifurcation.

References

1. Huffaker,C.B., Shea,K.P., and Herman,S.G., 1963, Experimental studies on predation : Complex dispersion and levels of food in an acarine predator-prey interaction. Hilgardia 34, No.9, pp.305-330.

2. Luckinbill,L.S., 1973, Coexistence in laboratory populations of Paramecium aurelia and its predator Didinium nasutum. Ecology 54, pp.1320-1327.

3. Rosenzweig,M.L., 1971, Paradox of enrichment : destabilization of exploitation ecosystems in ecological time, Science 171, pp.385-387.

4. Harrison,G.W., 1995, Comparing predator-prey models to Luckinbill's experiment with didinium and paramecium, Ecology 76 (2), pp.357-374.

5. Nakajima,F., 2008, A ratio-dependent predator-prey system model, Proceedings of RIMS of Kyoto Univ.(Koukyuroku), to be appeared.

Mathematical study on microbial coexistence mediated by syntrophic association

Shinji Nakaoka

JSPS PD Research Fellowship for Young Scientists
Graduate School of Mathematical Sciences, The University of Tokyo
with Chie Katsuyama, Yasuhiro Takeuchi and Kenji Katoh

Bacterial populations play a major role in a mineralization of organic compounds. Metabolically related bacterial populations occur within a given space. Some bacterial populations correlate strongly with each other in the expression of function, such an association is regarded as a microbial consortium. It is often the case that more than two species are synergistically involved in the degradation of organic compounds by syntrophic association in a consortium, suggesting that the degradation is mediated effectively by multiple species, rather than a single species.

Experiments were performed to figure out the character of xenobiotics degrading bacterial species, *Sphingomonas* sp. TFEE and *Burkholderia* sp. MN1 isolated from soil microcosm. It was revealed that *Sphingomonas* sp. TFEE is capable of degrading a xenobiotics, fenitrothion, to 3-methyl-4-nitropenol (3M4N) but not utilizing 3M4N as a sole carbon and energy source. By contrast, *Burkholderia* sp. MN1 grows based on the metabolite of fenitrothion, 3M4N, while it cannot degrade fenitrothion. Methylhydroquinone (MHQ), the intermediate of 3M4N, is utilized by both species. Based on these experimental observations, we developed a mathematical model that represents the syntrophic association composed of *Sphingomonas* sp. TFEE and *Burkholderia* sp. MN1. The variables S_0, S_1 and S_2 denote the concentrations of fenitrothion, 3M4N and MHQ, respectively. The population densities of *Sphingomonas* sp. TFEE and

Burkholderia sp. MN1 are denoted by x_1 and x_2. The model is given by

$$
\begin{aligned}
\frac{dS_0}{dt} &= \lambda - d_0 S_0 - \beta S_0 x_1 \\
\frac{dS_1}{dt} &= - d_1 S_1 + \beta S_0 x_1 - f_2(S_1)\frac{x_2}{\eta_2} \\
\frac{dS_2}{dt} &= - d_2 S_2 + \gamma f_2(S_1)\frac{x_2}{\eta_2} - f_1(S_2)\frac{x_1}{\eta_1} - f_2(S_2)\frac{x_2}{\eta_2} \\
\frac{dx_1}{dt} &= x_1\left(f_1(S_2) - \mu_1\right) \\
\frac{dx_2}{dt} &= x_2\left((1-\gamma)f_2(S_1) + f_2(S_2) - \mu_2\right)
\end{aligned}
\tag{Eq}
$$

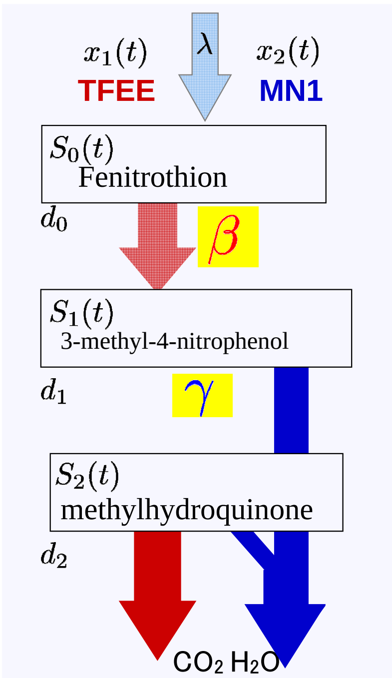

Figure 1: Scheme of fenitrothion degradation by two bacteria.

There are possibly three equilibria. *Null-degradation* equilibrium $E_F = (\frac{\lambda}{d_0}, 0, 0, 0, 0)$ always exists. All substrates and bacteria except fenitrothion have been diminished at this equilibrium. Sustainable degradation of fenitrothion requires the existence of at least one stable positive equilibrium. We analytically derived necessary and sufficient conditions for the existence of positive equilibria [1]. Under these conditions, two positive equilibria generically exist. *Syntrophic union* equilibrium $E_S :=$

$(S_0^+, S_1^*, S_2^*, x_1^+, x_2^+)$ is a stable equilibrium, representing the coexistence of two bacteria. Unstable equilibrium $E_U := (S_0^-, S_1^*, S_2^*, x_1^-, x_2^-)$ divides the region into two parts, namely, *associative* region and *dissociative* region (Fig. 2). On the associative region, all solutions tend to syntrophic equilibrium E_S, while on the dissociative region, all solutions tend to degradation-free equilibrium E_F. In this way, bistability between E_F and E_S is the common feature.

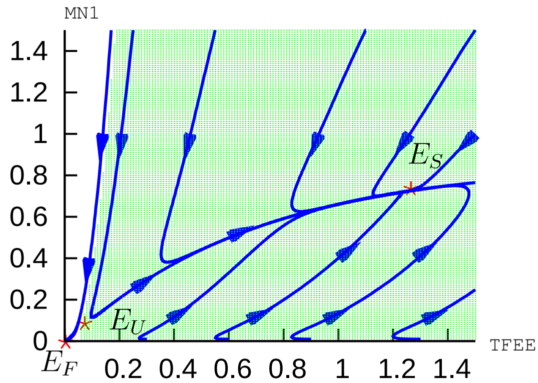

Figure 2: Dynamics of the syntrophic association. Both E_S and E_F are stable.

We further found that these two bacteria are characterized by mutual complementation; two species have complementary qualities to degrade pesticide completely. The degradative ability of one species facilitates the degradative activity of the other species and vice versa.

References

[1] C. Katsuyama, S. Nakaoka, Y. Takeuchi, K. Tago, M. Hayatsu and K. Katoh, Mathematical analysis of an experimental study of syntrophic association in pesticide degradation, in review.

[2] S. Nakaoka and Y. Takeuchi, Mathematical study on sharing metabolism, *RIMS Kokyuroku Bessatsu* **B3** (2007) 193–205.

Numerical and mathematical approaches to analyses of water-circulator-induced flow in ponds

T. Nakazawa* and H. Suito*†
* Graduate school of environmental science, Okayama University, Japan.
† JST PRESTO Researcher

1. Introduction

Pollution and muddiness of natural and artificial reservoirs that are used to supply water irrigation have become important problems in recent years in Japan. One cause of such turbid waters in small reservoirs, in which water flow is less active, is that stagnation of oxygen and water decrease aerobic decomposition capacity. Insolation stratifies the water in such small lakes and ponds according to a temperature gradient: a so-called thermocline. Consequently, vertically circulating flow is strongly suppressed.

A rotating propeller operating at low speed set on a lake surface is proposed because it is expected that the device can induce vertical circulating flow. Typically, a three- or four-bladed propeller forces rotation of the water of the surface and vertical circulating flow is induced because of the centrifugal force. Although various experiments have shown clearly that the water quality in a lake is improved by operation of such equipment, the flow mechanism is not fully understood. To optimize such equipment, mathematical methods are strongly required.

2. Formulation of the problem

- **Coordinate**

To survey such a fluid motion mathematically in a simple system, cylindrical coordinates (r, θ, z) are adopted. A radius of the cylindrical coordinate is r_1, a height of that is s and aspect ratio $\Gamma = \frac{s}{r_1}$. The flow confined between the top lid inducing a horizontal rotating flow, the bottom stationary lid, and the stationary wall are investigated here. Reynolds number is defined as

$$Re = \frac{\max(V(r,s))r_1}{\nu},$$

where $V(r,s)$ is the top boundary condition and ν is viscosity.

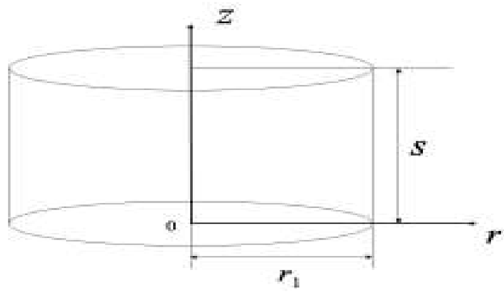

Fig. 1: Cylindrical coordinate.

The top lid

We set

$$V(r,s) = a \cdot r \cdot \exp(1 - a \cdot r) \quad (1)$$

as the top lid boundary condition, where a is selected due to $V(r_1, s) \approx 0$.

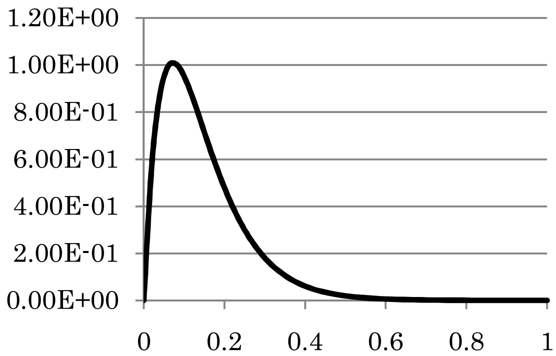

Fig. 2: A distribution of $V(r,s)$.

Governing equations

Since we hope to obtain steady-state solutions numerically for $\Gamma = 1$ and $Re = 50$ and 1000, we solve the time-dependent Navier-Stokes equation (2)-(4) and continuity equation (5) under some initial conditions and expect to obtain different steady-state solutions.

I. Momentum conversation law

$$\frac{\partial u}{\partial t} + u\frac{\partial u}{\partial r} + \frac{v}{r}\frac{\partial u}{\partial \theta} + w\frac{\partial u}{\partial z} - \frac{v^2}{r} = -\frac{\partial p}{\partial r} + \frac{1}{Re}\left(\frac{\partial^2 u}{\partial r^2} + \frac{1}{r}\frac{\partial u}{\partial r} + \frac{1}{r^2}\frac{\partial^2 u}{\partial \theta^2} + \frac{\partial^2 u}{\partial z^2} - \frac{u}{r} - \frac{2}{r^2}\frac{\partial v}{\partial \theta}\right) \quad (2)$$

$$\frac{\partial v}{\partial t}+u\frac{\partial v}{\partial r}+\frac{v}{r}\frac{\partial v}{\partial \theta}+w\frac{\partial v}{\partial z}+\frac{uv}{r}$$
$$=-\frac{1}{r}\frac{\partial p}{\partial \theta}+\frac{1}{Re}\left(\frac{\partial^2 v}{\partial r^2}+\frac{1}{r}\frac{\partial v}{\partial r}+\frac{1}{r^2}\frac{\partial^2 v}{\partial \theta^2}+\frac{\partial^2 v}{\partial z^2}+\frac{v}{r}+\frac{2}{r^2}\frac{\partial v}{\partial \theta}\right) \quad (3)$$

$$\frac{\partial w}{\partial t}+u\frac{\partial w}{\partial r}+\frac{v}{r}\frac{\partial w}{\partial \theta}+w\frac{\partial w}{\partial z}=-\frac{1}{r}\frac{\partial p}{\partial z}+\frac{1}{Re}\left(\frac{\partial^2 w}{\partial r^2}+\frac{1}{r}\frac{\partial w}{\partial r}+\frac{1}{r^2}\frac{\partial^2 w}{\partial \theta^2}+\frac{\partial^2 w}{\partial z^2}\right) \quad (4)$$

II. Mass conversation law

$$\frac{\partial u}{\partial r}+\frac{u}{r}+\frac{1}{r}\frac{\partial v}{\partial \theta}+\frac{\partial w}{\partial z}=0 \quad (5)$$

In numerical computations, we assume that steady-state solutions have been obtained when residuals are under 10^{-4}.

- **Initial conditions**

We survey three kinds of initial conditions, Case 1, Case 2 and Case 3.

$$\text{Case 1}\begin{cases}u=0\\ v=0\\ w=0\end{cases}, \text{Case 2}\begin{cases}u=0\\ v=V(r,s)\\ w=0\end{cases}, \text{Case 3}\begin{cases}u=0\\ v=V(r,z)\\ w=0\end{cases}$$

In Case 3, a velocity component for the azimuthal direction, $V(r,z)$, is set as follows;

$$V(r,z)=\sum_{l=1}^{\infty}A_l J_1(k_1 r)\sinh(k_l z) \quad (6),$$

where A_l is a constant number, J_1 is Bessel function of the first kind and k_l is zero points. $V(r,z)$ is zero on the axis and nearly equals zero on the wall.

3 Results and future works

- $\boldsymbol{Re=50}$

I. It is considered that Case 1 and Case 2 are the same distributions.
II. It is expected that flow fields converged the same distribution assuming Case 1 or Case 2 as initial conditions.
III. A distribution of Case 3 is different from those of Case 1 and Case 2.

- $\boldsymbol{Re=1000}$

I. It is expected that Case 1, Case 2 and Case 3 are not the same distributions.

It is planned that future works will include numerical investigations with respect to various Reynolds numbers and aspect ratios.

References

1. "Analysis of vertical convections in a cylindrical coordinate", T. Nakazawa and H. Suito, Abstract of 2007 annual meeting of Japan society of fluid mechanics, 308 (2007).
2. "Note on a class of solutions of the Navier-Stokes equations representing steady rotation-ally-symmetric flow", G. K. Bathelor, Q. J. Mech. Appl. Maths., 4, 29-41 (1951).
3. "Analytical solution for a steady flow of enclosed rotating disks", A. Khalili and H.J. Rath, Z. angew Math Phys., 45, 670-680 (1994).
4. "The flow in a cylindrical container with a rotating end wall at small but finite Reynolds number", Benson K. Muite, Phys. Fluids, 16(10), 3614-3626 (2004).
5. "Numerical solution of the Navier-Stokes equations for flows in the disk-cylinder system", Hsien-Ping Pao, Phys. Fluids, 15 (1), 4-11 (1972).
6. "Transitions of axisymetric flow between two corotating disks in an enclosure", T. Miura and J. Mizushima, Fluid Dyn. Res., 39, 193-208 (2007).
7. "Three-dimensional instability of axisymmetric flow in circulating lid-cylinder enclosure", A. Y. Gelfgat, P. Z. Bar-Yoseph and A. Solan, J. Fluid Mech, 438, 363-377 (2001).
8. "Observations of the flow produced in a cylindrical container by a rotating endwall", M. P. Escudier, Exp. Fluids, 2, 179-186 (1984).
9. "Aerodynamics aspects of disk files", E. Lennemann, IBM J. Res Develop., 18(6), 480-488 (1974).

Optimal Solutions to the Infinite Horizon Optimization Problems

Dapeng CAI (Nagoya University, cai@iar.nagoya-u.ac.jp) and Takashi Gyoshin NITTA (Mie University, nitta@edu.mie-u.ac.jp)

For economic growth models with infinite planning horizon, the infinite series of utility sequences may diverge, rendering the "maximization" of which meaningless. The discounting approach, widely used in intertemporal economics, avoids this problem as the discounted integral of utilities becomes finite under the "relentless force of compound interest" (Weitzman, 1998). However, economists have long been scathing about the ethical dimensions and logical difficulties of discounting since Ramsey's time (Ramsey, 1928; Pigou, 1932; Solow, 1974; Heal, 1998).[1]

There has been a large literature that analyzes the undiscounted growth models. In Ramsey's original work, he formulated the problem as minimizing the deviation from a given reference curve, the "bliss level," which avoids the problem that the sum of the objective function may not converge. A more general approach was later introduced by Von Weizsächer (1965) and Atsumi (1965) and further refined by Gale (1967) and Brock (1970). This approach uses the concept of the overtaking criterion, which replaces the comparison of infinite sums with a comparison of finite partial sums. Under the assumption of the existence of such a given reference curve, the existence and dynamical properties of the resultant optimal path have been considered in, for example, Michel (1990), Durán (2000), Kamihigashi (2001), and Le Van and Morhaim (2006). However, few studies have proposed how to explicitly construct the optimal paths for the undiscounted infinite horizon problems. Gale (1967) could be considered as a basis

[1] Stern (2007) argues that when considering climate change, "we [should] treat the welfare of future generations on a par with our own".

for such an approach. However, it involves checking, together with other assumptions, the existence of an optimal stationary path, which may be impossible for most problems.

Cai and Nitta (2007) present an alternative approach that explicitly constructs the optimal paths for the discrete time undiscounted infinite horizon optimization problems. They conclude that under a fairly general condition, the conjecture that "the limit of the solutions for the finite problems is optimal for the infinite horizon problem" is correct for the undiscounted problem, in the sense of a modified overtaking criterion.[2] However, as their analysis focuses on a particular example of the undiscounted infinite horizon problems, their approach is not directly applicable to most other problems. This paper aims at improving the applicability of their approach by extending their model to one in which both the utility and the production functions are allowed to depend on time. As a result, our proof of the conjecture and the analysis cover both the undiscounted and the discounted cases. This enables us to examine the impacts of discounting. We show that the higher the level of the productivity, the higher are the stationary values in the steady state. Moreover, we see that at extremely low levels of productivity, when $t \to \infty$, capital approaches zero at a positive discount rate, and a positive value when the rate is zero. In other words, the effects of discounting may be most disastrous when the level of productivity is extremely low.

Besides the modified overtaking criterion, we also consider another intertemporal optimality criterion: the sum-of-utilities criterion. We clarify the conditions under which the limits of the solutions for the finite horizon problem is optimal among all attainable

[2] The conjecture has been around for a while. The case when the discount factor is less than one has been examined in, for example, Stokey and Lucas (1989). Proving the conjecture involves establishing the legitimacy of interchanging the operators "max" and "$\lim_{T\to\infty}$", which has been "more challenging than one might guess" for the discounted case (Stokey and Lucas, 1989).

paths for the infinite horizon problem in the sense of a modified overtaking criterion, as well as the conditions under which such a limit is the unique optimum under the sum-of-utilities criterion.

For Reference, Refer to Finished Papers

1. Cai, D. and Nitta, T. G. Limit of the Solutions for the Finite Horizon Problems as the Optimal Solution to the Infinite Horizon Optimization Problems, arXiv:0803.4050

2. Cai, D. and Nitta, T. G. Constructing the Optimal Solutions to the Undiscounted Continuous-Time Infinite Horizon Optimization Problems, arXiv:0803.4046

3. Cai, D. and Nitta, T. G. Treating the Future Equally: Solving Undiscounted Infinite Horizon Optimization Problems, arXiv:math/0701371

A binary digit of memory induced by multiple covalent modifications and its application to molecular rhythm

(多重分子修飾による記憶の誘導とその分子リズムへの応用)

Isamu Ohnishi （大西　勇）

(Collaborated by Kazumi Ebisu（胡子　和実）and Tatsuo Shibata（柴田　達夫）)

Department of Mathematical and Life Sciences
Graduate School of Science
Hiroshima University

(広島大学大学院理学研究科数理分子生命理学専攻)

1 Introduction

Life can be considered to be a complex, but delicate, sensitive, and efficient system of organism obtaining high reproducibility and high evolvability in order to grow up, to undergo metabolic change, to react to stimulation, to control its feature, and so forth. For embodying these purposes, it is important to memorize and to communicate information on the past about themselves as precisely as possible. An organism can survive more stably, if the memorization is more correctly and more steadily, and if the communication is more rapidly. It is considered that these characters must be realized by a combination of some biochemical reactions. Especially, it is important how a strage element is constructed in a cell. In this paper we propose a kind of standard structure of mathematical model constructing a binary digit of storage element in a cell by use of covalent modifications and analyse it to elucidate its characteristic and important properties.

We consider a simple two-state (S and T) model for receptor proteins. This is based on and is modified the model a little in the classical work of Professors S. Asakura and H. Honda [1], where they have originally considered about the problem of temporary reaction and post-adaptation process in a cell. S stands for a state which has accepted attractants and is likely to take a convalent modifier, and T stands for the opposite state. S receives convalent modifiers one by one in a definite order, while T releases them in the reverse order. There are n possibly modifying sites receiving convalent modifiers in a receptor protein. Here we assume that a very rapid equilibrium of S and T is realized according to the mass-action law. We change some of important parameters' directions to get a kind of hysterecally switching structure of steady states, which is a foundation on the desirable storage element. In fact, the receptor protein constructs a binary digit in such a way that a state taking more convalent modifiers than a threshold number is regarded as "1", the inverse state as "0". In order to realize it, there must be a kind of bistability and hysterically switching mechanism of the system. In order to get this desirable nature, we adjust paramerers in the system in which the equilibrium between S and T goes to S side more, when the receptor protein has more convalent modifiers, and vice versa. This can make a state changing hysterically according to quantity of attractants, and as a result, it can make a digitally switching function robustly.

One of our important and interesting points is a correlation between the number of the possibly modifying sites and a kind of stability of the storage element. We therefore investigate how the width of hysteresis range varies, as the number of the sites tends larger. The result is that the wider the hysteresis range is, the bigger the number is. Thus it is considered that the existence of a lot of sites contributes the stability of the storage element. In order to verify usefulness of this fact more concretely, for example, later in §**??**, we apply this model to the phosphorylation–dephosphorylation circadian rhythm of clock proteins of *cyanobacteria*. *Cyanobacteria* are among the simplest organisms that show circadian rhythm. As this model is coupled with equations of attractants and repellents adequately as in Fig.2 and as time constant moves appropriately, the system undergoes Hopf bifurcation to get a time periodic solution, and moreover, the periodic solution survives more robustly, as the number of sites is larger. In a consequence, we elucidate a piece of significant meaning of existence of a lot of sites in the receptor protein. In fact, in the case of circadian rhythm of *cyanobacteria* (See for the details in [16], and [12]), a receptor protein monomer has two sites and it usually composes a hexamer, so that there are 12 sites per a hexamer of recepter protein. It seems that there is slightly many modification sites, but this contributes a stable oscillation daily. In our study, we ensure this fact by use of both deteministic and stochastic ways of simulations here. These two ways are not conflict with each other, but rather, these work to complement to each other. In fact, generally speaking, there may be fewer genes, proteins, and molecular than we can discuss about some qualitative and quantitative properties in a cell. In the case, it seems that we can hardly apply the model of differential equations to the interesting object. But in this paper, we ensure that the system preserves the hystrecally switching structure and robustness of time-periodical behavior of solutions even in the corresponding model system of stochastic way. Moreover, we compute the average and variance of rotation number of the time-periodical solutions of the stochastic model to verify the advantage of a lot of site numbers.

After we saw a kind of structural stability of the system in noisy field of biochemical reaction by poisson process simulation, we investigate several qualitative properties corresponding to some facts of biochemical experiments, for example in [4, 5, 6, 12, 16], by use of the system of the differential equations. Qualitative research for our system has meaning because of a paper of Kitayama et. al[6] in which it is seen that more than 10000 molecules of KaiA, KaiB, and KaiC exist in a cell of *cyanobacteria*, respectively. Then, *rescaling covariance property* is very useful. In fact, our system of equations has a kind of covariance according to rescaling the system. We call this covariance *rescaling covariance property* in this paper. This property permit rigorously and clearly that change of some reaction constants is restate by change of the total mass of some target proteins. We use this property of the system to understand that the system has oscillation solutions with same period in various ratios of total mass of the clock proteins under consideration, although some reaction coefficients should be changed appropriately. But only a few parameters should be changed here. *rescaling covarience property* is convenient for discussion because in simulation we are easy to change total values of proteins with preserving the hysterecal structure, and on the other hand, in biochemical experiment, they are easy to change reaction constants by use of mutants.

Furthermore, by *rescaling covariance property*, we can discuss about the period's varying according to changing environment. For example, surely, in constant dark condition, all the transcriptions and translations cease in *cyanobacteria*, but in natural condition, the ratio of all the clock proteins changes through the day. In spite of it, the circadian rhythm of phosphorylation–dephosphorylation in *cyanobacteria* is very stable. If there is a function adjusting the reaction parameters appropriately according to altering the conditions in *cyanobacteria*, then this kind of stability can be comprehensible by applying *rescaling covariance property*. In fact, at least in *cyanobacteria*, it is said that parameters can be adaptive to environment. *rescaling covariance property* can predict how parameters should change in a simple and clear manner. Moreover, we may also understand the temperature compensation in circadian rhythm of *cyanobacteria*, if the adjusting function works well for changing temperature. Finally, we remark that we do not take the re-regulation by light into account. Light makes the phase modulated and re-regulated in circadian rhythm by use of another principle, what is called phase syncronizing phenomena, whose effect is not considered in our system.

References

[1] S. Asakura and H. Honda, *Two-state Model for Bacterial Chemoreceptor Proteins –The Role of Multiple Methylation–*, J. Mol. Biol., **176** (1984), pp. 349-367.

[2] E. Emberly, and N. S. Wingreen,, Phys. Rev. Lett., **96** :038303.

[3] D. B. Forger, and C. S. Peskin, *A detailed predictive model of the mammalian circadian clock*, PNAS, **100** vol. 25 (2003), pp. 14806-14811.

[4] M. Ishiura, S. Kutsuna, S. Aoki, H. Iwasaki, C. R. Andersson, A. Tanabe, S. S. Golden, C. H. Johnson and T. Kondo, *Expression of a gene cluster kaiABC as a circadian feedback process in cyanobacteria*, Science, **281** (1998), pp. 1519-1523.

[5] H. Iwasaki, T. Nishiwaki, Y. Kitayama, M. Nakajima and T. Kondo, *KaiA-stimulated KaiC phosphorylation in circadian timing loops in cyanobacteria*, PNAS, **99** (2002), pp. 15788-15793.

[6] Y. Kitayama, H. Iwasaki, T. Nishiwaki and T. Kondo, *KaiB functions as an attenuator of KaiC phosphorylation in the cyanobacterial circadian clock system*, EMBO Journal, **21** (2003), pp. 2127-2134.

[7] G. Kurosawa, and Y. Iwasa, *Temperature compensation in circadian clock models*, J. Theor. Biol., **233** (2005), pp. 453-468.

[8] G. Kurosawa, A. Mochizuki, and Y. Iwasa, *Comparative study of circadian clock models, in seach of process promoting oscillation*, J. Theor. Biol., **216** (2002), pp. 193-208.

[9] G. Kurosawa, K. Aihara, and Y. Iwasa, *A model for the circadian rhythm of Cyanobacteria that maintains oscillation without gene expression*, Biophysical J., **91** (2006), pp. 2015-2023.

[10] A. Mehra, C.I. Hong, M. Shi, J. J. Loros, J.C. Dunlap, P. Ruoff , PLoS. Comput. Biol., **2** (2006), e96.

[11] T. Nakahira, M. Katayama, H. Miyashita, S. Kutsuna, H. Iwasaki, H. Oyama, and T. Kondo, , PNAS, **101**(2002), pp. 881-885.

[12] M. Nakajima, K. Imai, H. Ito, T. Nishiwaki, Y. Murayama, H. Iwasaki, T. Oyama and T. Kondo, *Reconstitution of Circadian Oscillation of Cyanobacterial KaiC Phosphorylation in vitro*, Science, **308** (2005), pp. 414-415.

[13] T. Nishiwaki, Y. Satomi, M. Nakajima, C. Lee, R. Kiyohara, H. Kageyama, Y. Kitayama, M. Temamoto, A. Yamaguchi, A. Hijikata, M. Go, H. Iwasaki, T. Takao and T. Kondo, *Role of KaiC phosphorylation in the circadian clock system of Synechococcus elongatus PCC 7942*, PNAS, **101**(2004), pp. 13927-13932.

[14] P. Ruoff, J. J. Loros, and C. Dunlap, *The relationship beween FRQ-protein stability and temperature compansation in the Neurospoura circadian clock*, PNAS, **102** vol. 49 (2005), pp. 17681-17686.

[15] H. Takigawa-Imamura, and A. Mochizuki, *Transcription autoreguration by phosphorylated and non-phosphorylated KaiC in Cyanobacterial circadian rhythm*, J. Theor. Biol., **241** (2006), pp. 178-192.

[16] J. Tomita, M. Nakajima, T. Kondo and H. Iwasaki, *No Transcription-Translation Feedback in Circadian Rhythm of KaiC Phosphorylation*, Science, **307** (2005), pp. 251-254.

[17] J. J. Tyson, K. C. Chen, and B. Novak, *Sniffers, buzzers, toggles and blinkers: dynamics of reguratory and signaling pathways in the cell*, Curr. Opin. Cell Biol.,, **15** (2003), pp. 221-231.

[18] M. Yoda, K. Eguchi, T. Terada and M. Sasai, *Monomer-Shuffling and allosteric transition in KaiC circadian oscillation*, Plos One, **5** (2007), pp. 1-8.

[19] J. S. Zon, D. K. Lubensky, P. R. H. Altena, and P. R. Wolde, *An allosteric model of circadian KAiC phosphorylation*, PNAS, **104** (2007), pp. 7420-7425.

Real option valuation of social systems

Kazumichi Ohtsuka[1] and Katsuhiro Nishinari[1, 2]

[1]*Dep. Aeronautics and Astronautics Engineering, University of Tokyo 7-3-1, Japan*

[2]*PRESTO, Japan Science and Technology Corporation, Japan*

I. INTRODUCTION

We introduce, in this paper, the method that identifies net present values of a queue by using a real option approach. The queueing model which we employ here is the one dimensional ASEP with open boundaries. This model shows various phenomena even though their interaction rules are simple. In particular, the ASEP forms a shock front (domain wall) under restricted boundary conditions. Motion of the domain wall follows a biased random walk [1]. Hence we apply the concepts of a real option approach[2–4] to estimate length change of a queue. Our approach make it possible to give a quantitative worth of present congestions.

II. ANALOGY BETWEEN THE ASEP AND REAL OPTION CONCEPT

We consider, in this article, the evaluation of congestion. For simplicity, we employ the one-dimensional ASEP as the model of a queuing system and apply this to pricing of a queue. At the boundaries of this system, particles are supplied at the left end with α, and removed at the right end with β. According to Ref. [1], motion of the domain wall to the left at rate α or to the right at rate β, so that the domain wall does a biased random walk with drift velocity $V = \beta - \alpha$ and diffusion coefficient $D = (\alpha + \beta)/2$. Positive (negative) values of velocity are defined that the domain wall moves to the left (right) boundary

Assume that the stochastic process $X(t)$, the length of a queue, follows an arithmetic Brownian motion:

$$dX = \mu dt + \sigma dz, \tag{1}$$

where μ is the drift of the domain wall per unit time, σ is the instantaneous standard deviation per unit time, and dz is the increment of a standard Wiener process. In the domain wall framework, μ and σ corresponds to $V = \beta - \alpha$ and $D = (\alpha + \beta)/2$ respectively. It means that values of a queue tail primarily depend both on entering and exit rates at boundaries. Note that our main interest is on changes of a queue length itsself, not on percentage changes (not on an geometric Brownian motion).

We define degree of human clogging as $\pi = X(t) - I$. The value π is a indicator which shows congestion (free flow) when its values are positive (negative). The variable I fixed at 0.5 which means a threshold queue length equal to half of the system size. In other word, we defined a queue is crowded when π is positive. Therefore, instant clogging from a queue, which we consider, is given by

$$\pi(X) = \max[X - I, 0]. \tag{2}$$

The value of a queue at time t can be expressed as the sum of the instantaneous clogging over the interval (t, dt) and the continuation value beyond $t + dt$. The value of queue is

$$J(x) \;=\; \pi(X)dt + e^{-\rho dt}E[J(X + dX)]. \tag{3}$$

To express weight of time, J is discounted at the rate ρ. Expanding the right-hand side using Ito's Lemma, we have

$$J(x) \;=\; \pi(X)dt + (1 - \rho dt + o(dt))[J(x) + J'(x)\mu dt + \frac{\sigma^2}{2}J''(x)dt + o(dt)], \tag{4}$$

where $o(dt)$ collects terms that go to zero faster than dt. Simplifying, dividing by dt, and $dt \to 0$, we get the differential equation

$$\frac{1}{2}\sigma J(X)'' + \mu J(X)' - \rho J(X) + \pi(X) = 0. \tag{5}$$

The solution of Eq. (5) can be written as where The solution of Eq. (5) can be written as

$$J(X) \;=\; \begin{cases} \frac{C_3 I}{\rho}\exp\Big(-\frac{\mu}{\sigma^2}(X-I)\Big)\sinh\Big(C_2 X\Big) & X < I \\ \Big[\frac{C_3 I}{\rho}\sinh\Big(C_2 I\Big) - \frac{\mu}{\rho^2}\Big]\exp\Big[-(C_1+C_2)(X-I)\Big] + \frac{X-I}{\rho} + \frac{\mu}{\rho^2} & X \geq I \end{cases}$$

where

$$C_1 \;=\; \frac{\mu}{\sigma^2},\; C_2 = \frac{\sqrt{\mu^2 + 2\rho\sigma^2}}{\sigma^2},$$

$$C_3 \;=\; \Big\{\frac{\sqrt{\mu^2 + 2\rho\sigma^2}}{\sigma^2}\exp\Big(\frac{\sqrt{\mu^2 + 2\rho\sigma^2}}{\sigma^2}I\Big) + \Big(\frac{\sqrt{\mu^2 + 2\rho\sigma^2} + \mu}{\sigma^2}\Big)\frac{\mu}{\rho^2}\exp\Big(\frac{\mu I}{\sigma^2}\Big)\Big\}^{-1}.$$

Note that the term $[(X_0 - I)/\rho] + \mu/\rho$ in the solution is the expected value of stream π when initial level is X_0. This is the net present value (NPV) of a queue obtained by

$$\text{NPV} = \int_0^\infty e^{-\rho t}\Big(X(t) - I\Big)dt = \frac{X_0 - I}{\rho} + \frac{\mu}{\rho}. \tag{6}$$

III. NONLINEAR PROPERTY OF REAL OPTION EVALUATION

To examine the relationship between J and the parameters, α and β dependences of J are plotted in Figs. 1(a) and 1(b). Figures show J does not have linear dependence on both parameters. For example, in Fig. 1(b), J does not monotonically decreases with β even if an exit rate of the system are increased. It means that a clogging of human flow (cumulative jamming signals) has intrinsically nonlinear properties.

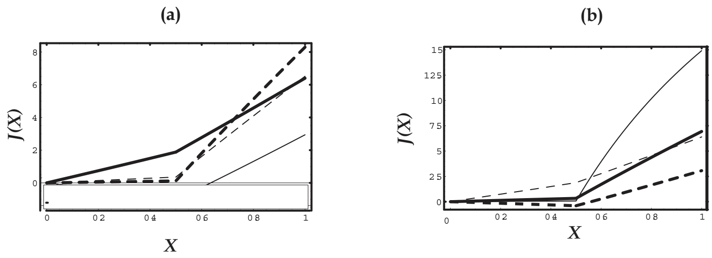

FIG. 1: (a)Dependence of $J(X)$ on α when (ρ, β, I)=(0.1, 0.25, 0.5). Thin solid line, thick solid line, thin dotted line and thick dotted line correspond to $\alpha = 0.2$, 0.25, 0.3 and 0.4. (b)Dependence of $J(X)$ on β when (ρ, α, I)=(0.1, 0.25, 0.5). Thin solid line, thick solid line, thin dotted line and thick dotted line correspond to $\beta = 0.1$, 0.2, 0.25 and 0.35

[1] Kolmeisky, A.B., Schütz, G.M., Kolmeisky, E.B., Straley, J. P.: Phase diagram pf one-dimensional driven lattice gases with open boundaries. J. Phys. A: Math. Gen. 31, 6911-6919 (1998)

[2] Hull, J.: Options, Futures and Other Derivatives, 6th ed. Princentice-Hall, Englewood Cliffs, New Jersey (2005)

[3] Dixit, A.K., Pindyck, R.S.: Investment under uncertainty, Princeton Univ. Press (1994)

[4] Øksendal, B.: Stochastic Differential Equations: An Introduction with Applications, 6th ed. Springer (2003)

Modelling forest transition: Bistability of forested and abandoned landscapes

Akiko Satake[1], and Thomas K. Rudel[2]

[1]*Creative Research Initiative Sousei, Hokkaido University, Sapporo, 001-0021.* [2]*Departments of Human Ecology and Sociology at Rutgers University, Rutgers University, NJ, USA.*

A historical generalization about forest cover change in which rapid deforestation gives way over time to forest restoration is called "the forest transition". Prior research on the forest transition leaves three important questions unanswered. (1) How does forest loss influence an individual landowner's incentives to reforest? (2) How does the forest recovery rate affect the likelihood of forest transition? (3) What happens after the forest transition occurs? The purpose of this paper is to develop a minimum model of the forest transition to answer these questions (Satake and Rudel, 2007). We assume that a forest is composed of many land parcels, each of which is in one of a finite list of land-use states. The land-use state of each land parcel changes stochastically. The transition probability is determined by two processes: the forest succession and the decision of landowners. The landowner tends to choose the land-use state which has a high expected discounted utility, i.e., the sum of the current and the future utilities of the land parcel. Landowners take the likelihood of future landscape changes into account when making decisions. We focus on a three-state model in which forested, agricultural, and abandoned states are considered (Figure). We assume that deforestation caused by landowners' decisions and forest regeneration initiated by agricultural abandonment have aggregated effects that characterize entire landscapes. These effects include feedback mechanisms called the 'forest scarcity' and 'ecosystem

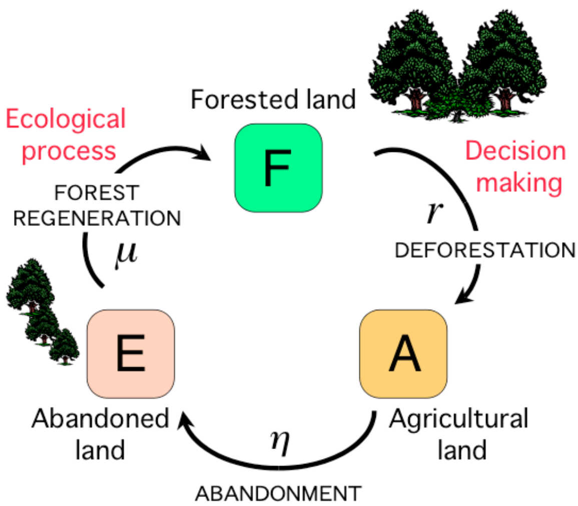

service' hypotheses. In the forest scarcity hypothesis, forest losses make forest products scarcer which increases the economic value of forests. In the ecosystem service hypothesis, the environmental degradation that accompanies the loss of forests causes the value of ecosystem services provided by forests to decline. We examined the impact of each mechanism on the likelihood of forest transition through an investigation of the equilibrium and stability of landscape dynamics. We found that the forest transition occurs only when landowners employ a low rate of future discounting. After the forest transition, regenerated forests are protected in a sustainable way if forests regenerate slowly. When forests regenerate rapidly, the forest scarcity hypothesis expects instability in which cycles of large-scale deforestation followed by forest regeneration repeatedly characterize the landscape. In contrast, the ecosystem service hypothesis predicts a catastrophic shift from a forested to an abandoned landscape when the amount of deforestation exceeds the critical level, which can lead to a resource degrading poverty trap. These findings imply that incentives for forest conservation seem stronger in settings where forests regenerate slowly as well as when decision makers value the future.

Reference

Satake, A., Rudel, T.K., 2007. Ecological Applications 17, 2024-2036.

Activities of Algicidal Bacteria and Their Influences on Microbial Communities

Kenichi SHIBATA[1], Takashi AMEMIYA[1], Kiminori ITOH[2]

1. Graduate School of Environment and Information Sciences, Yokohama National University, 79-7 Tokiwadai, Hodogaya-ku, Yokohama, 240-8501, Japan.
2. Graduate School of Engineering, Yokohama National University, 79-7 Tokiwadai, Hodogaya-ku, Yokohama, 240-8501, Japan.

It is said that algicidal bacteria can be used as biological control agents for algal blooms. We examined influences of algicidal bacteria on microbial communities in a laboratory experiment as a first step of ecological risk assessment. A microcosm, which consists of wild protozoa, bacterioplankton, and cultured *Microcystis aeruginosa* NIES 99, was constructed as a model microbial ecosystem of eutrophic lakes with algal blooms. *Lysobacter enzymogenes* subsp. *enzymogenes* AL-1 (DSM 1895) was added to the microcosm as an algicidal bacterium. Ciliates, flagellates, fungi, and *M. aeruginosa* NIES 99 were observed in control runs. In the runs with *L. enzymogenes* AL-1, although *M. aeruginosa* NIES 99 was not lysed, the other microbes disappeared. We address that applications of algicidal bacteria to actual lakes are considered to be ecologically risky contrary to the previous ideas.

Toxic cyanobacterial blooms have been widespread in lakes, reservoirs, and rivers throughout the world. The blooms cause livestock death and threaten human health and aquatic ecosystems[1]. Although several approaches have been proposed to eliminate the blooms, those approaches were hardly successful. There is no complete way to remove them. Therefore, we need various approaches to devise multiple strategies.

There are algicidal bacteria that kill algae and can be used as biological control agents. However, applications of algicidal bacteria for actual lakes or rivers may destroy the ecosystems. Since they can lyse several other microbes [2, 3, 4]. Nevertheless, there are no study for ecological risks of algicidal bacteria. We have microscopically observed the influences of algicidal bacteria on the microbial community using microcosms as a first step of ecological risk assessment.

Materials and Methods

Influences of algicidal bacteria on microbial community. *Microcystis aeruginosa* NIES 99 (obtained from microbial culture collection at national institute for environmental studies) was used as an algal bloom forming alga, and *Lysobacter enzymogenes* subsp. *enzymogenes* AL-1 DSM 1895 (obtained from Deutsche Sammlung von Mikroorganismen und Zellkulturen GmbH, abbreviate to AL-1) was used as an algicidal bacterium[3]. *M. aeruginosa* NIES 99 were routinely cultured in MA medium at 25℃ under 12 hours : 12 hours light-dark cycle. AL-1 was routinely cultured on trypticase soy agar.

Lake water was obtained from Lake Sagami (Kanagawa prefecture, Japan), and river water was obtained form Katsuragawa River, the upstream of Lake Sagami. The total nitrogen (TN) and total phosphorus (TP) were 3.78 ppm and 0.2 ppm respectively. The TN and TP of river water were adjusted to 1.6 ppm and 0.16 ppm by sodium nitrate and dipotassium hydrogen phosphate respectively.

M. aeruginosa NIES 99 was mixed with 1,200 ml of lake water, which was filtered through a sterile 5 μm filter, in a 2,000 ml Erlenmeyer flask. This microcosm was incubated over night. The microcosm was dispensed into four 500 ml Erlenmeyer flasks. The volumes were 270 ml for each.

Thirty milliliter of AL-1 stored in sterile distilled water (DW) for 3 days was added to two microcosms, and river water was added to another two microcosms as controls. Final concentrations of AL-1 were approximately 10^{10} cells/ml.

The compositions of microbes were observed by a phase-contrast microscope.

Testing conditions where algicidal bacteria are activated. AL-1 did not kill *M. aeruginosa* NIES 99 in the above experiment. Thus, we also examined the conditions where AL-1 kills *M. aeruginosa* NIES 99.

Seven condition were tested (Fig. 1). Shortly, 3 culture media (Fig.1 (i-a), (i-b), and (i-c)), 2 suspending solutions (Fig. 1 (ii-a) and (ii-b)), and 2 durations of starvation (Fig. 1 (iii-a) and (iii-b)) were tested.

Axenic *M. aeruginosa* NIES 99 was used to test the algicidal activities. Cultured *M. aeruginosa* NIES 99 was centrifuged at 5000 rpm (approx. 5000 × g) for 15 min. The supernatant was discarded and fresh MA medium was added onto the pellet. The pellet was broken down by pipetting. The concentration of *M. aeruginosa* NIES 99 was

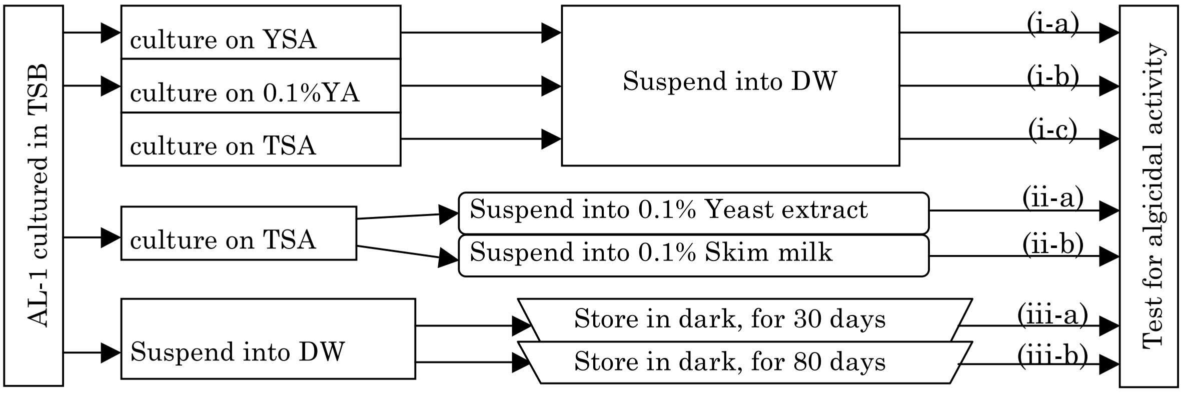

Fig.1 Seven conditions were tested. AL-1 was precultured in TSB (Torypticase Soy Broth). AL-1 was cultured (i-a) on YSA (Yeast extract Skim milk Agar) and suspended in to DW, or (i-b) on 0.1% YA (0.1% Yeast extract Agar) and suspended in to DW, or (i-c) on TSA (Trypticase Soy Agar) and suspended in to DW, then tested the algicidal abilities. AL-1 was cultured on TSA and (ii-a) suspended into 0.1% Yeast extract, or (ii-b) suspended into 0.1% Skim milk, then tested the algicidal abilities. AL-1 was cultured on TSA, suspended into DW, and stored in the dark at room temperature (iii-a) for 30 days or (iii-b) for 80 days.

adjusted to 1.5×10^5 cells/ml by adding fresh MA medium. Ten ml of it was dispensed into 30 ml test tubes. One ml of AL-1 under each conditions were added to the test tubes. The concentration of *M. aeruginosa* NIES 99 were measured for 3 days. Sterile DW was added to it instead of AL-1 as a control.

RESULTS

Influences of algicidal bacteria on microbial community. Flagellates, ciliates, yeasts, filamentous organisms, bacteria, and *M. aeruginosa* NIES 99 were observed in the control runs at the third day. Some of the microbes were showed in Fig. 1.

However, only small bacteria-like particles and some fine filaments, which might be some parts of filamentous organisms, were observed in runs with AL-1 (Fig. 2). Furthermore, *M. aeruginosa* NIES 99 increased from 1.75×10^5 cells/ml to 2.82 cells/ml (control : to 1.65 cells/ml).

Testing conditions where algicidal bacteria are activated. *M. aeruginosa* NIES 99 were increased after additions of AL-1 shortly after cultivation on any culture media (Fig. 4 (i-a), (i-b), and (i-c)).

Mixtures of AL-1 and 0.1% yeast extract decreased *M. aeruginosa* NIES 99 to 21% of control at 3rd day (Fig. 4 (ii-a)). mixtures of AL-1 and skim milk inhibited *M. aeruginosa* NIES 99 (Fig. 4 (ii-b)). The concentrations were 75% of control at 3rd day.

In runs with AL-1 stored for 30 days in DW, *M. aeruginosa* NIES 99 were not observed at the 3rd day (Fig. 4 (iii-a). AL-1 stored in DW for 80 days inhibited the growth of *M. aeruginosa* NIES 99 (iii-b). The concentrations of *M. aeruginosa* NIES 99 were 73% of control at 3rd day.

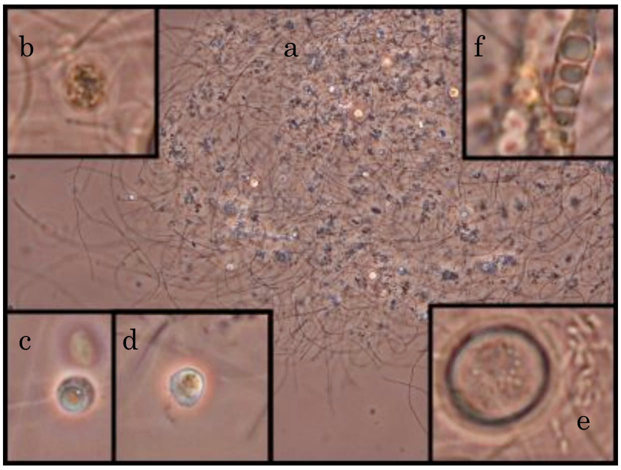

Fig. 2 The pictures of microbes observed in the control runs. a: biofilm (×400), b: *M. aeruginosa* NIES 99 (×1000), c and d: *Monas* spp. (×1000), e: yeast and some bacteria (×1000), f: fungi (×1000). The organisms showed in c to f were observed in or around the biofilms (a).

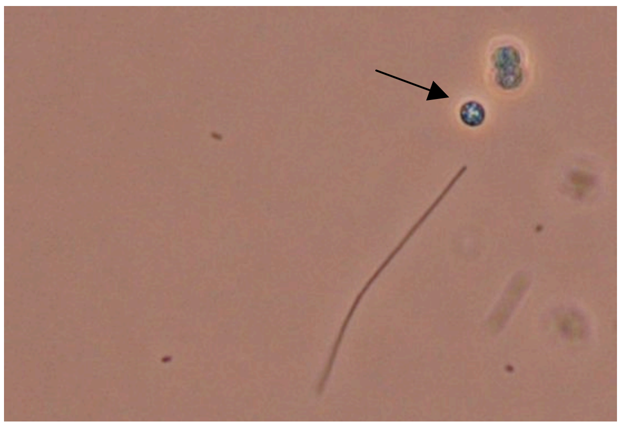

Fig. 3 The picture of microbes observed in the runs with AL-1. Only some filaments, bacteria-like particles, and *M. aeruginosa* NIES 99 (indicated by an arrow) were observed in runs with AL-1 (×400). Nonetheless, the other organisms were not observed at all.

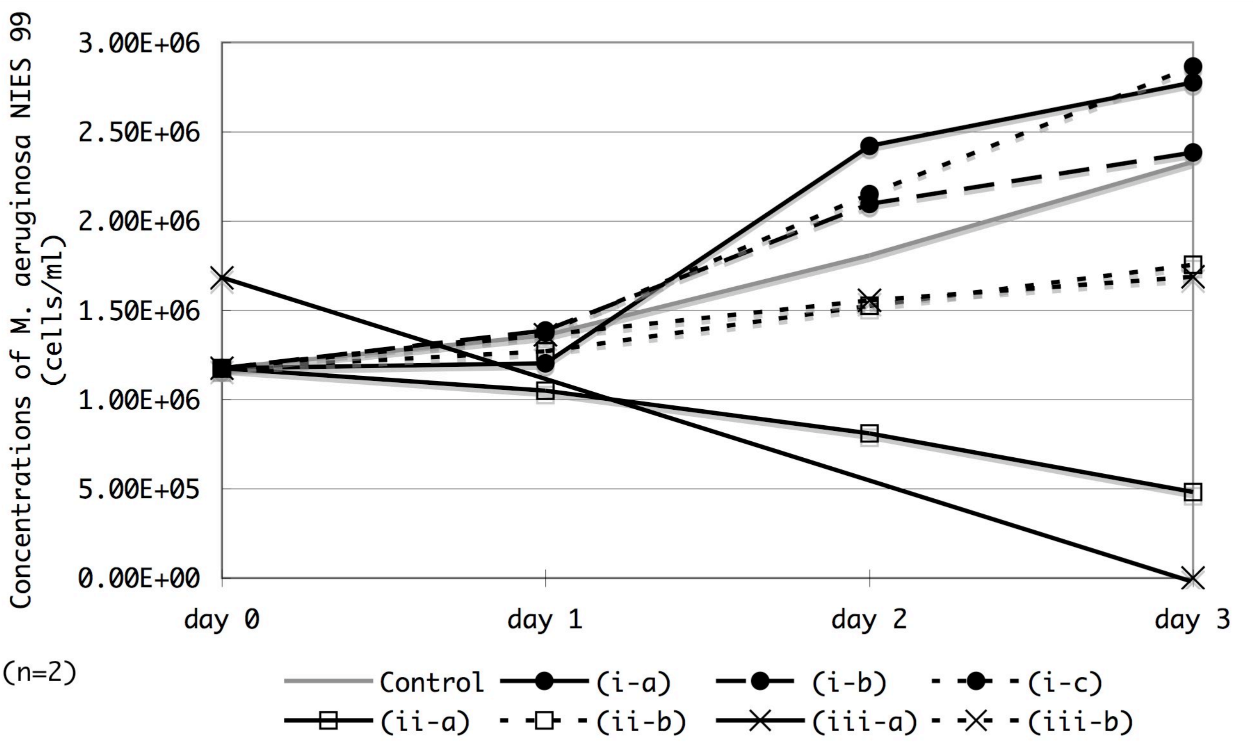

Fig.4 The changes of concentrations of *M. aeruginosa* NIES 99. (i-a), (i-b), (i-c), (ii-a), (ii-b), (iii-a), and (iii-b) are same as Fig.1. DW was added instead of AL-1 in control.

DISCUSSION

Influences of algicidal bacteria on microbial community. Although AL-1 did not lysed *M. aeruginosa* NIES 99; ciliates, flagellates, yeasts, and fungi were lysed. These microbes play important roles on nutrient cycle. Consequently, this would result stagnations of nutrient cycle and large amount of detritus. Moreover, some of the microbes are known as predators of phytoplankton. For instance, *Monas* spp. (Fig. 2 c and d) are predators of *Microcystis*[6]. Therefore, addition of algicidal bacteria might cause increase of algal bloom. Furthermore, extinction of these microbes provides chances of mass propagations for surviving phytoplankton, and results only a shift of its algal composition without eliminating it.

The influences of algicidal bacteria on microbial communities are clearly hazardous. We need to address the influences, and assess the risks.

Testing conditions where algicidal bacteria are activated. AL-1 did not decreased *M. aeruginosa* NIES 99 shortly after cultivation on any agar media. They need to be under specific conditions to decrease *Microcystis* spp.

They decreased *M. aeruginosa* NIES 99 with dilute yeast extract. This was reported that the AL-1 lyses various bacteria that cultured in 1% yeast extract broth[2].

Some of algicidal bacteria related with *Lysobacter* or *Myxobacter* secrete proteolytic enzyme[2]. Those enzyme are known as one of algicidal substances. Since skim milk is protein, they secrete proteolytic enzyme to digest it. However, AL-1 with 0.1% skim milk slightly inhibited *M. aeruginosa* NIES 99, but did not decrease them. AL-1 would need other substances that helps proteolytic enzyme to lyse *M. aeruginosa* cells, or have other mechanisms to kill them.

AL-1 drastically lysed *M. aeruginosa* NIES 99 in 3 days after 30 days storage in DW. Starvations are effective stimulating method of algicidal ability. However, AL-1 stored for 80 days only inhibited and could not decrease them. Excessive starvations deactivate the algicidal ability. There must be an optimal duration of starvation.

Eventually, adding yeast extract and 30 days starvation were effective. However, additions of yeast extract causes further eutrophication of the lakes. Thus, storage in DW is thought to be useful activating method. Nonetheless, the minimal concentrations of AL-1 to lyse *M. aeruginosa* NIES 99 are too high to apply actual lakes. We need to isolate effective algicidal bacteria. These activating methods would roughly apply to the other algicidal bacteria.

REFERENCES

1) I. Chorus, *et al.* (2000) *J Toxicol Environ Health B*, **3**, 323.
2) J. C. Ensign and R. S. Wolfe (1965) *J Bacteriol*, **90**, 395.
3) M. Shilo (1970) *J Bacteriol*, **104**, 435.
4) J. R. Stewart *et al.* (1969) *Science*, **164**, 1523.
5) J. R. Stewart (1971) *Arch Microbiol*, **80**, 176.
6) T. Saito (2003) *Environ Technol*, **24**, 143.

Motion of Aquatic Plants Interacting with Water Flows

H. Suito *† and K. Tanino*
* Graduate School of Environmental Science, Okayama University, Japan,
† JST PRESTO researcher

1 Introduction

In this study, an interaction between motions of sea grasses and sea water flows is studied numerically in order to optimize the way of transplanting sea grasses. Transplantation of sea grasses is widely tried in many places in Japan because sea grass field is playing a very important role in coastal ecosystems: it yields oxygen by photosynthesis, provides egg-laying site for fishes, and so on. However, it has been widely lost by shore protection works, reclamation works, and etc. The objectives of this study are to simulate motions of sea grasses by wave actions and to provide useful information to transplantation of sea grasses.

2 Governing Equations

2.1 Motion of a sea grass

A Motion of a sea grass is assumed to be governed by the following balance equation;

$$\rho_a \frac{\partial^2 \boldsymbol{x}}{\partial t^2} + c_a \frac{\partial \boldsymbol{x}}{\partial t} + EI \frac{\partial^4 \boldsymbol{x}}{\partial s^4} - \frac{\partial}{\partial s}\left(T \frac{\partial \boldsymbol{x}}{\partial s}\right) = \boldsymbol{f}, \tag{1}$$

where $\boldsymbol{x}$ is a position vector at s, c_a is a dumping coefficient, EI is a bending stiffness and T is a tension along the plant body. A sea grass is assumed to be incompressible;

$$\left|\frac{\partial \boldsymbol{x}}{\partial s}\right|^2 = 1 \tag{2}$$

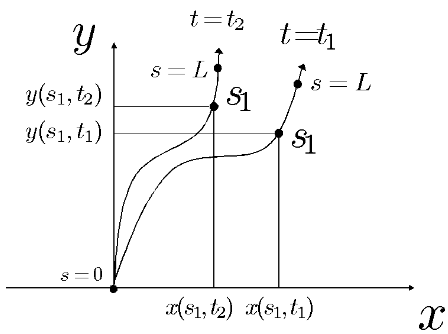

Figure 1: Geometry

Equations (1) and (2) are discretized for time as follows;

$$\rho_a \frac{\boldsymbol{x}^{n+1} - 2\boldsymbol{x}^n + \boldsymbol{x}^{n-1}}{\Delta t^2} + c_a \frac{\boldsymbol{x}^{n+1} - \boldsymbol{x}^n}{\Delta t} + EI \frac{\partial^4 \boldsymbol{x}^{n+1}}{\partial s^4} - \frac{\partial}{\partial s}\left(T^{n+1} \frac{\partial \boldsymbol{x}^{n+1}}{\partial s}\right) = \boldsymbol{f}^n, \tag{3}$$

$$\left|\frac{\partial \boldsymbol{x}^{n+1}}{\partial s}\right|^2 = 1 \tag{4}$$

Then, by taking the inner product between (3) and $\frac{\partial \boldsymbol{x}^{n+1}}{\partial s}$, differentiating it with respect to s, and substituting (4) into it, an equation for the tension T^{n+1} is obtained;

$$\frac{\partial^2 T^{n+1}}{\partial s^2} - T^{n+1}\left(\frac{\partial^2 \boldsymbol{x}^{n+1}}{\partial s^2}\right)^2 = \frac{\rho_a}{\Delta t^2}\left(1 - 2\frac{\partial \boldsymbol{x}^{n+1}}{\partial s} \cdot \frac{\partial \boldsymbol{x}^n}{\partial s} + \frac{\partial \boldsymbol{x}^{n+1}}{\partial s} \cdot \frac{\partial \boldsymbol{x}^{n-1}}{\partial s}\right)$$
$$+ \frac{c_a}{\Delta t}\left(1 - \frac{\partial \boldsymbol{x}^{n+1}}{\partial s} \cdot \frac{\partial \boldsymbol{x}^n}{\partial s}\right) + EI \frac{\partial^4 \boldsymbol{x}^{n+1}}{\partial s^4} \cdot \frac{\partial \boldsymbol{x}^{n+1}}{\partial s} - \frac{\partial \boldsymbol{f}^n}{\partial s} \cdot \frac{\partial \boldsymbol{x}^{n+1}}{\partial s} \tag{5}$$

2.2 Motion of sea water

A motion of sea water around sea grasses are governed by incompressible Navier-Stokes equations;

$$\frac{\partial \boldsymbol{u}}{\partial t} + (\boldsymbol{u} \cdot \nabla) = \frac{1}{\rho_w} \nabla p + \nu \nabla^2 \boldsymbol{u} - c\chi(\boldsymbol{u} - \boldsymbol{u}_a), \tag{6}$$

$$\nabla \cdot \boldsymbol{u} = 0, \tag{7}$$

where the existence of sea grasses is represented by fictitious domain method. χ is a characteristic function of sea grasses and $\boldsymbol{u}_a$ is the moving velocity of sea grasses. External force f in the motion equation for the sea grass is computed by an integration of pressure p around the plant body and a gravitational force.

3 Numerical Results

Figures (2), (3) and (4) show the shapes of sea grasses and velocity vectors of sea water.

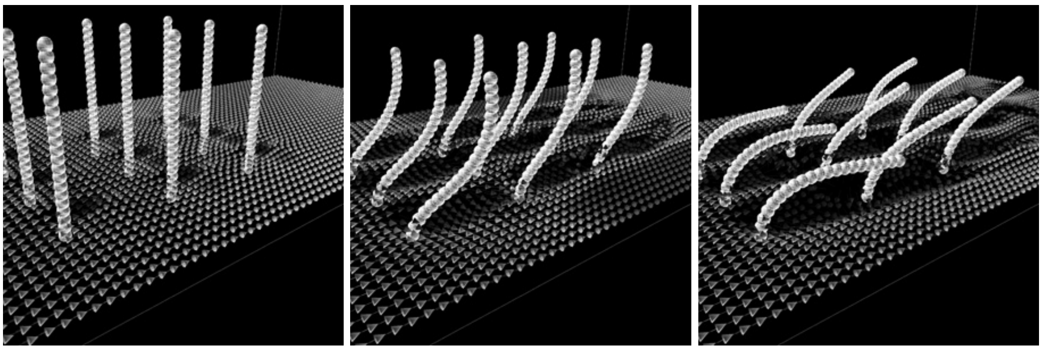

Figure 2: Shapes of sea grasses and a flow field (horizontal cross sections)

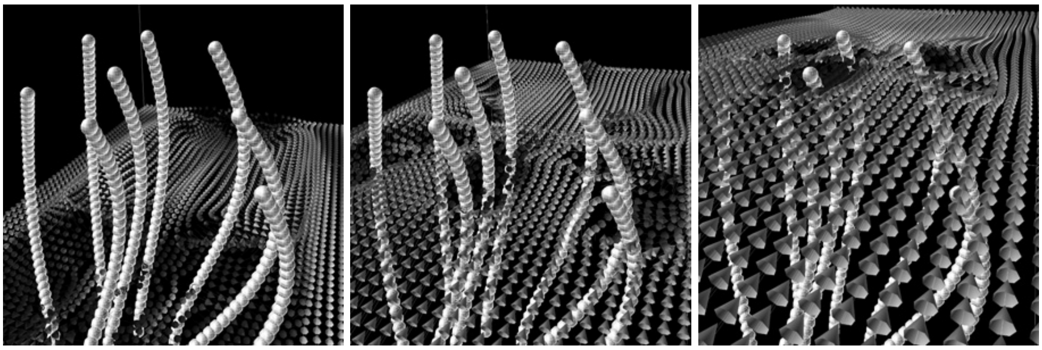

Figure 3: Shapes of sea grasses and a flow field (horizontal cross sections)

Figure 4: Shapes of sea grasses and a flow field (vertical cross sections)

4 Conclusions

In this study, a numerical model for computing the motions of sea grasses interacting with water flow is presented. Although further investigation for more accurate and realistic numerical model is required, this kind of simulation is expected to be helpful for understanding the mechanisms of its motion and to provide useful information to transplantation of sea grasses.

5 Acknowledgement

The authors would like to thank Prof. H. Tamaki at Ishinomaki-Senshu University for providing real-site data for sea grass fields.

References

[1] H. Kawarada and H. Suito: Numerical method for a free surface flow on the bases of the fictitious domain method, East-West J. Numer. Math., Vol. 5, No. 1, pp. 57-66, 1997

[2] S. Ikeda, T. Yamada, Y. Toda: Numerical study on turbulent flow and honami in and above flexible plant canopy, International Journal of Heat and Fluid Flow, Vol. 22, pp. 252-258, 2001

[3] H. Suito and H. Kawarada: Numerical simulation of spilled oil by fictitious domain method, Japan Journal of Industrial and Applied Mathematics, Vol. 21, No. 2, pp. 219-236, 2004

Fuel Loss and Jams due to Pausing Railroad Crossings

Akiyasu Tomoeda and Katsuhiro Nishinari
Department of Aeronautics and Astronautics,
Graduate School of Engineering, University of Tokyo,
and
PRESTO, Japan Science and Technology Corporation,
Hongo, Bunkyo-ku, Tokyo 113-8656, Japan.

Yoshiaki Harada
Member of the Diet, Liberal Democratic Party, Japan.
(Dated: July 9, 2008)

In Japan, all cars must pause before crossing the railroad for avoiding the accidents. This rule was established by a law in 1960. In fact, however, railroad crossings come to the serious bottlenecks because of this pausing rule and this bottleneck causes heavy jams. In this study, by using cellular automaton model we have investigated the traffic flow at railroad crossings in two cases: with pausing and without pausing. Moreover, the lost time due to pausing at railroad crossings have been also quantitatively estimated by both numerical simulations and analytical calculations. As the results, we have found that these estimations are good agreement with the data by actual measurements.

I. INTRODUCTION

In recent years, many kinds of environmental efforts have been made all over the world. One of the important challenges to prevent the environmental pollution is to reduce the traffic jams, since traffic jams make cars idle away and unwanted exhaust gas are emitted. In this study, we focus on the traffic flow at railroad crossings. In Japan, all cars must pause before crossing the railroad for avoiding the accidents. This rule was established by a law in 1960, since, at that time, the accuracy of crossing gates is insufficient. However, nowadays, the crossing gates have been grown in performance and the mechanical errors are more or less on naught. In order to abolishing the pausing rule, we contribute in terms of mathematical theory of "Jammology".

This paper is organized as follows, in Sec. 2 the surveys on railroad crossings are reported. In Sec. 3, one of the major traffic model, which is described as the stochastic cellular automaton model, is improved and applied to one-dimensional road where the railroad crossing are included. The results of numerical simulations and analytical calculations about traffic flow and lost time are shown in Sec. 4, and conclusions are given in Sec. 5.

II. SURVEYS ON RAILROAD CROSSINGS

TAB. I shows the number of top three accidents at railroad crossings. The leading case of railroad accidents is that cars are stuck on the railroad. This kind of accidents is actually caused by engine stall due to pausing and accounts for about half of the total number of accidents. Note that, the accidents due to neglect of pausing rule do not happen.

According to Japanese law, it is admitted as a special case that cars do not need to pause at the railroad crossing with traffic signal, when crossing gates are open and traffic signal is green. However, we have never seen that the signal is red and gate is open. From comparative table (TAB. II), there is no difference between the traffic signals and the crossing gates. Thus, it would not be an exaggeration to say that these plants result in the wasteful overlapping investment.

Accident Cases	Number
Be stuck by closed crossing gates	105
Ignore closed crossing gates	61
At railroad crossings without a security alarm	29

TABLE I: The number of accidents about the top three

Traffic Light	Green	Yellow	Red
Railroad Crossing	Open	Alarm	Close

TABLE II: Comparative table between traffic signals and railroad crossing

In terms of traffic flow, abolishing the pausing rule leads to removing the bottleneck and doubling the traffic flow, which has major economic effects (two hundred billion yen) as well as the idea of Electronic Toll Collection (ETC) System. In terms of environmental conservation, the amount of oil consumption is reduced by 510 thousand kilo liter per year and environmental burdens are also reduced by 1.18 million ton per year. For all of these reasons, abolishing the pausing rule becomes excellent amendment for resolving jams, energy saving, environmental pollution and reducing accidents.

However, it is an undeniable fact that we have some misgivings about abolishing the pausing rule. One of the possible accidents is that cars may be left at a railroad as seen in an intersection. Cars often enter into the intersection though the front road is bumpy and cars strand in the intersection. If a similar phenomenon is happened at the railroad, this situation leads to the horrible accidents. One possibility for avoiding this kind of accident is painting a road indication, where cars must not stopping and standing. Actually, this indication is used in front of a fire station or police station, since an emergency vehicle can rush immediately to the site without blockage in front of the station.

III. RAILROAD CROSSING MODEL BASED ON M-SOV MODEL

In this section, we explain the modified stochastic optimal velocity (m-SOV) model, which is improved the established stochastic optimal velocity (SOV) model[1], and apply this m-SOV to the traffic model at railroad crossing. One of the advantages of SOV model is that the two significant stochastic models, which are the asymmetric simple exclusion process (ASEP)[2] and the zero range process (ZRP)[3], are reduced in the limit of low or high sensitivity of drivers. These two stochastic models are quite useful to calculate analytically, since they are exactly solvable in the sense that the probability distribution in the steady state can exactly calculated.

In SOV model, it is possible that a car stops even if the front cell is empty. This phenomenon occurs from stochastic behavior of model (not intentionally) and the car keeps its current velocity. In contrast, it is naturally possible that a car stops if the front cell is not empty. This phenomenon occurs from physical behavior (intentionally), but a car keeps its current velocity as well as the stochastic stop. That is, in SOV model, if a car stops at any time step, its velocity does not change to 0 until the car stay the same place for a long time, since those two situations of stopping are treated exactly the same. In fact, however, those two situations are entirely different. Thus, we suggest modified SOV model by discriminating the case that a car stops *stochastically (not intentionally)* from the case that a car stops *physically (intentionally)*. If next cell is not empty and a car stops, its velocity change to 0, since the stop is treated as *intentional*. In contrast, if next cell is empty, a car stops

	Stochastically Stop $1-v_i^t$	Physically Stop
SOV model	In both cases, the velocity is updated by $v_i^{t+1}=(1-a)v_i^t+aV_{opt}(\Delta x_i^t)$. (†)	
M-SOV model	The velocity is updated by (†).	The velocity is updated by $v_i^{t+1}=0$

TABLE III: Comparative table of velocity update between SOV model and m-SOV model.

not intentionally and its velocity is treated the same way as the SOV model. Thus, we decide its velocity equals to 0 only if a car stops *physically (intentionally)*(TAB. III).

Let us imagine that the road partitioned into L identical cells such that each cell can accommodate at most one car at a time, and we set the number of cars equals to M. 3 cells at the center of the one dimensional road are set down as the area of railroad crossing, where cars can not stop (FIG. 1). Moreover, we impose periodic boundary conditions and adopt *parallel update*. In these simulations, we set that 1 cell corresponds to 6 meters and 1 time step corresponds to 0.72 seconds, since the mean velocity in city traffic is about 30 kilometers per hour and mean headway distance is about 6 meters.

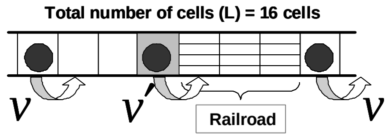

FIG. 1: Schematic view of the CA model with railroad crossing.

For comparison of traffic flow, we consider two situations: one situation is that cars must pause in front of the railroad crossing (at the shaded cell in FIG. 1) and another situation is that cars can enter into the railroad crossing without pausing.

- *With pausing*
  In this case, cars must pause in front of the railroad crossing, even if the cell over the railroad is empty. The velocity is updated by

$$v_i^{t+1} = \begin{cases} 0 & \text{(pausing and physically stopping)} \\ (1-a)v_i^t + aV_{\rm opt}(x_{i+1}^t - x_i^t) & \text{(otherwise).} \end{cases} \tag{1}$$

- *Without pausing*
  In this case, cars do not need to pause in front of the railroad crossing. The velocity is updated by

$$v_i^{t+1} = \begin{cases} 0 & \text{(only physically stopping)} \\ (1-a)v_i^t + aV_{\rm opt}(x_{i+1}^t - x_i^t) & \text{(otherwise).} \end{cases} \tag{2}$$

IV. SIMULATION RESULTS AND ANALYTICAL CALCULATIONS

The typical space-time plots of railroad crossing simulations are given by FIG. 2. From this figure, we have found that the jam at the bottleneck is resolved by abolishing the pausing rule.

FIG.3 shows the flow-density plots, so-called *the fundamental diagram*. This figure demonstrates that the traffic capacity (the maximum value of traffic flow) without

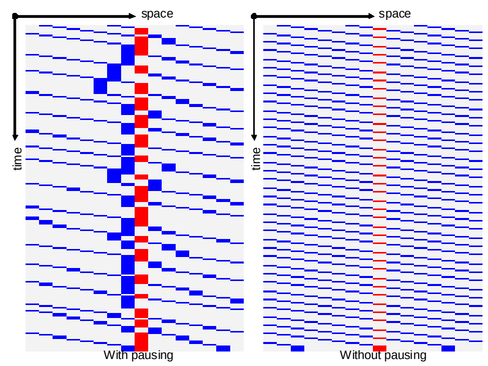

FIG. 2: Space-time plots for parameter values ($M = 3, L = 16$, (about 100 meters), $a = 0.1$, $0 \leq$time≤ 200). In the case with pausing, cars must pause at the center (red) cell.

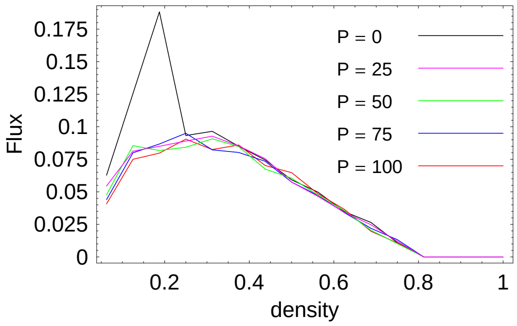

FIG. 3: The fundamental diagram for parameter values ($L = 16, a = 0.1$). The symbol P is used to denote the rate of cars of pausing. For example, $P = 50$ corresponds to the case that a half of cars pauses at the railroad crossing.

pausing ($P = 0$) becomes about twice as large as the capacity with pausing ($P \neq 0$) around $\rho = 0.2$, where ρ is the density of cars. However, since the flow except $P = 0$ is quite similar, we have found that the flow hardly changes, until all car do not pause at the railroad crossing.

In FIG. 4, we plot the difference of lap-time between with pausing and without pausing. It is found that the time difference at low density equals to about 9.5 time steps regardless of the system size. Moreover, the time difference of all cases reaches the maximum value at around critical density ($\rho \sim 0.2$).

Now, we have estimated the time difference analytically at the low density. At the low density we can assume that the headway distance of each cars is significantly large, i.e. we put $V_{opt}(\Delta x_i^{t-1}) = 1$. Furthermore, we also put $v_i^0 = 0$ as the initial condition, since our aim is to estimate the lost time due to pausing. Under these assumptions, velocity updating formula ((†) in TAB. III) is reduced to

$$v_i^{t+1} = (1-a)v_i^t + a. \tag{3}$$

By solving this recurrence formula with initial condition

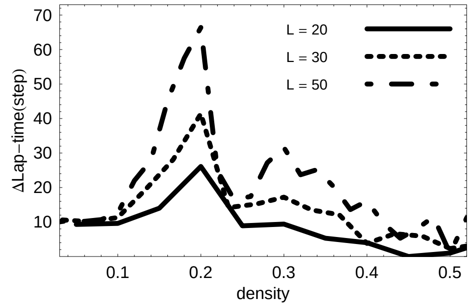

FIG. 4: The plots of the time difference between with pausing and without pausing for the parameter $a = 0.1$.

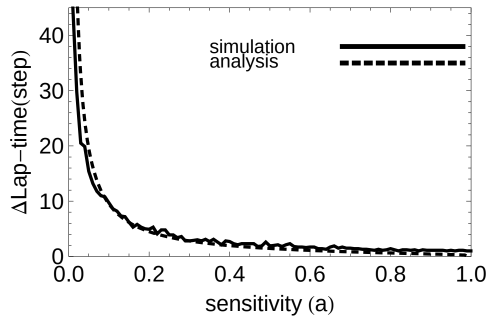

FIG. 5: The time difference plots of computer simulations and analytical calculations for the parameter $M = 1$.

($v_i^0 = 0$), we obtain

$$v_i^t = 1 - (1-a)^t. \tag{4}$$

Since this formula can be regarded as the cumulative distribution function, the probability density function is

$$\frac{\partial v_i^t}{\partial t} = -(1-a)^t \log(1-a). \tag{5}$$

Hence, the expectation value of time ($T(a)$) is

$$\begin{aligned} T(a) &= \int_0^\infty t \frac{\partial v_i^t}{\partial t} dt \\ &= -\frac{1}{\log(1-a)}. \end{aligned} \tag{6}$$

As long as the density is low, we have reasonably good agreement between the analytical calculations (6) and the corresponding numerical data obtained from computer simulations (see FIG. 5). For example, in the case $a = 0.1$, we get the estimates $T(0.1) = 9.49122$ from analytical calculations. The corresponding number obtained from direct computer simulations is 9.5, which is shown at the low density limit in FIG. 4.

V. CONCLUSIONS

Japanese law obliges that cars must pause in front of the railroad crossing before enter into the railroad and this pausing rule causes heavy jams by bottleneck effect. In order to estimate the impact of pausing rule on traffic flow, we have first improved the SOV model and suggested the modified SOV model by discriminating two stopping behavior of cars : *stochastically* and *physically*. Next, we have applied this m-SOV model to the traffic model at railroad crossing and compare the traffic flow with pausing to the flow without pausing. As the results, we have found that the traffic flow without pausing becomes about twice as large as the flow with pausing around the critical density. In particular, we have found that the flow hardly changes, until all car do not pause at the railroad crossing. Moreover, the lost time due to pausing is estimated by both computer simulations and analytical calculations and we have obtained the lost time is about 9.5 steps (about 6.8 seconds).

[1] M.Kanai, K.Nishinari and T.Tokihiro, Phys. Rev. E **72**, 035102 (2005)
[2] B. Derrida, E. Domany, and D. Mukamel, J. Stat. Phys. **69**, 667 (1992).
[3] F. Spitzer, Adv. Math. **5**, 246 (1970).

Easing Pedestrian Jam for Preventing Global Warming

Daichi Yanagisawa[1,2] and Katsuhiro Nishinari[1,3]
[tt087068, tknishi]@mail.ecc.u-tokyo.ac.jp
[1] Department of Aeronautics and Astronautics,
School of Engineering, The University of Tokyo.
7-3-1, Hongo, Bunkyo-ku, Tokyo 113-8656, Japan.
[2] Research Fellow of the Japan Society of the Promotion of Science.
[3] PRESTO, Japan Science and Technology Corporation.

I. INTRODUCTION

Pedestrian Dynamics is studied by simulations and experiments vigorously over last decades [1, 2]. The main goal of the study is to solve the congestion in the city and find the safety way to evacuate in the emergency situation. However, easing the pedestrian jam does not solve these problems, but is also effective to save the energy and prevent the global warming.

It is said that one human has same power as a 100 [W] light ball. Thus, the temperature of a place, where many people are gathering, is higher than a vacant place, and need much energy for air conditioner. For example, the congested commuters' trains in Japan use a lot of energy for air conditioner in summer. Therefore, we can save energy for air conditioner by dispersing people.

In summer, large buildings such as theaters use air conditioner to cool inside of them. However, when many people get out from them, warm air comes into the buildings. Therefore, we can decrease it coming into the buildings by shorten the total egress time by applying the way of shortening the evacuation time in emergency situation, and save the energy for air conditioner.

We consider how pedestrians disperse and the way of fast evacuation. We will show how people disperse in the case there are two exits by the theoretical analysis. We find that the egress time is shortened when people evacuate in several lines than when people go out freely and also verify that putting an obstacle is effective for the fast evacuation. The both cases are studied by the experiments and the theoretical analysis.

II. THE WAY OF PEOPLE DISPERSING

We consider the situation as in Fig. 1 (a). Eighteen pedestrians try to get out from the room. There are two exits which are Exit A and Exit B, and Exit A is much nearer than Exit B for the pedestrians. If the all pedestrians go to the Exit A, a big jam is formed and the temperature around the Exit A goes up (Fig. 1 (b)). It is stressful for them to stay for a while in the jam. If the pedestrians disperse to the two exits, the size of the jam becomes much smaller (Fig. 1 (c)). The total evacuation time is also shorter in the dispersion case (Fig. 1 (c)) than the concentration case (Fig. 1 (b)).

We analyze how people disperse by using game theory.

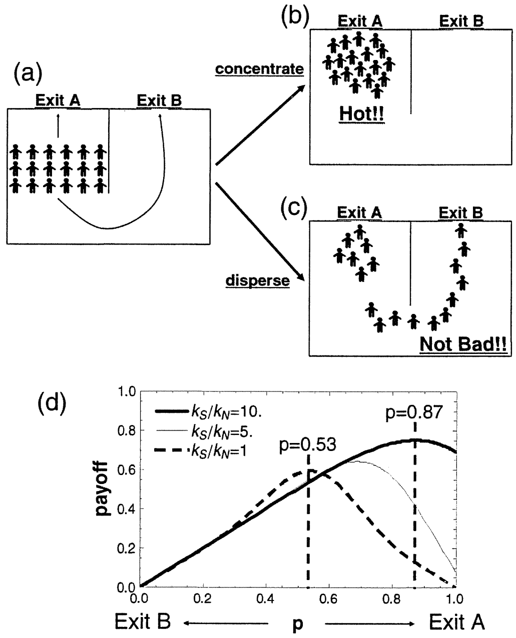

FIG. 1: (a), (b), and (c) Schematic views of the evacuation from the room, which has two exits. (d) The value of payoff as a function of p.

The payoff function of the pedestrians is determined as payoff$(S_X, N_X) = \exp(-k_S S_X - k_N N_X)$, where S_X is the distance to the Exit X, N_X is the number of pedestrians going to the Exit X, k_S is the pedestrians' intensity of going to the nearest exit, and k_N is the pedestrians' intensity of avoiding the congestion. Since S_X and N_X are multiplied by minus signs, payoff decreases when S_X and N_X increases. Thus, if a pedestrian choose a near exit and there are few other pedestrians, he/she can get large payoff. We decide p as the probability of going to the Exit A, i.e., the pedestrian go to the Exit B with probability $1-p$. Figure 1 (d) shows the payoff as a function of p in the case $k_s/k_N = 10,\ 5,\ 1$, $S_A = 1$, and $S_B = 3$. We clearly find that the maximum payoff is attained at the value of p. We call it optimal p notated as p_{opt} here after. In the case $k_s/k_N = 10$, i.e., the pedestrians tend to choose the nearest exit without considering a congestion, the value of $p_{opt} = 0.87$, therefore most of the pedestrians go to the Exit A. However in the case $k_s/k_N = 1$, i.e., the pedestrian try to avoid a congestion as well as

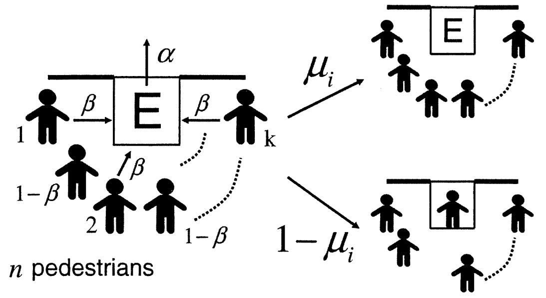

FIG. 2: Schematic view of the extended model at the exit.

go to the nearest exit, the value of $p_{opt} = 0.53$, therefore pedestrians disperse to the two exits.

III. THE RELATION BETWEEN PEDESTRIAN OUTFLOW AND A WAY OF EVACUATION

We consider a situation that every pedestrian in a room moves to the same one exit. We extend the floor field model [3] to focus on the pedestrians' behavior at the exit (Fig. 2). The normal floor field model uses the Neumann neighboring cells, however, we consider the situation that there are n neighboring cells of the exit cell and k pedestrians are trying to move to the exit cell. The case $n = 3$ and $n = 5$ corresponds to the FF model using the Neumann neighborhood and Moore neighborhood, respectively. The transition probability to the exit cell determined by the Static FF is represented as $\beta \in [0, 1]$ for simplicity. $\alpha \in [0, 1]$ is a probability of getting out through the exit.

We consider three new factors to reproduce the realistic pedestrians' behavior at the exit.

First, we introduce the clogging and sticking effect by the *friction function.*

Due to the use of parallel dynamics of the floor field model, it happens that two or more pedestrians choose the same target cell in the update procedure. Such situations are called conflicts in this paper. To describe the dynamics of a conflict in a quantitative way, *friction parameter* $\mu_0 \in [0, 1]$ was introduced in Ref.[4]. It describes clogging and sticking effects between the pedestrians. In a conflict the movement of *all* involved pedestrians is denied with probability μ_0, i.e., all pedestrians remain at their cell. Therefore, the conflict is solved with probability $1 - \mu_0$, and one of the pedestrians is allowed to move to the exit cell (Fig. 2). The pedestrian which actually moves is then chosen randomly with equal probability.

However, the friction parameter, which represents the strength of clogging and sticking between pedestrians, is a constant and does not take account of the difference of the number of the pedestrians involved in the conflict. In reality, the clogging effect is stronger when three pedestrians conflict each other than when two pedestrians conflict each other. Therefore, we newly introduce the friction function μ_1 and μ_2, which are functions of $k \in \mathbf{N}$, i.e., the number of pedestrians involved in the conflict. μ_1 and μ_2 are described as follows:

$$\begin{aligned} \mu_1(\zeta_1, k) &= 1 - \exp[-\zeta_1(k-1)] \\ \mu_2(\zeta_2, k) &= 1 - (1-\zeta_2)^k - k\zeta_2(1-\zeta_2)^{k-1}. \end{aligned} \tag{1}$$

$\zeta_1 \in [0, \infty)$ and $\zeta_2 \in [0, 1]$ are friction coefficient, which represent the strength of the clogging irrelevant to k. When ζ_1 and ζ_2 increases, μ_1 and μ_2 increase, respectively. The details of μ_1 and μ_2 are described in Ref. [5].

The second factor is the effect of turning around at an exit. The pedestrians, who move to the exit cell from lateral direction as the pedestrian 1 and k in Fig. 2, have to turn their face to the outside of the room at the exit cell to get out from the room, thus their walking speed decreases. The third factor is the zipper effect. When many pedestrians egress through the narrow exit, we often see that pedestrians in the left area and pedestrians in the right area go through the exit one after the other, and the outflow increases since the number of conflicts between pedestrians deceases dramatically. This phenomenon is called zipper effect. We introduce these factors to the model. The details of them are described in Ref. [6].

We did the evacuation experiments (Fig. 3) to verify the relation between the three new factors and the average pedestrian outflow $\langle q \rangle$ [persons/(m · sec)], which is the average number of pedestrians going through the 1 [m] width exit in 1 [sec].

The results of the experiments and theoretical analysis are described in Fig. 4. There are three remarkable points in this figure. First, we see that the pedestrian outflow decreases in $n \geq 2$. This indicates that when the number of pedestrians at the neighboring cells of the exit increases, the outflow decreases. Second, the maximum outflow is attained in the case (B), i.e., two-parallel-line case. We observe the zipper effect, i.e., pedestrians in the left line and the right line go through the exit one after the other, in our video. Pedestrians are intelligent enough to avoid conflicts by their selves. Third, the pedestrian outflow in the case (G) ($n = 4$) and the average of pedestrian outflow in the case (H) and (I) (Fig. 4 (H&I)) are similar. This indicates that there are approximately four pedestrians at the exit in the normal evacuation situation (H) and (I) when the width of the exit is 50 cm.

Comparing the theoretical and experimental results, we see that the results of the friction functions agree with those of the experiments very well, however, the results of the friction parameter does not. Since the friction functions consider the difference of n, they reproduce the value of the experiments, while the friction parameter does not.

IV. THE EFFECT OF AN OBSTACLE

We study the effect of an obstacle put in front of the exit in this section. We did the two kind of evacuation

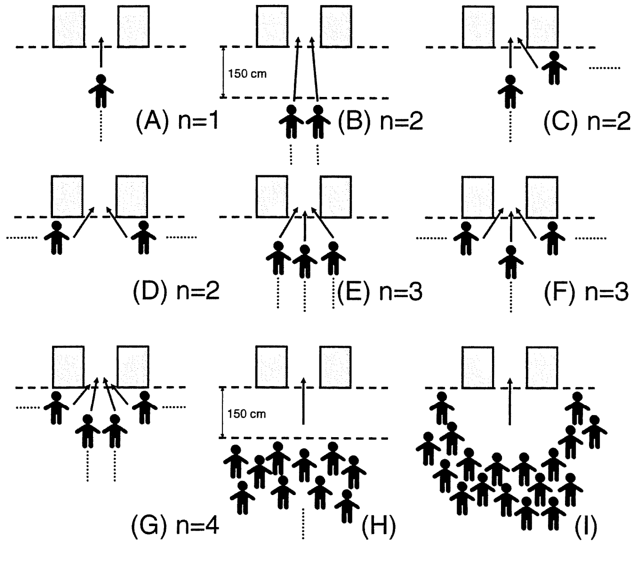

FIG. 3: Schematic views of nine initial conditions of the experiments.

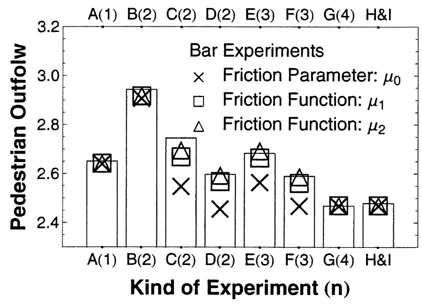

FIG. 4: Pedestrian outflows of the experiments and the theoretical calculation using μ_0, μ_1, and μ_2.

experiments at the NHK TV studio in Japan. In one case, pedestrians egress from the room through the 50 [cm] exit as in Fig. 5 (a) and the other case, pedestrians egress from the room through the 50 [cm] exit with an obstacle as in Fig. 5 (b).

The pedestrian outflow in the case (a) is 2.75 and that in the case (b) is 2.93. We surprisingly find that the outflow of the experiment (b), i.e., the experiment putting an obstacle in front of the exit, is larger than the experiment (a), which is a normal evacuation.

We explain this phenomenon by our theory. Looking the video of the experiments, we see that the obstacle blocks the participant moving to the exit. In the Sec. III, we found that in the normal evacuation there are approximately four pedestrians at the exit, i.e., $n = 4$ in the experiment (a) (Fig. 5 (a)). When the obstacle is put in front of the exit, there are approximately three pedestrians at the exit, since it blocks one pedestrian moving to the exit. Therefore, we consider that $n = 3$ in the experiment (b) (Fig. 5 (b)). We obtain the value of the pedestrian outflow from the theoretical analysis as follows: (Case μ_0: 2.75), (Case μ_1: 2.94), and (Case μ_2: 3.00). We find that the pedestrian outflows of the friction functions μ_1 and μ_2 agree with that of the experiment (b) well again, while the pedestrian outflow of the friction parameter is much smaller. This result justifies our assumption that the obstacle increase the pedestrian outflow since it decreases n, which is the number of pedestrians at the neighboring cells of the exit cell.

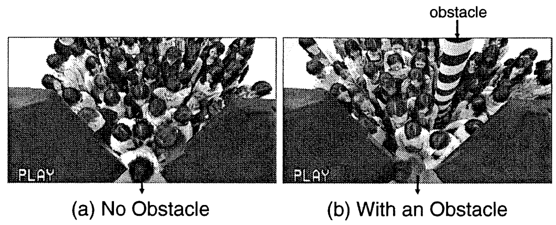

FIG. 5: Snap shots of the experiments. (a) Normal evacuation. (b) There is an obstacle in front of the exit.

V. CONCLUSION

In the former part in this paper, we study how pedestrian disperse to the two exits. In the latter part, we introduce the *friction function*, which changes its value against the number of pedestrians involved in a conflict. By using the friction functions, we obtain the more realistic figure of the pedestrian outflow through an exit, which corresponds to the result of the experiments very well. We have also found that the evacuation in the two-parallel-line case is the fastest and that the pedestrian outflow increases by putting an obstacle in front of the exit in the experiments.

Acknowledgements

This work is supported by Japan Society for the Promotion of Science. The experiments in Sec. IV, was supported by the NHK TV program *Science Zero.*

[1] D. Helbing, Rev. Mod. Phys. **73**, 1067 (2001).
[2] D. Yanagisawa *et al*, Phys. Rev. E, 76, 061117 (2007).
[3] C. Burstedde *et al*, Physica A **295**, 507 (2001).
[4] A. Kirchner *et al*, Physica A **324**, 689 (2003).
[5] D. Yanagisawa, *et al*, Proceedings of the Pedestrian and Evacuation Dynamics 2008, (to be published).
[6] D. Yanagisawa *et al* (in preperation).